2018

Electrochemical Methods To Study Real-Time In Vivo Neurochemistry

Aya Abdalla
University of South Carolina

ELECTROCHEMICAL METHODS TO STUDY REAL-TIME *IN VIVO* NEUROCHEMISTRY

by

Aya Abdalla

Bachelor of Science
American University of Sharjah, 2013

Bachelor of Chemical Engineering
American University of Sharjah, 2013

Submitted in Partial Fulfillment of the Requirements

For the Degree of Doctor of Philosophy in

Chemistry

College of Arts and Sciences

University of South Carolina

2018

Accepted by:

Parastoo Hashemi, Major Professor

Stephen L. Morgan, Committee Member

Linda Shimizu, Committee Member

Jim Fadel, Committee Member

Cheryl L. Addy, Vice Provost and Dean of the Graduate School

DEDICATION

This dissertation is dedicated,

To my loving parents, for inspiring me to always be a better human, and loving me for who I am.

To my siblings, for always having each other's backs.

To my girls, for all the memories made and yet to be made.

To Saffron, for always making me laugh at your crazy, no matter how bad of a day I am having.

ACKNOWLEDGEMENTS

After a long journey, to be sitting here writing this, seems like a dream I thought would never come to pass. The metaphorical tunnel, a lot of times, felt endless, and the light at the end, an unattainable goal. But, it has finally come to pass. These past 5 years were filled with more emotions and experiences than I can fit into a few sentences. There were shouts of joy at successful endeavors, and tears of frustration at unsuccessful ones. Through all those memorable moments, both wonderful and challenging, I had people who stood by me, and taught me to stand strong and proud.

First, my advisor, Dr. Parastoo Hashemi. You have been an inspiring force in my life, showing me the kind of researcher, mentor, and human, both in science and outside, that I should aim to be. I will always be grateful for everything you have taught me and all the obstacles you helped me through.

Second, I would like to thank my committee members both at USC and Wayne State; Dr. Stephen Morgan, Dr. Linda Shimizu, Dr. Jim Fadel, Dr. Andrew Cisneros, and Dr. Mary Rodgers, for all your help and guidance throughout my PhD. Your helpful comments have allowed me to be a better scientist. In addition, I am grateful to all our collaborators, Dr. Stephen Morgan, Dr. Michael Heien, Dr. David Linden, Dr. Michael Reed, Dr. Janet Best, Dr. Fred Nijhout, and Dr. Edsel Pena, for broadening my horizons and teaching me that science can remain exciting, no matter how long you have been doing it for. Furthermore, I will forever

remain indebted to my undergraduate professors, who saw something in me and instructed me to never stop dreaming or ever put limits on how far I think I can go.

Next, special thanks have to go to the Hashemi lab. Kevin, Thushani, Rachel, Srimal, Shane, Matt, Pavithra, Shirley, Anisa, Rhiannon, Megan, Jordan, Melinda, Alyssa, Anna Marie, Damian, Bruce, Audrey, and Ellen. Thank you all for more than I can say; for great friendships, great mentoring and just making a special journey all the more special by being memorable parts of it. Thank you for being there when I needed help whether it was in science, or more importantly, in life in general.

I would like to also thank all those friends, whether in USC or at Wayne who have always made me feel like I am part of something bigger than just me, I am thankful to have met all of you. You will always remain with me wherever my road takes me next.

To my second family, Ayoosh, Bedo, Borra, Shahooda and Yamoonti, I would like to send some very special thanks. You girls have taught me that family is not limited to blood. You have been with me every step of the way for the last 9 years and if it was not for your constant support and friendship, I would not have reached where I am today. My appreciation and thanks will never be enough.

Finally, to the most important people in my life, my family, I would like to send never ending thanks, love, and appreciation. I am truly blessed in my life by the people who surround me, but you are all, by every count, an even bigger blessing. To have parents and siblings who always make you feel special, smart, and loved is truly something to remain eternally grateful for.

In the end, I would like to thank Allah, whose love has kept me strong, and who guided me to where I am today, blessing me with everything I need to succeed as well as with people who would motivate me to always keep moving forward.

ABSTRACT

Serotonin neurotransmission has multiple facets that are challenging to characterize, due to the lack of analytical tools that can measure serotonin in the brain. In addition, the mechanisms of serotonin modulation by other neurotransmitters, such as histamine, are not well understood. These limitations make the study and treatment of disorders in which serotonin is implicated problematic. This dissertation presents novel electrochemical methods, in addition to the well-established serotonin fast-scan cyclic voltammetry (FSCV), to better understand the dynamics of serotonin and histamine neurotransmission *in vivo*. In Chapter 1, a method, known as fast-scan controlled adsorption voltammetry, was optimized to selectively and sensitively measure ambient serotonin levels *in vivo*. In Chapter 2, this newly developed method was combined with FSCV and triple staining immunohistochemistry to confirm that serotonin transporter density affects the reuptake kinetics and ambient levels of serotonin in the CA2 region of the hippocampus and the medial prefrontal cortex. Subsequently, to study the serotonin modulation by histamine, in Chapter 3, an FSCV voltammetry waveform for *in vivo* measurement of histamine was optimized, that is stable, selective, and sensitive. Through electrical stimulation of the MFB and measuring the evoked histamine signal in the posterior hypothalamus, we showed that serotonin can be simultaneously measured alongside histamine. In Chapter 4, our work was able to demonstrate that histamine has an inhibitory effect on serotonin via the H-3

receptors. This dissertation showcases novel electrochemical techniques that will help pave the way towards a more detailed understanding of the different mechanisms that regulate serotonin neurotransmission *in vivo*, including neuromodulatory effects by other neurotransmitters. This will enable further work to be carried out in disease models.

PREFACE

Chapter 2: **Abdalla A**, Atcherley CW, Pathirathna P, Samaranayake S, Qiang B, Peña E, Morgan SL, Heien ML, Hashemi P (2017) *In Vivo* Ambient Serotonin Measurements at Carbon-fiber Microelectrodes. Anal Chemistry 89:9703-9711.

Chapter 4: Samaranayake S, **Abdalla A**, Robke R, Wood KM, Zeqja A, Hashemi P (2015) *In Vivo* histamine voltammetry in the mouse premammillary nucleus. Analyst 140:3759-3765.

Chapter 5: Samaranayake S, **Abdalla A**, Robke R, Nijhout HF, Reed MC, Best J, Hashemi P (2016) A voltammetric and mathematical analysis of histaminergic modulation of serotonin in the mouse hypothalamus. J Neurochem 138:374-383.

TABLE OF CONTENTS

LIST OF FIGURES

LIST OF ABBREVIATIONS

5-HIAA ……... 5-hydroxyindolacetic acid

5-HT …….. Serotonin (5-hydroxytryptamine)

5-HTP …… 5-hydroxytryptophan

AA ..…… Ascorbic Acid

AADC…….. Aromatic Amino Acid Decarboxylase

CFM ..…….. Carbon Fiber Microelectrode

CNS ..……..… Central Nervous System

CV ..…….. Cyclic Voltammogram

DA ..…….. Dopamine

DAT ..……..…… Dopamine Transporter

DRN ..…….. Dorsal Raphe Nucleus

FIA ..……..…… Flow Injection Analysis

FSCV ..…….. Fast Scan Cyclic Voltammetry

FSCAV ..... Fast Scan Controlled-Adsorption Voltammetry

GFP ..... Green Fluorescent Protein

HA ..... Histamine

HNMT ..... Histamine N-methyl Transferase Enzyme

HSW ..... Histamine Selective Waveform

MAO ..... Monoamine Oxidase

MD ..... Microdialysis

MFB ..... Medial Forebrain Bundle

mPFC ..... medial Prefrontal Cortex

NE ..... Norepinephrine

NET ..... Norepinephrine Transporter

OCT ..... Organic Cation Transporter

PH ..... Posterior Hypothalamus

PM ..... Premammillary Nucleus

SERT ..... Serotonin Transporter

SNr ..... Substantia Nigra Pars Reticulata

SSRI ..... Selective Serotonin Reuptake Inhibitor

TMN ..... Tuberomamillary Nucleus

UA ..... Uric Acid

VMAT ..... Vesicular Monoamine Transporter

CHAPTER 1: INTRODUCTION

The human brain is arguably regarded as nature's most complex system. Neurotransmitters, the brain's signaling molecules, control various brain functions in regionally distinct localities. The four amine systems, dopamine (DA), histamine (HA), norepinephrine (NE) and serotonin (5-HT), play essential roles in brain chemistry.[1] These roles could range from serotonin being responsible for regulating mood and sleep, to dopamine's part in our reward system, or histamine's role in the brain's immune response.[2-5] This makes the study of these biogenic amines important in furthering the understanding of different brain functions. My lab has specific interests in serotonin and histamine.

Serotonin was first identified in the central nervous system in 1953.[6] Since its discovery, dysregulation in the serotonergic system has been linked to numerous neuropsychiatric and neurodegenerative diseases, such as depression, anxiety, and schizophrenia.[7-9] Unfortunately, the treatment of these disorders remains challenging due to the poor characterization of serotonin neurochemistry in healthy and disease models and the lack of information on neuromodulators that affect it, such as histamine (HA).

HA is another important monoamine in the brain with various functions, the most important being modulation of other neurotransmitters. It is also widely implicated in the brain's immune response.[5] Compared to dopamine and serotonin,

HA is an understudied neurotransmitter, due to the complicated electrooxidation mechanisms of this analyte.[10] There is evidence that HA modulates serotonin transmission[11] and since HA and serotonin coexist in many brain regions, we find it of merit to understand the functions of the histamine system along with the serotonin system.

1.1 THE SEROTONIN SYSTEM

Serotonin is a neuromodulator, responsible for several functions in the central nervous system (CNS) and the body's peripheral nervous system. Only 2% of the serotonin in the body is found in the brain while the other 98% is found in the body.[12] Serotonin is thought to be responsible for an extensive array of behavior and motor functions, such as mood, appetite, and the circadian rhythm.[13] Due to the vast and varied role it plays, serotonin has been implicated in diseases like Alzheimer's, Autism, Parkinson's disease, and depression.[14] The biochemistry of serotonin is complicated, with pharmacological manipulations affecting many direct and indirect pathways. To further understand the role serotonin plays in the different neurodegenerative, neuropsychiatric disorders, and neurological diseases, it is critical to better comprehend the neurochemical functions of serotonin in the brain.

L-Tryptophan, the precursor for serotonin, is introduced to the body through diet. Once in the brain, L-Tryptophan is hydroxylated to 5-hydroxytryptophan (5-HTP) via enzyme tryptophan hydroxylase and transported into neurons. Subsequently aromatic amino acid decarboxylase (AADC) is responsible for converting 5-HTP into serotonin. Serotonin in then packaged into different vesicles

at the serotonin neuron terminals by the vesicular monoamine transporter (VMAT). When the neuron receives an action potential, the vesicles undergo exocytosis to release a part of their contents into the extracellular space. Upon release, serotonin will interact with various receptors, to propagate an electrical signal. Serotonin autoreceptors regulate serotonin in the extracellular space by autoinhibiting release. Serotonin is then removed via different transporters, the most important of which is the serotonin transporter (SERT), then broken down by monoamine oxidase (MAO) into its different metabolites such as 5-hydroxyindolacetic acid (5-HIAA).[12]

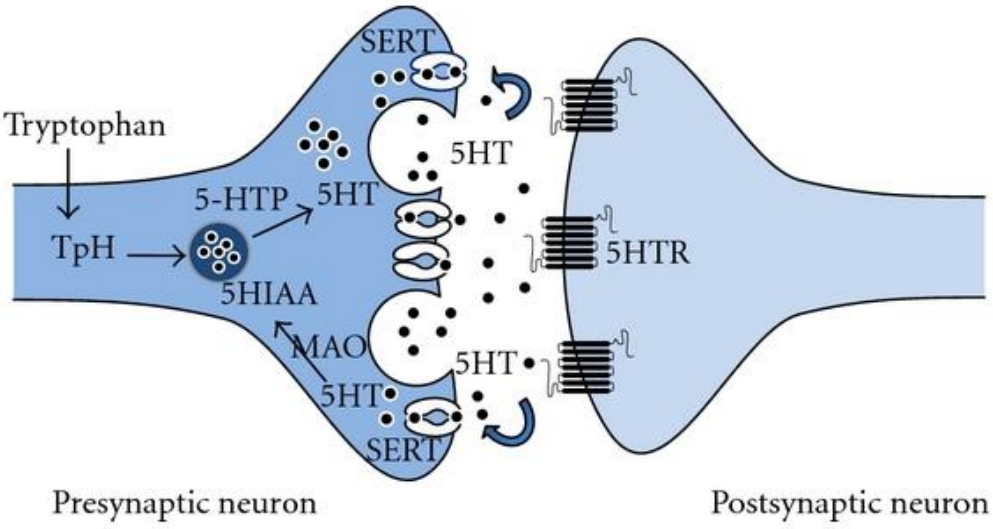

Figure 1.1. The synthesis, packaging, release, reuptake and metabolism of serotonin at a serotonin neuron terminal. TpH - tryptophan hydroxylase, 5-HTP – 5-hyroxytryptophan, 5HIAA – 5-hydroxyindolacetic acid, MAO – monoamine oxidase, 5HT – serotonin, SERT – serotonin, SERT – serotonin transporter, 5HTR – serotonin receptor.[9]

The regulation of serotonin in the brain has been under a lot of scrutiny and review in the past few years. This is mainly because many drugs that are thought

to act on the serotonin system, such as serotonin-selective reuptake inhibitors (SSRI's), exhibit variable efficacies.[15] Additionally, what is known about serotonin's neurochemistry reveals that it is quite different from other neurotransmitters. One of these differences is the level of its regulation: while other neurotransmitters are easily found in the extracellular space at high concentrations, serotonin is only found at low concentrations, in addition to having various mechanisms in place to prevent these levels from increasing.[15]

In 2014 our group described 2 reuptake mechanisms, while studying serotonin in the substantia nigra pars reticulata (SNr), and used a Michaelis-Menten kinetic model to model the data. They observed three types of serotonin responses in the SNr. In some mice, serotonin was released then cleared quickly, referred to as a "fast" response. In others, the released serotonin took a longer time to clear, termed "slow" responses. A hybrid between the two was when the released serotonin exhibited both fast and slow responses. This means that there are two mechanisms for serotonin uptake into cells. 'Uptake 1' is clearance through the SERTs which have high affinity to serotonin but are not very efficient as was described by the high K_m and low V_{max} values calculated through the Michaelis-Menton equation. 'Uptake 2' is performed by non-serotonin transporters (non-SERTs) like dopamine transporters (DATs) or norepinephrine transporters (NETs) that have low affinity for serotonin but have comparatively faster rates as seen by the lower K_m values and the higher V_{max} values. The difference in clearance times between fast, slow, and hybrid were related to the percent of the clearance by

SERTs versus non-SERT's. The following is the model developed to describe these findings, which also includes an autoreceptor function.

$$\frac{d[S\,(t)]}{dt} = R\,(t)\big(1 - A(t)\big) - \alpha\frac{V_{max1}[S\,(t)]}{K_{m1}+[S\,(t)]} - \beta\frac{V_{max2}[S\,(t)]}{K_{m2}+[S\,(t)]} \qquad \textbf{(1)}$$

Where, S(t) is the concentration of serotonin in the extracellular space, R(t) the rate of serotonin release, and A(t) is the fraction of stimulated autoreceptors. The constants α and β represent the contribution of each of the uptake mechanisms, and V_{max} and K_m are Michaelis-Menton variables, where the slow uptake is denoted by the 1 and the fast by 2. Thus, when the response is slow, the β term is zero and α is 1 whereas when it is fast the opposite holds true. The hybrid response model incorporates a value for both α and β. V_{max} and K_m values for uptake 1 were calculated to be 17.5 nM/s and 5nM respectively while those for uptake 2 were 780 nM/s and 170nM respectively.[15]

The regulation of serotonin by autoreceptors and the different uptake mechanisms is only part of the picture. Other mechanisms are also responsible for the regulation of serotonin levels in the brain, including modulation by histamine.[16]

1.2 THE HISTAMINE SYSTEM

HA is a very important chemical in the brain and in the body. It is involved in several physiological functions, such as allergic and immune reactions to foreign substances. Additionally, HA is important for regulation of digestion via gastric secretion. [17] As a neurotransmitter, HA is implicated in many neurological

disorders such as Alzheimer's and Parkinson's diseases;[18] the same diseases that serotonin is thought to play such an important role in.

HA, like serotonin, does not pass through the blood brain barrier. It is synthesized from the amino acid L-histidine, that we intake through our diet and that gets into the brain through the L-amino acid transporter. L-histidine is converted to HA through the enzyme L-histidine decarboxylase. HA is then stored into vesicles by VMAT, where it stays until an action potential causes depolarization of the neuron and the exocytosis of the vesicles. Once in the extracellular space, HA interacts with a variety of receptors and autoreceptors. Unlike other neurotransmitters, there is no known mechanism for the reuptake of HA back into the neuron. The common belief is that instead of being reuptaken, HA is metabolized through two pathways. The first, is by histamine N-methyltransferase which degrades HA to tele-methylhistamine by a methylation process. Tele-methylhistamine is further metabolized by MAO-B to tele-methylimidazole acetic acid. The second method has HA oxidized to imidazole acetic acid by diamine oxidase. In vertebrates, the first method is the primary method of HA metabolism and there is little evidence of the second process occurring, due to the lack of detection of diamino oxidase in vertebrates. [19]

Release of HA into the extracellular space, causes it to interact with various histamine receptors, some of which are present on non-histaminergic neurons. This causes the neuromodullatory effects of HA on other neurotransmitters, like serotonin. This makes it critical to not only study the histaminergic or the serotonergic system exclusively, but to also find a way to study the modulation of

histamine on the serotonergic system, and its impacts on disorders that were once thought to only be caused by imbalances in the serotonergic system.

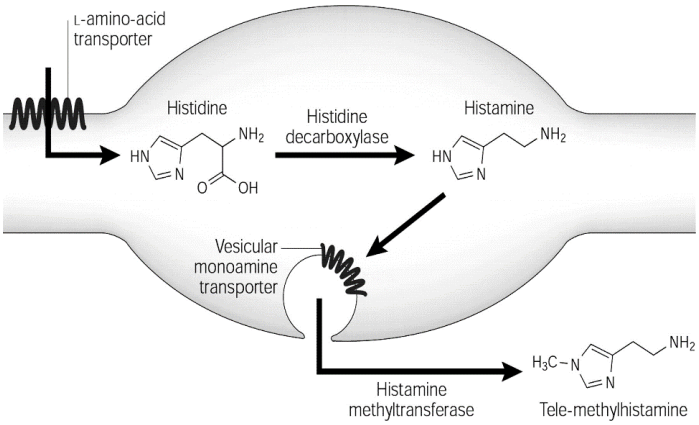

Figure 1.2. The synthesis, packaging, release, and metabolism of histamine at a histamine neuron terminal.[15]

Serotonin has been associated with a plethora of neurological and neuropsychiatric disorders, making the study of the different mechanisms and neurotransmitters that control and modulate the neurochemistry of serotonin such as histamine of critical importance. A major limitation in this endeavor is the lack of analytical tools able to study these two aminergic systems *in vivo*.

1.3 TOOLS FOR *IN VIVO* NEUROTRANSMISSION STUDY

Each of the different aminergic systems innervates certain regions of the brain, and most times, there will be multiple aminergic innervations to the same brain region. The hippocampus, for example, which is a brain region most known for memory consolidation,[21] has innervations from all 4 aminergic systems.[22-25] This makes the brain a heterogeneous environment, that is very difficult to probe.

1.3.1 CRITERIA FOR IDEAL *IN VIVO* MEASUREMENTS

The brain presents many unique challenges for analytical studies, and any analytical method must take into account 4 different criteria to be successful. These criteria, which Hashemi first referred to as the four S's, are size, sensitivity, selectivity and speed.[1]

The brain is an extremely physically delicate organ that is very sensitive to disruption and damage. Inserting a probe into the brain must cause minimal damage to avoid destroying cells and activating the brain's immune mechanisms, which would inherently change the local environment surrounding the probe. Thus, it is imperative that, first, the probe used is **small**. Second, the probe needs to be **sensitive** enough to effectively measure analytes present at low concentrations in the brain. Molecules in the brain range from picomolar to millimolar in concentration. Therefore, depending on the analyte being studied, the technique should be able to measure concentration through a wide linear range. Third, due to a myriad of substances present, many of which have similar molecular characteristics, it is essential that the chosen analytical tool has high **selectivity** to the molecule being measured. If the method is unable to differentiate between the molecule of interest and other analytes present, the outcome will not result in meaningful data. The final criteria to meet is the **speed** of measurement. Neurotransmission is a process that occurs on a sub-second time scale. Accordingly, *in vivo* measurements need to have high temporal resolution to visualize the changes occurring in real-time.

In recent decades, various methods have been developed following these criteria and employed to achieve a better understanding of the roles and function of neurotransmitters *in vivo*.

1.3.2 CURRENT ANALYTICAL METHODS FOR NEUROTRANSMITTER ANALYSIS

Different methods have been used to measure different neurotransmitters in the brain. Each method was able to further the understanding of the neurochemistry of monoamines, such as dopamine and serotonin, but due to the difficulty of meeting all 4 criteria mentioned above, it has been challenging to obtain a complete picture. Microdialysis, chronoamperometry, optogenetics, *etc.* are methods that have all been used to delve deeper into the chemistry of the brain. However, each method is not without limitations.

1.3.2.1 MICRODIALYSIS SAMPLING

One of the most common methods employed to monitor neurotransmitters is microdialysis (MD). MD is accomplished by implanting a probe with a semipermeable membrane (l = 7 - 12 mm; d = 220 - 380 μm) into the brain. A solution is perfused through the probe, and analytes diffuse across the membrane according to their concentration gradient and are collected.[26] Importantly, MD is a sampling technique that must be coupled to an appropriate analytical method to separate and detect analytes of interest. MD possesses inherent limitations, namely in temporal and the damage done to the brain by the implantation of the probe. The large size of the MD probe (100 – 500 μm) damages brain tissue. This damage has been well characterized by the Michael group, and results in

measurements being performed from damaged, unhealthy tissue.[27] In addition, most MD measurements are made on a minute time scale, making it hard to study neurotransmission, which occurs in milliseconds. This limitation in temporal resolution is due primarily to the analysis of MD samples: for offline analysis, the temporal resolution of traditional MD is limited by the volume required for handling and subsequent analysis; for online analysis, the temporal resolution is limited by the flow rate and the analysis time, which is dependent on the analytical instrument coupled to MD.[26] However, there has been outstanding progress made towards answering these limitations, where some research labs are now able to make measurements at a second-time scale, through manipulating the dialysate being collected. This work was pioneered by the Kennedy group, who improved the temporal to 2 s, through the collection of the dialysate in the form of droplets, separated by oil, that form over a 2 second period,[28] thus overcoming many of the limitations of microdialysis analysis.

There still remains, however, the issue of tissue damage caused by the large probes. The Kennedy group has made notable progress in this field through the introduction of microfabricated MD probes that are 45 µM in diameter and 180 µM in length.[29] These probes, although smaller, are still large enough to cause damage, albeit on a smaller scale than traditional MD probes.[27]

1.3.2.2 ELECTROCHEMICAL TECHNIQUES

1.3.2.2.1 CHRONOAMPEROMETRY

Chronoamperometry is one of the most common electrochemical methods utilized for monoamine analysis. In chronoamperometry, potential is applied to the

electrode surface in a square pulse form. The initial potential is selected so that the analyte of interest has no redox activity. This potential is then stepped to a second potential selected so as to be more positive than the oxidation potential of the analyte under investigation. This results in constant oxidation, which generates a detectable current, and causes the concentration of analyte at the electrode surface to fall to zero, thus creating a concentration gradient and generating a decaying current-time trace. When the potential is stepped back, it causes the reverse to occur and the oxidized analyte is now reduced. The decaying current profiles of both processes can be used to study the diffusion properties of analytes, as well as the release and reuptake of the neurotransmitters *in vivo*. The ratio of oxidation and reduction decay slopes can also be used to somewhat identify the analyte being measured.[30] Unfortunately, this square pulse waveform generates a large capacitative (non-faradaic) current every time the potential is switched. Although this current decays within a few milliseconds, it still makes it problematic to study the current-time traces generated by this method.[31] Most groups have found a way around this limitation, by only studying the last 70 – 80% of the current – time trace.[32] This has been very successful in tissue slices as well as cell studies, but to be able to successfully use this method *in vivo*, higher selectivity is required and depending on the ratio of decaying curves is not adequate enough. Thus, to overcome this, studies *in vivo* have used exogenous neurotransmitter injections close to the electrode surface so as to insure the identity of measured analyte.[30]

1.3.2.2.2 FAST-SCAN CYCLIC VOLTAMMETRY (FSCV)

In the early 1980's FSCV was developed by Millar and Wightman for monitoring dopamine *in vivo*.[33,34] This technique employs carbon fiber microelectrodes (CFM) with micrometer dimensions (l = 50-150 μm; d = 7 μm) that are implanted into the brain and offer a minimally invasive approach providing selectivity, sensitivity, and biocompatibility.[2] Owing to its high temporal and spatial resolution, FSCV was able to uncover mechanistic details about dopamine neurotransmission. More recently, the Hashemi lab has been able to advance FSCV to various new frontiers, and are pioneers for using this method for serotonin and histamine analysis.[2,10] In addition, we were the first to extend FSCV to metal ions, specifically Cu(II) and Pb(II) speciation studies.[35,36]

FSCV requires a set of instructions, known as a waveform, be applied to the CFM. This waveform is optimized for the selective detection of the analyte to be studied. It is applied at high scan rates, meaning that data is collected within milliseconds. The waveform typically consists of an anodic wave, a cathodic wave, and a resting potential as seen in the serotonin waveform, developed by Brad Jackson et al. in the mid 90s, depicted in **Figure 1.1A**.[37]

During the anodic sweep, the analyte undergoes oxidation at its oxidation potential (left to right on **Figure 1.1B**). Likewise, during the cathodic wave the analyte will be reduced at its reduction potential (right to left on **Figure 1.1B**). The resting potential between waveform application allows for the maximum adsorption of the analyte to the carbon fiber surface.

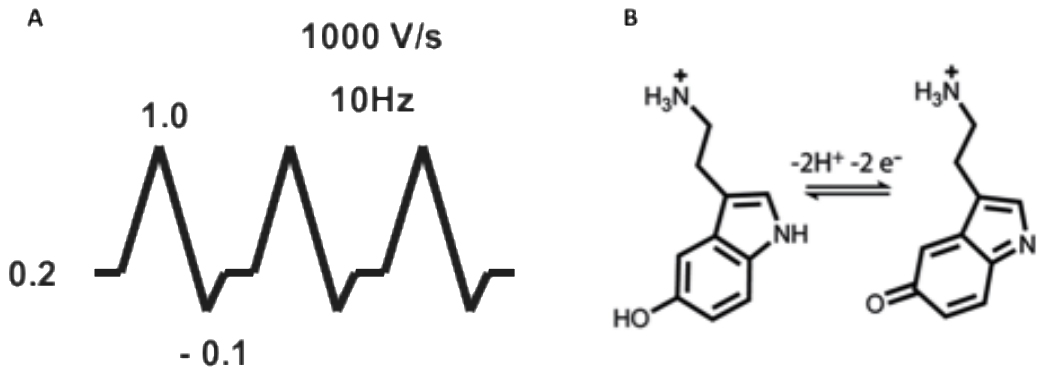

Figure 1.3. (A) The serotonin waveform applied at a 1000 V/s and 10Hz. The anodic sweep in this waveform is 0.2 to 1.0 V, while the cathodic sweep is 1.0 to -0.1 V, and the resting potential is 0.2 V. **(B)** Serotonin's 2 electron, 2 proton redox reaction.

The electron transfer process occurring at the carbon fiber's surface produces a faradaic current through the CFM, as seen in **Figure 1.1B** for serotonin. The current generated is detected and subsequently plotted versus applied voltage, to create a cyclic voltammogram (CV). A CV is analyte specific (in a given media) due to the analyte's unique oxidation and reduction potential. Thus, it is possible to qualitatively determine the analyte being measured from studying the CV.

Waveforms are applied at fast scan rates that range from 100 V/s to 10^6 V/s, whereas classic cyclic voltammetry typically scans at or below 1 V/s. These fast scan rates provide FSCV with the temporal resolution required to perform sub-second measurements. However, fast scan rates also produce a large capacitative current (or non-faradaic current) that is many times larger than the faradaic current of interest. To successfully measure the faradaic current, the non-faradaic current (or background) must be subtracted from obtained current. Thus, FSCV is a

background-subtracted technique, which creates the main limitation of FSCV, in that it only detects concentration changes. Particularly for neurotransmitters, this limitation translates into requiring the stimulated release of a given molecule for analysis. This requirement makes it impossible to analytically determine the analyte's ambient level. Even with this limitation, FSCV is still able to provide a wealth of information about neurotransmitters, such as release and reuptake mechanisms, making it a powerful tool for *in vivo* studies.

In FSCV, a single CV is collected in a few milliseconds, thus to obtain a more complete picture, multiple CVs are collected over a 30 s period. The CVs are then aligned together to generate a color plot, which is a 3D compilation of the data that can also be viewed as a 2D plot (**Figure 1.2A**). Using the color plot generated, a horizontal strip can be extracted to generate a current vs. time (i-t) plot, hence enabling us to quantitatively study the analyte, as can be seen in **Figure 1.2B**. CVs can also be re-generated through the extraction of vertical strips from the color plot. The green event at 0.7 V in **Figure 1.2A** represents serotonin oxidation, whereas the blue event at around 0.0 V represent the serotonin reduction. Calibrations are then used to convert current into concentration, and as a result, the analyte's concentration changes over time can be monitored.

1.3.3 THE NEED FOR AMBIENT LEVEL MEASUREMENTS

As mentioned above, FSCV is able to provide valuable information about the dynamics of neurotransmission, provided that a change is first introduced to the system. *In vivo* we induce this change occurs via electrical stimulation. However, due to background subtraction ambient levels cannot be determined.

This level is critical for better understanding the mechanisms that control extracellular serotonin levels. In 2015, Atcherley et al. developed a method capable of measuring ambient levels of dopamine *in vivo*, and coined the technique fast-scan controlled adsorption voltammetry (FSCAV).[38]

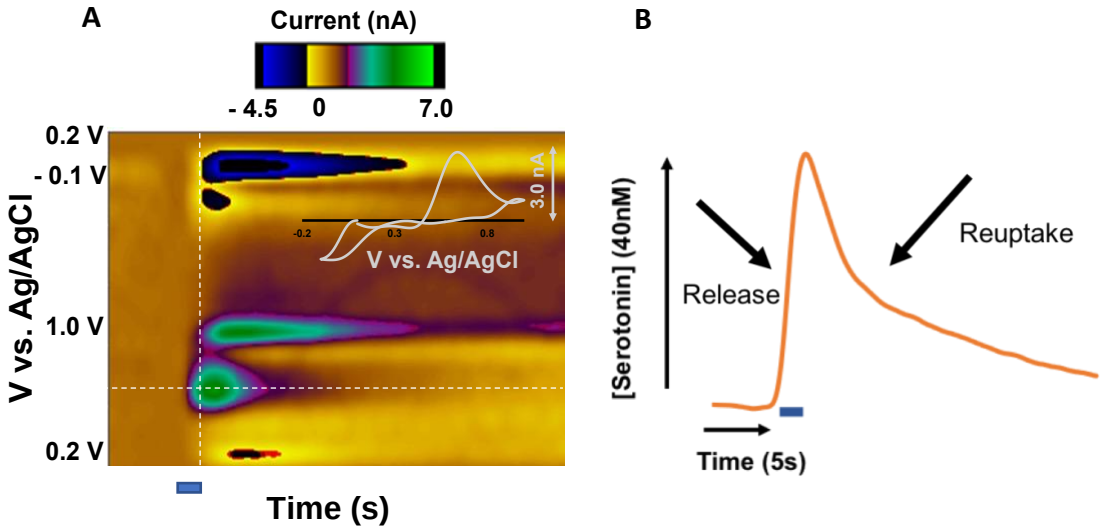

Figure 1.4. (A) 2D depiction of a representative color plot. Inset displays a current – voltage (CV) plot extracted from the white vertical dashed line. The green event at 0.7 V represents serotonin oxidation. The blue event around 0 V represents serotonin reduction. (B) Representative current versus voltage extracted from the horizontal dashed line in A. Blue rectangular bar represents period of electrical stimulation (2 s).

FSCAV depends on controlled adsorption to measure basal levels of analytes. It is performed by applying a waveform at a high frequency for 2 seconds followed by a period of controlled adsorption, where the potential is held at a constant value that maximizes adsorption of a specific molecule to be measured, onto the CFM surface. After adsorption, the waveform is reapplied, causing the rapid oxidation and reduction of all the analyte adsorbed onto the electrode surface. The redox reaction generates a current which is measured and converted

to concentration, allowing for the basal concentration value to be determined.[38,39] This process can be seen in **Figure 1.5**.

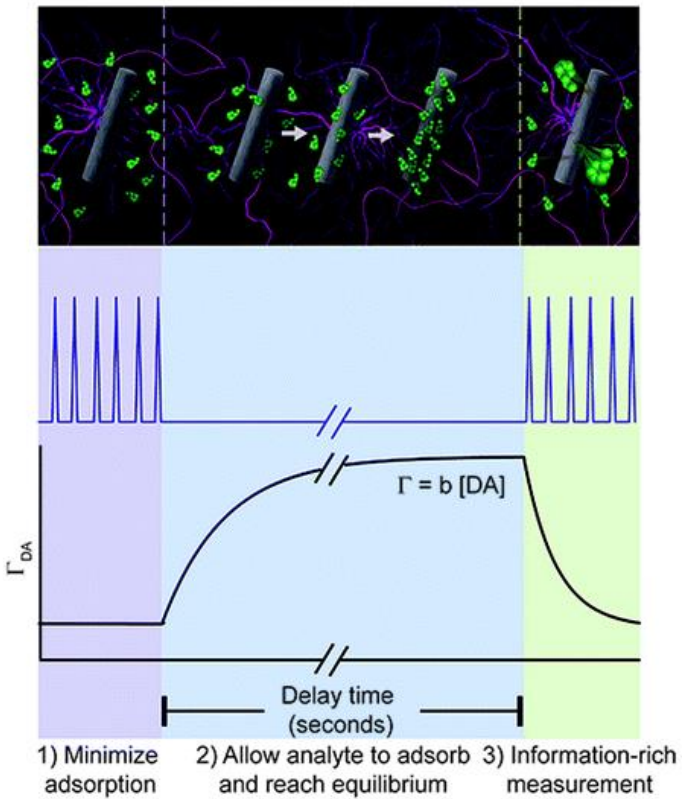

Figure 1.5. The stages of FSCAV: first minimized adsorption followed by controlled adsorption and finally reapplication of waveform, where data is collected through oxidation of analyte.

In this dissertation, FSCAV will be expanded to include the analysis of serotonin in various different brain regions of the mouse.

1.4 SCOPE OF THE DISSERTATION

This dissertation will first start by introducing how FSCAV was developed for ambient serotonin measurements *in vivo*. Next, it will describe the characterization of two new voltammetric circuitries; namely the hippocampus

(CA2 region) and the prefrontal cortex (pFc). These are areas with serotonin innervations that have been linked to psychiatric illnesses such as Alzheimer's disease, depression, and schizophrenia, among many others. The next focus was histamine, where *in vivo* measurements of histamine were made in the hypothalamus region, specifically the premammillary nucleus. Subsequently, we moved to study the histamine modulation of serotonin within the same region. The work done in this dissertation introduces new possibilities in the study of serotonin, allowing us now to look at the different facets of serotonin neurotransmission, and introducing modulation factors, that presents new targets to pharmaceutical agents.

The scope is outlined by chapter below:

Chapter 1: Introduction

Chapter 2: This chapter describes the development of fast-scan controlled adsorption voltammetry for ambient, extracellular serotonin measurements that is sensitive, selective, and stable both *in vitro* and *in vivo*. The signal is confirmed *in vivo*, both electrochemically and pharmacologically, in addition to developing a statistical model (in collaboration with statisticians) to allow for more accurate analysis of *in vivo* data, specifically the pharmacological administrations.

Chapter 3: In this chapter two new voltammetric stimulation circuitries are characterized for serotonin. *In vivo* serotonin FSCV has previously focused on measurements in the SNr with dorsal raphe nucleus (DRN) or MFB stimulation. The SNr was chosen because of the dense innervation of serotonin. It was vital however to shed light on other brain areas because of their implications in specific

diseases. In this chapter, evoked (FSCV) serotonin was measured specifically in the mouse prefrontal cortex and hippocampus which are important in a variety of disorders including depression, autism spectrum disorder, and addiction. Furthermore, triple staining immunohistochemistry with single-photon microscopy was performed to visualize the SERTs density in these discrete localities. Finally, FSCAV was utilized to measure ambient serotonin levels in both regions to determine effects of SERT density on basal levels.

Chapter 4: This chapter describes the optimization of a FSCV waveform for HA detection. *In vitro* experiments were performed to verify stability, selectivity, and sensitivity of HA measurements over other common analytes. *In vivo* measurements were collected in the premammillary nucleus, with stimulation in the medial forebrain bundle. Pharmacological manipulations were carried out to ascertain that it was a robust HA signal.

Chapter 5: This section describes *in vivo* measurements performed to demonstrate histamine modulation of serotonin and to determine the histamine receptor responsible for this modulation, through pharmacological intervention. Additionally, a mathematical model was generated to further our understanding of this modulation.

Chapter 6: Conclusions and future directions. This section summarizes the work carried out towards my PhD along with the future work that will be carried out based on my findings.

1.5 REFERENCES

(1) Lama, R. D.; Charlson, K.; Anantharam, A.; Hashemi, P. Anal. Chem. (Washington, DC, U. S.) 2012, 84, 8096-8101.

(2) Hashemi, P.; Dankoski, E. C.; Petrovic, J.; Keithley, R. B.; Wightman, R. M. Anal Chem 2009, 81, 9462-9471.

(3) Portas, C. M.; Bjorvatn, B.; Ursin, R. Prog Neurobiol 2000, 60, 13-35.

(4) Fischer, A. G.; Ullsperger, M. Front Hum Neurosci 2017, 11, 484.

(5) Juric, D. M.; Krzan, M.; Lipnik-Stangelj, M. Pharmacol Res 2016, 111, 774-783.

(6) Preston, A. R.; Eichenbaum, H. Curr Biol 2013, 23, R764-773.

(7) Kobayashi, K.; Umeda-Yano, S.; Yamamori, H.; Takeda, M.; Suzuki, H.; Hashimoto, R. PLoS One 2011, 6, e18113.

(8) Otmakhova, N. A.; Lisman, J. E. J Neurosci 1999, 19, 1437-1445.

(9) Vizi, E. S.; Kiss, J. P. Hippocampus 1998, 8, 566-607.

(10) Haas, H. L.; Konnerth, A. Nature 1983, 302, 432-434.

(11) Rachel A Saylor, S. R. T. a. S. M. L., Michael, G. S. W. A. C., Ed.; World Scientific: Compendium of *In Vivo* Monitoring in Real-Time Molecular Neuroscience, 2017, pp 1 - 45.

(12) Jaquins-Gerstl, A.; Michael, A. C. J Neurosci Meth 2009, 183, 127-135.

(13) Wang, M.; Slaney, T.; Mabrouk, O.; Kennedy, R. T. J Neurosci Methods 2010, 190, 39-48.

(14) Lee, W. H.; Ngernsutivorakul, T.; Mabrouk, O. S.; Wong, J. M.; Dugan, C. E.; Pappas, S. S.; Yoon, H. J.; Kennedy, R. T. Anal Chem 2016, 88, 1230-1237.

(15) Huffman, M. L.; Venton, B. J. Analyst 2009, 134, 18-24.

(16) Zhang, B.; Heien, M. L.; Santillo, M. F.; Mellander, L.; Ewing, A. G. Anal Chem 2011, 83, 571-577.

(17) Kuhr, W. G.; Ewing, A. G.; Caudill, W. L.; Wightman, R. M. J Neurochem 1984, 43, 560-569.

(18) Stamford, J. A.; Kruk, Z. L.; Millar, J. Brain Res 1984, 299, 289-295.

(19) Samaranayake, S.; Abdalla, A.; Robke, R.; Wood, K. M.; Zeqja, A.; Hashemi, P. Analyst (Cambridge, U. K.) 2015, 140, 3759-3765.

(20) Pathirathna, P.; Yang, Y.; Forzley, K.; McElmurry, S. P.; Hashemi, P. Anal Chem 2012, 84, 6298-6302.

(21) Yang, Y.; Pathirathna, P.; Siriwardhane, T.; McElmurry, S. P.; Hashemi, P. Anal. Chem. (Washington, DC, U. S.) 2013, 85, 7535-7541.

(22) Atcherley, C. W.; Wood, K. M.; Parent, K. L.; Hashemi, P.; Heien, M. L. Chem Commun 2015, 51, 2235-2238.

(23) Atcherley, C. W.; Laude, N. D.; Parent, K. L.; Heien, M. L. Langmuir 2013, 29, 14885-14892.

(24) Twarog, B. M.; Page, I. H.; Bailey, H. American Journal of Physiology 1953, 175, 157-161.

(25) Abi-Dargham, A.; Laruelle, M.; Aghajanian, G. K.; Charney, D.; Krystal, J. J Neuropsychiatry Clin Neurosci 1997, 9, 1-17.

(26) Owens, M. J.; Nemeroff, C. B. Clinical Chemistry 1994, 40, 288-295.

(27) Nikolaus, S.; Muller, H. W.; Hautzel, H. Rev Neurosci 2016, 27, 27-59.

(28) Seitz, A.; Bandiera, S. M. Biomed Chromatogr 2017.

(29) Best, J.; Nijhout, H. F.; Reed, M. Theor Biol Med Model 2010, 7, 34.

(30) Buller, K. M.; Wixey, J. A.; Reinebrant, H. E. Neurol Res Int 2012, 2012, 650382.

(31) Wood, K. M.; Hashemi, P. ACS Chem. Neurosci. 2013, 4, 715-720.

(32) Samaranayake, S.; Abdalla, A.; Robke, R.; Nijhout, H. F.; Reed, M. C.; Best, J.; Hashemi, P. J Neurochem 2016.

(33) Lieberman, P. Ann Allergy Asthma Immunol 2011, 106, S2-5.

(34) Nuutinen, S.; Panula, P. Adv Exp Med Biol 2010, 709, 95-107.

(35) Hough, L. B. In Basic Neurochemistry: Molecular, Cellular and Medical Aspects. 6th edition., George J Siegel, B. W. A., Wayne Albers, Stephen K Fisher, and Michael D Uhler, Ed.; Lippincott-Raven: Philadelphia, 1999.

(36) Haas, H. L.; Sergeeva, O. A.; Selbach, O. Physiol Rev 2008, 88, 1183-1241.

(37) Jackson, B. P.; Dietz, S. M.; Wightman, R. M. *Anal Chem* **1995**, *67*, 1115-1120.

(38) Atcherley, C. W.; Wood, K. M.; Parent, K. L.; Hashemi, P.; Heien, M. L. *Chem Commun* **2015**, *51*, 2235-2238.

(39) Atcherley, C. W.; Laude, N. D.; Parent, K. L.; Heien, M. L. *Langmuir* **2013**, *29*, 14885-14892.

CHAPTER 2: *IN VIVO* AMBIENT SEROTONIN MEASUREMENTS AT CARBON-FIBER MICROELECTRODES

Reprinted with permission from Analytical Chemistry

Abdalla, A., Atcherley, C. W., Pathirathna, P., Samaranayake, S., Qiang, B., Peña, E., Morgan, S. L., Heien, M. L., Hashemi, P., *In Vivo* Ambient Serotonin Measurements at Carbon-fiber Microelectrodes. Anal Chemistry 2017, 89 (18), 9703 – 9711

2.1 ABSTRACT

The mechanisms that control extracellular serotonin levels *in vivo* are not well-defined. This shortcoming makes it very challenging to diagnose and treat the many psychiatric disorders in which serotonin is implicated. Fast-scan cyclic voltammetry (FSCV) can measure rapid serotonin release and reuptake events but cannot report critically important ambient serotonin levels. In this paper, we use fast-scan controlled adsorption voltammetry (FSCAV), to measure serotonin's steady-state, extracellular chemistry. We characterize the 'Jackson' voltammetric waveform for FSCAV and show highly stable, selective, and sensitive ambient serotonin measurements *in vitro*. *In vivo*, we report basal serotonin levels in the CA2 region of the hippocampus as 64.9 nM ± 2.3 nM (n=15 mice, weighted average ± standard error). We electrochemically and pharmacologically verify the selectivity of the serotonin signal. Finally, we develop a statistical model that incorporates the uncertainty in *in vivo* measurements, in addition to electrode variability, to more critically analyze the time course of pharmacological data. Our novel method is a uniquely powerful analysis tool that can provide deeper insights into the mechanisms that control serotonin's extracellular levels.

Keywords

Fast-scan controlled adsorption voltammetry (FSCAV), fast-scan cyclic voltammetry (FSCV), hippocampus (CA2), basal, baseline, tonic, extracellular, steady state, 5-HT

2.2 INTRODUCTION

Dysfunctions of the serotonin system are thought to underlie numerous neuropsychiatric disorders such as depression, anxiety, and schizophrenia.[1-3] A better interpretation of serotonin neurochemistry is crucial for understanding the roles of this neurotransmitter but insight into serotonin's chemistry has been limited by the difficulty of *in vivo* chemical measurements. Serotonin is particularly challenging to detect electroanalytically *in vivo* because of an inauspicious combination of low extracellular concentrations and the propensity of serotonin and serotonin metabolites to foul electrodes.[4]

In 2009, we optimized fast-scan cyclic voltammetry (FSCV) for measurement of endogenous serotonin release and reuptake *in vivo* using carbon fiber microelectrodes (CFMs).[5] Since then, we have uncovered various important aspects of serotonin neurochemistry. For example, evoked serotonin release is under much tighter regulation than dopamine (DA),[6] being subject to prolonged autoreceptor control and multiple reuptake mechanisms.[7] Furthermore, a single dose of a selective serotonin reuptake inhibitor (SSRI) rapidly alters serotonin neurochemistry;[8] an important finding because a chronic SSRI regimen must often be followed for clinical therapy.[2]

While FSCV continues to provide important insights into the mechanisms that regulate extracellular *in vivo* serotonin, the method has limitations. In particular, because FSCV is background-subtracted, it only reports information about concentration changes. These changes allow us to probe serotonin release

and reuptake, however it would be invaluable to also determine serotonin's ambient (steady-state, extracellular or basal) concentrations.

There are very few methods that can quantitatively measure extracellular serotonin concentrations. By far, the most commonly used method is microdialysis which reports extracellular serotonin levels in the lower nanomolar range.[9-13] We thus sought to design a reliable and accurate method for measuring serotonin's ambient concentrations with our carbon fibers, that we could couple to our FSCV measurements.

We recently made basal measurements of dopamine with fast-scan controlled-adsorption voltammetry (FSCAV), which exploits the adsorption capabilities of activated CFMs. The method is robust, selective, fast, and sensitive with the additional allure that CFMs measure from discrete brain localities[14] where tissue damage is minimized.[15] Our studies revealed a fundamental coaction between evoked and ambient dopamine.[16] Here, we orient this method towards serotonin.

We find that unique FSCAV serotonin signals (that resemble FSCV responses) are stable during repeated recordings over 120 minutes *in vitro*. We confirm that the majority of interfering analytes are unlikely to contribute to the serotonin FSCAV signal, bar serotonin's major metabolite, 5-hydroxyindoleacetic acid (5-HIAA) which gives a small signal at high concentrations. Subsequently we show that 5-HIAA is unlikely to contribute to the signal when at physiological concentrations. Next, our method is utilized to report ambient, *in vivo* serotonin levels in the mouse hippocampus as 64.9 nM ± 2.3 nM (n = 15 mice, weighted

average ± standard error) using a functional linear statistical model that we developed based on electrode and *in vivo* variability. Using a pharmacological approach, the *in vivo* signal is validated and interferences by 5-HIAA, dopamine, and norepinephrine[17-21] are disqualified. Finally, we take a closer statistical look at the time course of the pharmacological data using a chemometric approach incorporating the uncertainty inherent to *in vivo* recordings as well as the variability between CFMs to show that the drug response is significant earlier than shown by conventional statistical tests.

Accurate measurements of ambient serotonin are essential for establishing serotonin's physiological impact and here we present an ideal tool and analyses for this measurement. Furthermore, FSCV and FSCAV can be combined at a single sensor, providing the distinctively powerful analytical capability of measuring both phasic and ambient serotonin.

2.3 EXPERIMENTAL SECTION

Solutions

Dopamine hydrochloride, serotonin hydrochloride, 5-hydroxyindole acetic acid, ascorbic acid, 3,4-dihydroxyphenylacetic acid, uric acid, norepinephrine hydrochloride, hydrogen peroxide, adenosine, histamine hydrochloride, pargyline hydrochloride, desipramine hydrochloride, and GBR 12909 were purchased from Sigma Aldrich (St. Louis, MO). Liquion™ (LQ-1105, 5% by weight Nafion®) was purchased from Ion Power Solutions (New Castle, DE). Buffer solution was composed of 15 mM Tris, 126 mM NaCl, 2.5 mM KCl, 25 mM $NaHCO_3$, 2.0 mM

NaH_2PO_4, 1.2 mM Na_2SO_4, 1.2 mM $CaCl_2$, and 2.0 mM $MgCl_2$ (all purchased from Sigma Aldrich (St. Louis, MO)).

Carbon-Fiber Microelectrodes

The carbon-fiber microelectrodes were assembled by aspirating a single T-650 carbon fiber (7 μm, Goodfellow, Coraopolis, PA) into cylindrical glass capillaries (internal diameter: 0.4 mm, external diameter: 0.6 mm, A-M Systems, Carlsborg, WA). The carbon filled capillaries were positioned vertically in a pipette puller (Narishige Group, Setagaya-Ku, Tokyo, Japan) to form a carbon – glass seal under gravity. The carbon fibers were then cut to approximately 150 μm in length. Nafion solution (Liquion-1105-MeOH, Ion Power, DE) was electrodeposited on the exposed carbon fibers as previously described.[5] The microelectrode was dried at 70° for 10 minutes.

Data Collection

FSCV and FSCAV were performed using software (WCCV 3.05) and instrumentation developed by Knowmad Technologies LLC (Tucson, AZ). FSCAV was performed using a CMOS precision analog switch, ADG419 (Analog Devices) to control the application of the computer-generated waveform to the electrode. The logic was controlled programmatically and either a series of ramps (0.2 V to 1.0 V to -0.1 V to 0.2 V, scan rate = 1000 V/s) was applied every 10 ms (100 Hz), or a constant potential (0.2 V) was applied to the electrode for a specified period (10 s) (controlled adsorption period).

Flow Injection Analysis

FSCV *in vitro* analyses were performed using flow injection analysis (FIA). CFMs were placed into a flangeless short 1/8 nut (PEEK P-335, IDEX, Middleboro, MA) with 2 mm of the tip exposed from the nut. The microelectrode-containing nut was fastened into a modified HPLC union (Elbow PEEK 3432, IDEX, Middleboro, MA). The other end of the elbow union was secured into the out-flowing stream of the FIA buffer. Two holes were drilled into the union to incorporate a reference electrode and a 'waste' flow stream. The flow was maintained using a syringe infusion pump (kd Scientific, model KDS-410, Holliston, MA) at a rate of 2 mL min^{-1}. Serotonin was introduced using a rectangular pulse into the flow stream for 10 s through a six-port HPLC loop injector (Rheodyne model 7010 valve, VICI, Houston, TX).

Data Analysis

FSCV and FSCAV signals were processed using software written in-house using LabVIEW 2009. The processing includes filtering, smoothing, and signal deconvolution. For FSCAV, the cyclic voltammogram (CV) of the 3rd scan (after controlled adsorption period) was extracted and the peak that occurred between approximately between 0.4V to 0.85V was integrated. The resulting charge value in pC was plotted vs. serotonin concentration to create calibration curves which were then utilized to report *in vivo* values.

Statistical Analysis

Based on the calibration data, linear models relating charge with both concentration and different electrodes were developed. These linear models

incorporated interactions between the concentration and the electrode to accommodate for the inherently varying responses between electrodes.[22,23] These models allow different intercept and slope in the linear relationship between charge and concentration for each electrode. The fitting was performed using linear model via the *lm* command in the R programming package. The results show significant differences in the intercept and slope for each electrode (**Figure S-1** in Supplementary information). Using these fitted linear models and given charge measurements collected *in vivo* at successive time points, estimates of the concentration levels at each time point were obtained. This was done by `inverting' the fitted linear relationship between concentration and charge, and a weighted pooling of the concentration estimates from each of the electrodes was performed to obtain an overall concentration level estimate at each time point. The weights are based on the inverse of the estimated variance of the concentration estimates. Point-wise confidence intervals (CI) were constructed by fitting the functional model to the time and concentration values. These 95% point-wise confidence intervals were constructed when the functional model was fitted to the pairs of time and concentration values using the *predict.lm* command in the R package.

Exclusion Criteria

FSCV was performed before FSCAV collection *in vivo* to verify the presence of serotonin. CVs collected during an evoked response in mice were compared with previously well-established signals.[5] Mice in which the CVs did not match the characteristics of a serotonin CV were excluded from this study. Furthermore, mice

that died before the end of the collection time were excluded. All other mice were included in this study.

Animal Surgeries

6 – week old male C57BL/6J mice, 20-25 g, were purchased from Jackson Laboratories (Bar Harbor, ME). The mice were housed in 12-h light/dark cycles and were offered food and water *ad libitum*. Animal care and procedures were in agreement with the Guide for the Care and Use of Laboratory Animals, accepted by the Institutional Animal Care and Use Committees (IACUC) of the University of South Carolina. After an intraperitoneal (*i.p.*) injection of the anesthetic urethane, (25% dissolved in 0.9% NaCl solution, Hospira, Lake Forest, IL) at a volume of 7 µL per 1 g mouse weight, stereotaxic surgeries (David Kopf Instruments, Tujunga, CA) were performed. A heating pad from Braintree Scientific was used to maintain ideal mouse body temperature of 37° C. Bregma was used as a reference for stereotaxic coordinates of Medial Forebrain Bundle (MFB) [APL: -1.58, ML: +1.0, DV: -4.8 to -5.0] and CA2 [AP: -2.9, ML: +3.35, DV: -2.5 to -3.0] from Franklin and Paxinos (2008). In order to access the CA2 and MFB, holes were drilled in accordance to the stereotaxic coordinates. A stainless-steel electrode (diameter 0.2 mm; Plastics One, Roanoke, VA) was implanted into the MFB for stimulation. The nafion coated CFM was then lowered into the CA2. A silver wire (diameter: 0.010 in; A-M Systems, Sequim, WA), electroplated with chloride by immersion of the wire in hydrochloric acid (0.1 M, 4 V vs. tungsten), was implanted into the opposite hemisphere of the CA2 electrode placement. A 60 Hz biphasic 350 µA, 120 pulse stimulation, 2 ms per phase was employed through linear constant

current stimulus isolator (NL800A Neurolog; Digitimer Ltd.). All drugs were administered *i.p.*; Pargyline at a dose of 75 mg kg^{-1} and GBR 12909 at a dose of 15 mg kg^{-1}, both dissolved in 90% saline and injected at a volume of 0.1ml $20g^{-1}$.

2.4 RESULTS AND DISCUSSION

Serotonin FSCAV

A robust analytical measurement of ambient serotonin would lend nuance to our understanding of this complex neurotransmitter. Researchers have conventionally relied on microdialysis for basal measurements; however, it is greatly desirable to us to measure this ambient concentration at CFM's. Because FSCV relies on background-subtraction to remove a large charging current, FSCV could not, until recently, report basal neurotransmitter concentrations. We recently described a novel modification to the FSCV technique that allowed us to measure ambient *in vivo* DA levels, which we coined FSCAV.[16] FSCAV is similar in concept to adsorptive stripping voltammetry whereby analytes adsorb onto the electrode surface for a controlled period of time before electrochemical characterization. We utilize the terminology 'ambient' to denote a measurement made at a temporal resolution (20 s) that is neither on the same scale as FSCV (milliseconds) or microdialysis (minutes). The temporal scale of FSCV allows it to measure phasic changes whereas microdialysis can measure tonic or basal changes in the brain. Conversely, FSCAV is an average of both. Here, FSCAV was applied to serotonin analysis.

Electrochemical measurements of serotonin are fundamentally challenging because of serotonins' and serotonin metabolites' detrimental effects on the

electrode surface. In 1995, Jackson *et al.* developed a solution for electrode fouling for serotonin measurements by developing a waveform, at a very high scan rate, to 'outrun' fouling reactions.[4] The 'Jackson waveform' was later combined with an electrodeposited Nafion coating on the CFM for *in vivo* serotonin FSCV.[5] We therefore applied the Jackson waveform (0.2 V to -0.1 V to 1.0 V to 0.2 V, 1000 V s^{-1}) to a Nafion coated CFM for *in vivo* serotonin FSCAV (100 Hz) with a 10 s controlled adsorption period.

Figure 2.1A(i) shows a color plot of 100nM serotonin collected *in vitro* with FSCV using the Jackson Waveform at 10Hz. **Figure 2.1A (ii)** shows a color plot of 100 nM serotonin *in vitro* with FSCAV using the same waveform at 100Hz. The black area in **Figure 2.1A (ii)** is the controlled adsorption period, and the CV taken at the 3rd scan (denoted by star) after waveform re-application is shown in **Figure 2.1B.** Importantly, this CV contains peaks characteristic of serotonin's redox potentials.[4,5] This CV is superimposed onto a CV taken from an FSCV color plot (denoted by star). The orange lines illustrate the integration limits used for FSCAV analysis (see experimental section). The CVs show good agreement, with the exception of a slight potential shift in the FSCAV signal which we attribute to the higher waveform application frequency (100 Hz vs 10 Hz for FSCV).[24]

Second, we identified 9 electroactive species in the hippocampus that could potentially interfere with the FSCAV signal.[18,25-32]

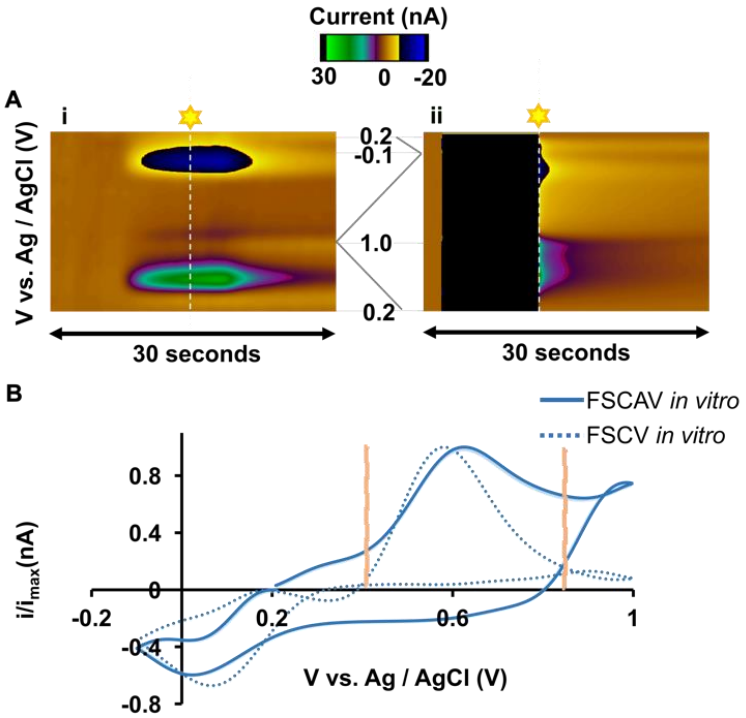

Figure 2.1. (A) Representative FSCV (i) and FSCAV (ii) color plots of 100nM serotonin *in vitro*. B) Cyclic voltammograms extracted from the vertical dashed lines in A(i) and A(ii) after normalization (current / maximum current). Vertical orange dashed lines represent integration limit.

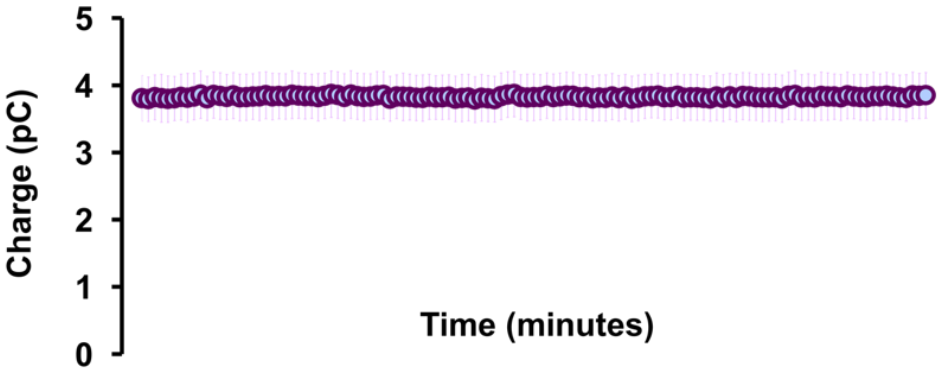

Figure 2.2. Repeated FSCAV measurements over 120 minutes in 100 nM serotonin (n=4 electrodes ± SEM)

Figure 2.3 shows CVs collected from these different species at concentrations that mimic a range of reported or predicted physiological values.[4,5,16,24,29,33-39]

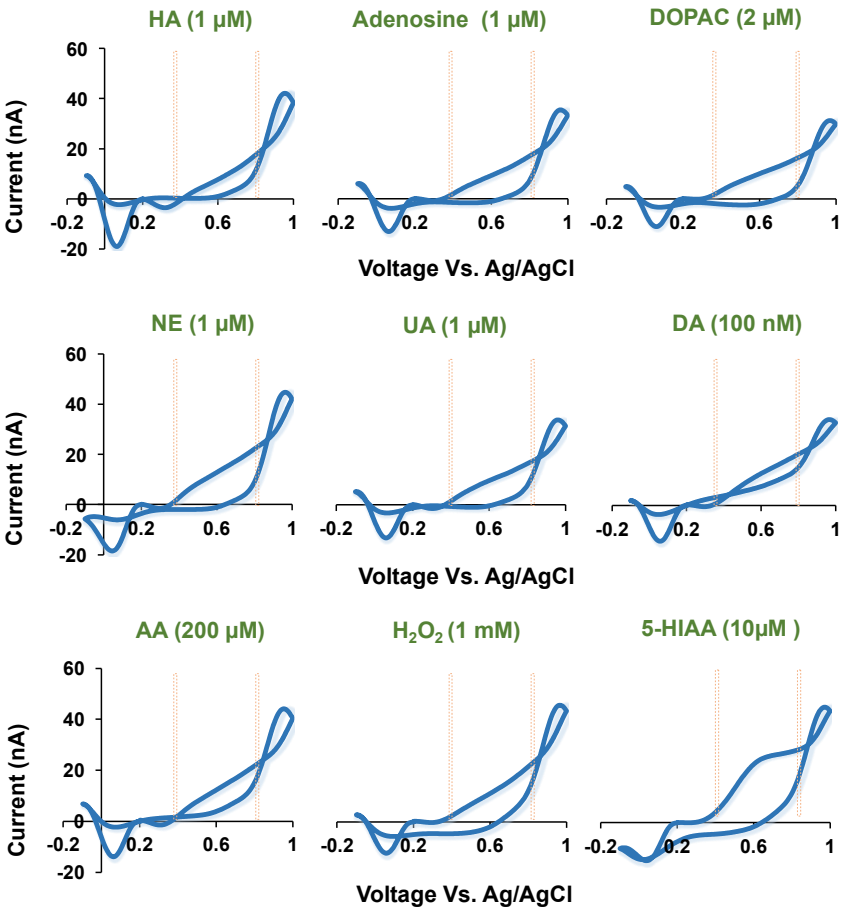

Figure 2.3. CVs for HA (1 µM), adenosine (1 µM), DOPAC (2 µM), NE (1 µM), UA (1 µM), DA (100 nM), AA (200 µM), H2O2 (1 mM) and 5-HIAA (10 µM). Vertical dashed lines represent integration limits utilized for serotonin analysis.

We applied the integration limits for serotonin analysis (+0.4 V to +0.85 V) and analyzed these CVs. Histamine (HA) (1 µM), adenosine (1 µM), DOPAC (2 µM), norepinephrine (NE) (1 µM), uric acid (UA) (1 µM), DA (100 nM), ascorbic acid (AA) (200 µM), and hydrogen peroxide (H_2O_2) (1 mM) showed no significant

features within the serotonin integration limits (n=4). 5-HIAA (10 µM)[5] could prove problematic due to the presence of a peak within the integral limits.

We show that 5-HIAA interference is unlikely in **Figure 2.4**. In this **Figure**, charge is plotted against concentration for serotonin (orange). Here, the linear portion of the serotonin calibration is shown with orange markers with the following linear regression:

$$y=0.0207\ (\pm\ 0.0005)\ x + 1.51(\pm\ 0.14),\ R^2 = 0.997 \qquad (1)$$

The serotonin plot shows linearity up to 600 nM, with a sensitivity of 0.021 ± 0.0005pC nM^{-1} (n=4 ± SEM), and a limit of quantification of 5 nM. When both serotonin and 5-HIAA are present in solution, we postulate that there is a competition for adsorption sites on the carbon fiber surface. The rationale here is that the analyte with higher adsorption equilibrium constant (K_{ads}) on the CFM will exhibit a more favorable thermodynamic adsorption profile and will thus outcompete the other.[40] A Langmuir monolayer adsorption isotherm model was used with FSCAV data to calculate K_{ads} for serotonin and 5-HIAA. K_{ads} for serotonin and 5-HIAA were 9.57 x 10^{10} and 7.02 x 10^{8}, respectively. The much higher K_{ads} for serotonin adsorption onto CFMs means that 5-HIAA added to serotonin does not affect the signal as shown in the inset in **Figure 2.4**. The green stars signify a separate data set where approximately 100x more concentrated 5-HIAA was added to the serotonin solution and the blue markers show the signal. The close agreement of the blue and orange markers make it clear that 5-HIAA, at physiological concentrations (typically 10 µM),[41] would not impact the signal. In

addition to favorable adsorption, the much improved sensitivity for serotonin vs. 5-HIAA can be credited to Nafion on the CFM.[5]

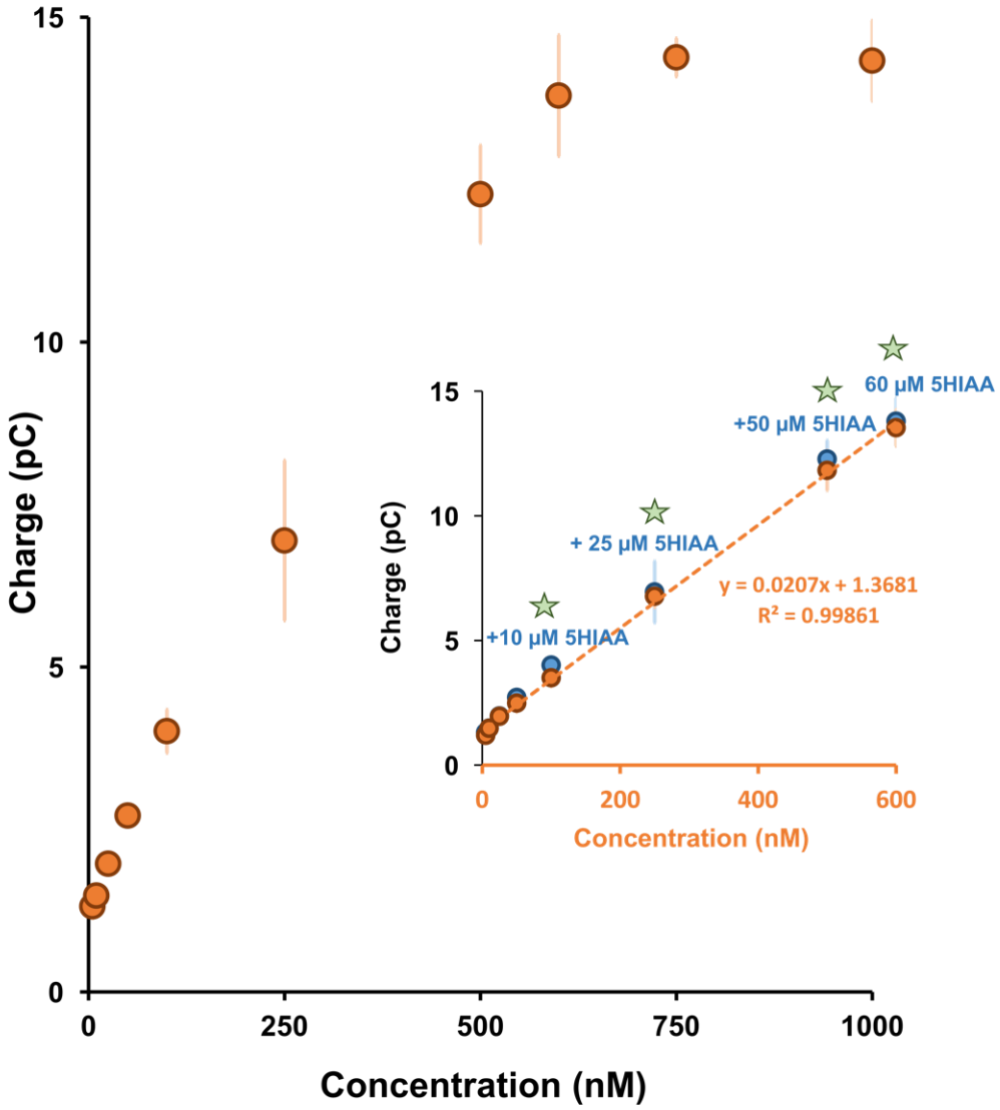

Figure 2.4. Serotonin selectivity curve (n=4 electrodes ± SEM). Inset shows linear serotonin range (orange markers), The green stars represent the addition of 5-HIAA to serotonin. All blue markers represent serotonin / 5-HIAA mixture with 5-HIAA being a 100 times the serotonin concentration. All inset calibrations are n=4 electrodes ± SEM.

In Vivo Serotonin FSCAV

To apply FSCAV to *in vivo* serotonin measurements, we first employed a retrograde stimulation of the Medial Forebrain Bundle (MFB) and confirmed electrically stimulated serotonin release in the CA2 region of the mouse hippocampus (example of evoked release can be seen in **Figures 2.6 and 2.7**). Subsequently FSCAV was performed at the same electrode. **Figure 2.5A** shows the *in vivo* FSCAV color plot (i) adjacent to a color plot of 100 nM serotonin *in vitro* (ii).

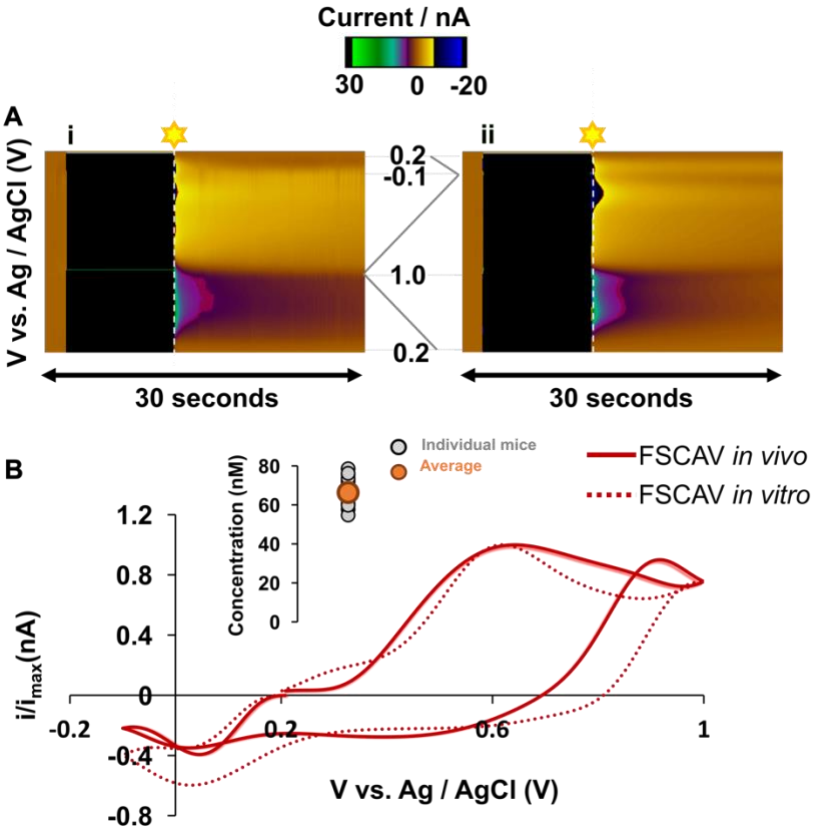

Figure 2.5. (A) Representative FSCAV color plots of serotonin *in vivo* (i) and *in vitro* (ii). (B) CVs extracted from the 3rd scan indicated by vertical dashed lines in A(i) and A(ii). Inset shows ambient serotonin measurements in CA2 region of mouse hippocampus. Grey markers represent individual mice and orange marker represents weighted averaged response (n=15 mice ± standard error).

The close agreement of the CVs shown in **Figure 2.5B** is strong evidence that this signal is serotonin. We took a chemometric approach to report the concentration *in vivo* with uncertainty that incorporated not only *in vivo* variability but also the variability of individual electrodes. These variations occur mainly due to the non-uniformity between carbon fiber surfaces that arise as a result of the fabrication process. A linear functional model was developed using the calibration data of the different electrodes used in the *in vivo* experiments. In 15 mice, the weighted average extracellular serotonin level was 64.9 nM ± 2.3 nM (n = 15 mice, weighted average ± standard error) (see inset in **Figure 2.5B**).

Previous reports of ambient serotonin with microdialysis in different brain regions have estimated extracellular serotonin in low nanomolar to 10's of nanomolar. [9-13] Our value is slightly above this range. Our method is performed on a fundamentally different spatial scale. For example, commercial microdialysis probes typically have a diameter of 200 µm and are 2 mm in length, whereas CFMs are 7 µm in diameter and 150 µm in length. The tissue volume impacted by a CFM is orders of magnitude smaller than that of a typical microdialysis probe,[15] and because we optimize the electrode's placement based on stimulated serotonin release, the electrode is in a 'hot spot' (area of high serotonin activity), accounting for slightly higher levels.

Above, we assessed FSCAV's selectivity *in vitro*, however, the *in vivo* matrix is far more complicated than can be reproduced on the bench. It is therefore critical to verify the signal pharmacologically *in vivo*. For this task, we employed pargyline (75 mg kg^{-1}), an irreversible monoamine oxidase B (MAO-B) inhibitor. By inhibiting

MAO-B, and hence the metabolism of serotonin in the brain, an increase in serotonin and a decrease in 5-HIAA is expected.[42,43] **Figure 2.6** shows experiments that test the effects of pargyline on the FSCAV signal. First, FSCV was used to optimize the position of the CFM by evoking serotonin release (a representative example color plot is shown inset on the top left). Individual animal FSCAV responses (faint blue makers) and the averaged response (dark blue dots) 60 min before and 60 min after an *i.p.* injection of pargyline are shown on the central trace. Using conventional statistical analysis, pargyline administration caused a significant increase in the FSCAV signal at 29 min and thereafter (two way repeated measures anova: $p<0.0001$, n=5 mice ± SEM with Dunnett's multiple comparison post hoc, $p<0.01$, n=5 mice ± SEM). The effects of pargyline were verified with FSCV following FSCAV data collection (inset top right color plot is a representative color plot and [serotonin] vs. time traces pre (α; pre and β:post drug)), where pargyline increased evoked serotonin amplitude and reduced the rate of reuptake as previously seen in rats.[6] This experiment eliminates the possibility of 5-HIAA interference and would verify our signal as serotonin, save for one final concern; that DA and NE are also substrates for MAO-B [44,45] and are present at appreciable levels in the CA2 region of the hippocampus.[17,19-21]

Very little sensitivity was established *in vitro* for DA or NE. To further verify no interference from DA we administered GBR 12909, a potent DA transporter inhibitor, to a separate set of mice. We have previously shown that GBR 12909 causes an increase in ambient DA,[16] but not in evoked serotonin levels.[5]

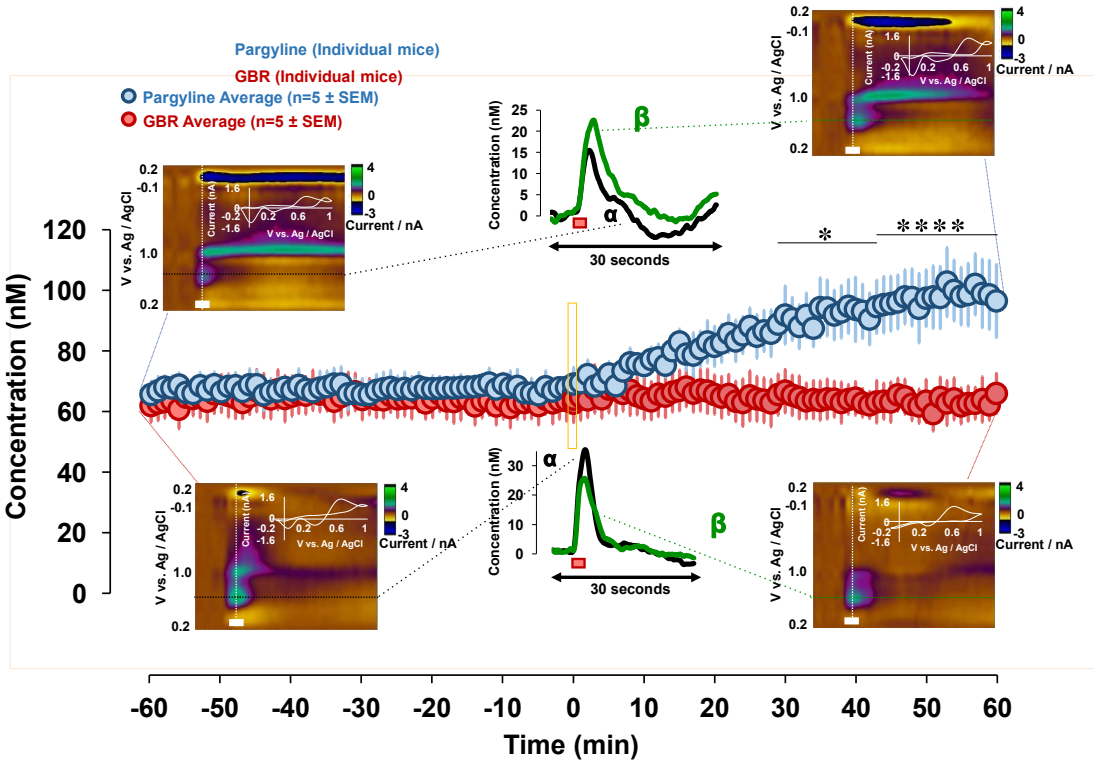

Figure 2.6. Faint blue markers represent individual mouse responses to *i.p*. Pargyline (75 mg kg^{-1}) and faint red markers represent individual mice responses to *i.p*. GBR 12909 (15 mg kg^{-1}). Files were collected 60 minutes before and after drug administration. Dark blue dots represent averaged Pargyline response (n=5 mice ± SEM) and dark red dots represent averaged GBR 12909 response (n=5 mice ± SEM). Yellow bar at 0 min is injection time. Representative FSCV color plots and CVs before and after FSCAV file collection are inset (top – Pargyline, bottom – GBR 12909). White bars at bottom of color plot denotes stimulation (2s). Inset center are [serotonin] vs. time traces taken from color plots). Red bars below [serotonin] vs. time is the stimulation. (∗ above solid blue markers indicate post hoc test, ∗p<0.05, ∗∗∗∗p<0.0001).

The faint, red markers in **Figure 2.6** show individual FSCAV animal responses to 15 mg per kg GBR 12909, while the dark red dots show the averaged responses 60 min before and after *i.p*. administration (n=5 mice ± SEM). As above, FSCV was used to assess the effects of this manipulation on the evoked serotonin response. The lack of an increase in the FSCAV signal (two way repeated

measures anova, p>0.05, n=5 mice ± SEM with Dunnett's multiple comparison post hoc, p>0.05, n=5 mice ± SEM) and FSCV signal allows us to exclude DA as

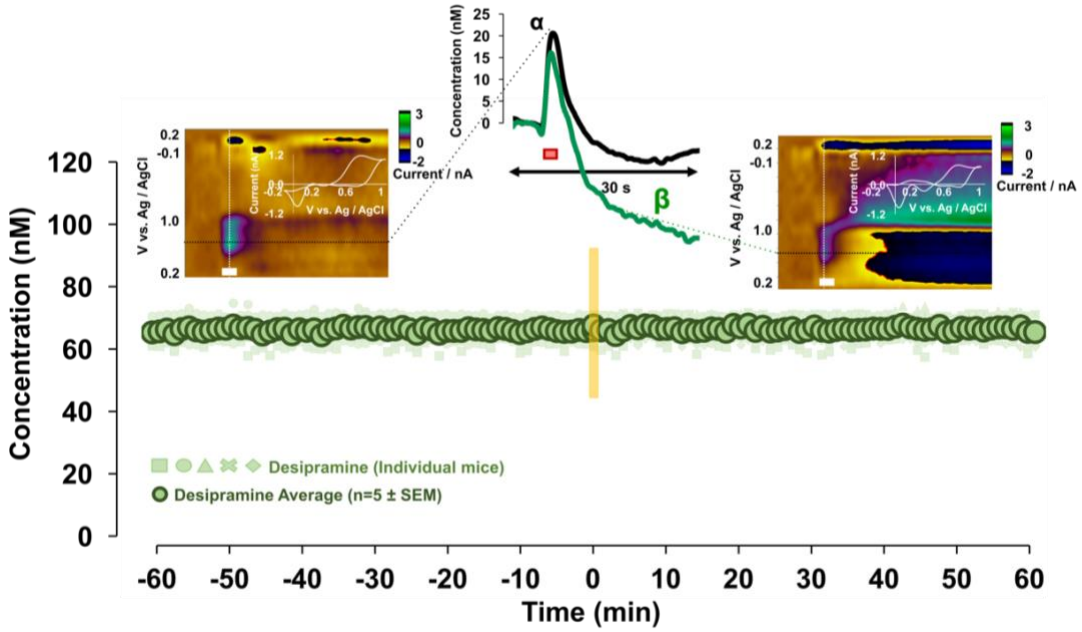

interference.

Figure 2.7. Faint green markers represent individual mice responses and dark green dots represent averaged response to *i.p*. Desipramine (15 mg kg^{-1}) (n=5 mice ± SEM). Files were collected 60 minutes before and after drug administration. Yellow bar at 0 min is injection time. Representative FSCV color plots and CVs before and after FSCAV file collection are inset. White bars at bottom of color plot denotes time of stimulation (2s). Inset center are representative [serotonin] vs. time traces of evoked serotonin response before (black) and after (green) drug administration. Red bars below [serotonin] versus time is stimulation period (2s).

To eliminate the possibility of interference from NE, we administered desipramine (15 mg kg^{-1}) to a separate set of mice. Desipramine is a norepinephrine transporter (NET) inhibitor that selectively blocks NETs but has negligible effect on DA or 5HT transporters.[46,47] The faint green, markers in **Figure 2.7** represent the individual FSCAV responses, while the dark green dots represent the averaged response 60 minutes before and after *i.p*. drug administration (n=5

mice ± SEM). Injection is immediately before first data point at 0 min (yellow bar). FSCV color plots and CVs taken before and after FSCAV data collection from a representative experiment are inset. There was no change in the FSCAV signal (two way repeated measures anova, $p>0.05$, n=5 mice ± SEM with Dunnett's multiple comparison post hoc, $p>0.05$, n=5 mice ± SEM). There was no increase in the release amplitude as measured with FSCV, however there was a dramatic dip below baseline after stimulation. We previously showed that dips such as this were mediated by prolonged autoreceptor activation[7] and because desipramine has agonist activity at the 5H1B receptor, [48,49] it is likely we are observing a potentiation of the autoreceptor effect. This experiment allows us to exclude norepinephrine as a possible interference.

Conventional statistical tests (two way repeated measures anova with Dunnett post hoc test) show that the serotonin levels increase significantly 29 minutes after pargyline administration. However, visually it is seen that the serotonin levels begin to rise much earlier than that. To address this, we expanded the fitted linear model to encompass the concentration values prior to and post pargyline, GBR 12909, and desipramine administration. The equations of the model were as follows,

$$\text{Serotonin/Pargyline: } C(t) = 65.217 + 0.0041*t + 0.5268*[\max(0, 62.6-t)] - 0.0042*[\max(0, 62.6-t)]^2 \quad (2)$$

$$\text{Serotonin/GBR12909: } C(t) = 58.82 + 0.0055*t - 0.000088*t^2 \quad (3)$$

$$\text{Serotonin/Desipramine: } C(t) = C(t) = 71.54 + 0.0013*t - 0.000004*t^2 \quad (4)$$

where C(t) is change in concentration with time, t is time and max (a, b) is the larger value between a and b. The fitted model (blue line) over the averaged serotonin data (black dots) with pargyline, GBR 12909, and desipramine administration is seen in **Figure 2.8A, B** and, **C** respectively.

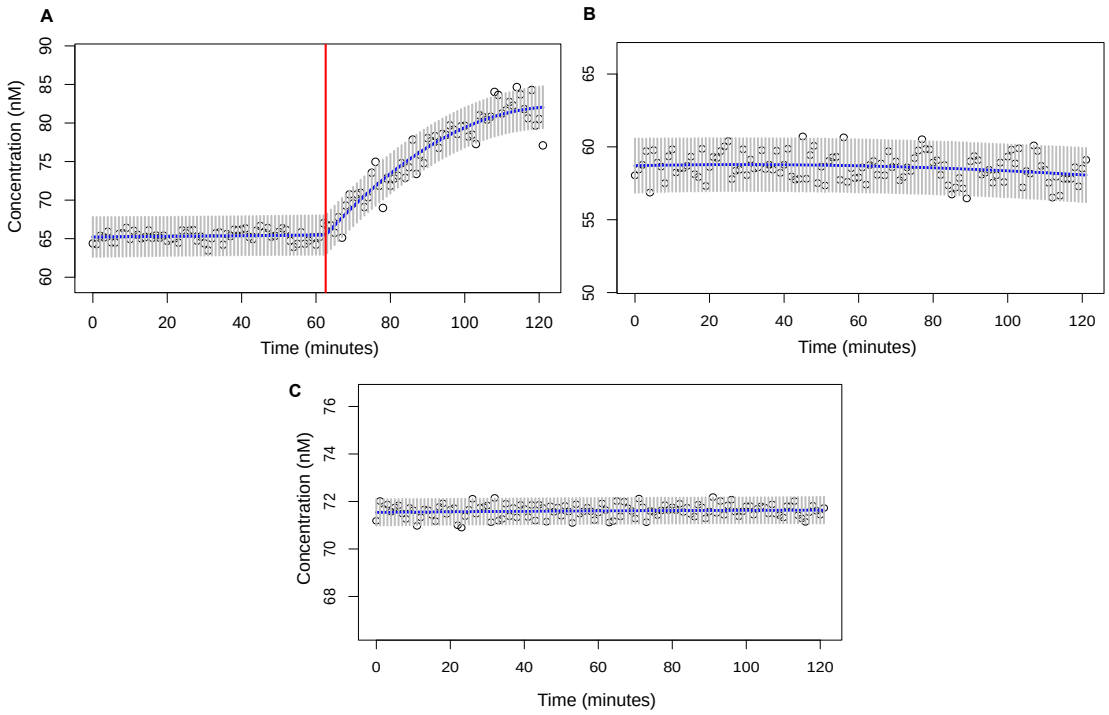

Figure 2.8. Files were collected 60 minutes before and after (**A)** Pargyline, **(B)** GBR 12909, and **(C)** Desipramine administration. Circles represent averaged serotonin response (n=5 mice ± 95% CI). Vertical grey lines represent 95% confidence intervals, and the blue line is the fitted model. Red vertical line in A represent point of change after drug administration, i.e. 2.60 minutes.

For pargyline, the functional continuous model consisted of a linear part over the time portion where no drugs were administered plus a time lag Delta (0 to 60+Delta) and is parabolic over the time interval from 60+Delta to 120 (**Figure 2.8A**). Using this model, the estimate for this time lag Delta or simply the time point where the drug causes a change in the slope is 2.60 minutes. This estimate is obtained by maximizing the coefficient of determination (R^2) with respect to the

possible values of Delta. Note that the final fitted model has a high R^2 equal to about 95%, indicating an excellent fit of the linear-parabolic model for relating concentration to time for this serotonin study.

For the GBR 12909 and desipramine, the model showed no effect of time on serotonin concentration and there was basically no change over the whole period of study. The plot of this fitted model is presented in **Figure 2.8B** and 2.**8C** respectively, which is almost flat, together with the estimated concentration levels (the solid circles) at each of the time points, and the 95% point-wise confidence intervals.

It is important to note that using repeated measures anova with Dunnett test, the only information that was available is the time point at which pargyline caused a change that was statistically significant ($p<0.05$, 29 mins). On the other hand, through employing a statistical model that was built to take into account electrode variability, we were able to determine the point at which pargyline changed the ambient serotonin concentrations as soon as 2.60 minutes. This may be a more accurate reflection of the pharmacological profile of this agent.

The combination of electrochemical and pharmacological characterizations performed *in vivo* and *in vitro* allows us to confidently assert that FSCAV is able to selectively measure ambient serotonin *in vivo.* The synergy with a chemometric approach introduces a new wealth of information that allows for more accurate electrode calibrations and a more comprehensive understanding of the time course of *in vivo* data.

2.5 CONCLUSIONS

Imbalances in serotonin neurochemistry are important to study in the context of neuropsychiatric disorders. While FSCV can provide real-time chemical information, the method reports only phasic changes. Ambient serotonin levels are critical to establishing the fundamental extracellular mechanisms that control serotonin. Here, we reported FSCAV for ambient serotonin measurements. We performed a characterization of the FSCAV waveform for sensitive and selective serotonin measurements. *In vivo*, we utilized the waveform to report a basal serotonin level in mouse CA2 as 64.9 nM ± 2.3 nM (n = 15 mice, weighted average ± standard error). We pharmacologically verified the *in vivo* signal against perceived interferences. Finally, we developed a statistical model to further analyze the FSCAV readings and report the uncertainty caused by measuring *in vivo* using different CFM's. Serotonin FSCAV yields information about serotonin's basal behavior *in vivo* and when coupled with FSCV at a single CFM will provide a deeper chemical insight into serotonin's mechanisms in the brain.

2.6 ACKNOWLEDGEMENTS

The authors would like to thank Kevin Wood, Anisa Zeqja, Matthew Jackson, Megan Connolly and Thushani Siriwardhane for experimental assistance and helpful conversations. The University of South Carolina start-up funds (PH), the Eli Lily Young Investigator Award (PH), NIH (MH106563) (PH), and NIH (DA034975) (MLH) funded this research. Portions of the statistical analysis were provided by the Biometry Core of the Center for Colon Cancer Research under NIH support P30GM103336-01A1.

Competing financial interest

Dr. Michael Heien declares an actual or potential financial conflict of interest and is co-founder/equity holder in Knowmad Technologies, a licensee of University of Arizona (UA) intellectual property used in this research. This relationship has been disclosed to the UA Institutional Review Committee and is managed by a Financial Conflict of Interest Management Plan.

Supporting Information. Detailed description of mathematical model, statistical parameters obtained from model, standard errors and tests of significance of the coefficients.

Basal SI 072817. The Supporting information includes a more elaborative explanation of the mathematical model used in the paper including the raw data that shows the variability between the different electrodes. In addition, it contains the standard errors and tests of significance of the coefficients obtained from the data of each of the three drugs administered.

2.7 REFERENCES

(1) Abi-Dargham, A.; Laruelle, M.; Aghajanian, G. K.; Charney, D.; Krystal, J. *J Neuropsychiatry Clin Neurosci* **1997**, *9*, 1-17.

(2) Owens, M. J.; Nemeroff, C. B. *Clinical Chemistry* **1994**, *40*, 288-295.

(3) Nikolaus, S.; Muller, H. W.; Hautzel, H. *Rev Neurosci* **2016**, *27*, 27-59.

(4) Jackson, B. P.; Dietz, S. M.; Wightman, R. M. *Anal Chem* **1995**, *67*, 1115-1120.

(5) Hashemi, P.; Dankoski, E. C.; Petrovic, J.; Keithley, R. B.; Wightman, R. M. *Anal. Chem. (Washington, DC, U. S.)* **2009**, *81*, 9462-9471.

(6) Hashemi, P.; Dankoski, E. C.; Lama, R.; Wood, K. M.; Takmakov, P.; Wightman, R. M. *Proc. Natl. Acad. Sci. U. S. A.* **2012**, *109*, 11510-11515, S11510/11511-S11510/11512.

(7) Wood, K. M.; Zeqja, A.; Nijhout, H. F.; Reed, M. C.; Best, J.; Hashemi, P. *J. Neurochem.* **2014**, *130*, 351-359.

(8) Wood, K. M.; Hashemi, P. *ACS Chem. Neurosci.* **2013**, *4*, 715-720.

(9) Mathews, T. A.; Fedele, D. E.; Coppelli, F. M.; Avila, A. M.; Murphy, D. L.; Andrews, A. M. *J Neurosci Methods* **2004**, *140*, 169-181.

(10) Zhang, J.; Jaquins-Gerstl, A.; Nesbitt, K. M.; Rutan, S. C.; Michael, A. C.; Weber, S. G. *Anal Chem* **2013**, *85*, 9889-9897.

(11) Gardier, A. M.; David, D. J.; Jego, G.; Przybylski, C.; Jacquot, C.; Durier, S.; Gruwez, B.; Douvier, E.; Beauverie, P.; Poisson, N.; Hen, R.; Bourin, M. *J Neurochem* **2003**, *86*, 13-24.

(12) Parsons, L. H.; Justice, J. B., Jr. *J Neurochem* **1993**, *61*, 1611-1619.

(13) Lee, W. H.; Ngernsutivorakul, T.; Mabrouk, O. S.; Wong, J. M.; Dugan, C. E.; Pappas, S. S.; Yoon, H. J.; Kennedy, R. T. *Anal Chem* **2016**, *88*, 1230-1237.

(14) Sames, D.; Dunn, M.; Karpowicz, R. J.; Sulzer, D. *Acs Chemical Neuroscience* **2013**, *4*, 648-651.

(15) Jaquins-Gerstl, A.; Michael, A. C. *J Neurosci Meth* **2009**, *183*, 127-135.

(16) Atcherley, C. W.; Wood, K. M.; Parent, K. L.; Hashemi, P.; Heien, M. L. *Chem. Commun. (Cambridge, U. K.)* **2015**, *51*, 2235-2238.

(17) Kobayashi, K.; Umeda-Yano, S.; Yamamori, H.; Takeda, M.; Suzuki, H.; Hashimoto, R. *PLoS One* **2011**, *6*, e18113.

(18) Sfikakis, A.; Papadopoulou-Daifotis, Z.; Bikas, N. *Behav Brain Res* **2002**, *128*, 41-52.

(19) Yoshitake, T.; Kehr, J.; Yoshitake, S.; Fujino, K.; Nohta, H.; Yamaguchi, M. *Journal of Chromatography B* **2004**, *807*, 177-183.

(20) Morishima, M.; Harada, N.; Hara, S.; Sano, A.; Seno, H.; Takahashi, A.; Morita, Y.; Nakaya, Y. *Neuropsychopharmacol* **2006**, *31*, 2627-2638.

(21) Huang, F.; Li, J.; Shi, H. L.; Wang, T. T.; Muhtar, W.; Du, M.; Zhang, B. B.; Wu, H.;

Yang, L.; Hu, Z. B.; Wu, X. J. *J Neurosci Meth* **2014**, *229*, 8-14.

(22) Fox, J. *applied linear regression analysis and generalized linear models*, 3rd ed.; Sage Publications: Thousand Oaks, CA, 2016.

(23) John Fox, S. W. *An R Companion to Applied Regression*, 2nd ed.; Sage Publications: Thousand Oaks, CA, 2011.

(24) Atcherley, C. W.; Laude, N. D.; Parent, K. L.; Heien, M. L. *Langmuir* **2013**, *29*, 14885-14892.

(25) Vizi, E. S.; Kiss, J. P. *Hippocampus* **1998**, *8*, 566-607.

(26) Otmakhova, N. A.; Lisman, J. E. *J Neurosci* **1999**, *19*, 1437-1445.

(27) Hemat, R. A. S.; ebrary Inc.; Urotext,: Blackrock, 2003, p 224.

(28) Sperlagh, B.; Vizi, E. S. *Curr Top Med Chem* **2011**, *11*, 1034-1046.

(29) Laatikainen, L. M.; Sharp, T.; Bannerman, D. M.; Harrison, P. J.; Tunbridge, E. M. *J Psychopharmacol* **2012**, *26*, 1561-1568.

(30) Klann, E.; Thiels, E. *Prog Neuropsychopharmacol Biol Psychiatry* **1999**, *23*, 359-376.

(31) O'Neill, R. D.; Gonzalez-Mora, J. L.; Boutelle, M. G.; Ormonde, D. E.; Lowry, J. P.; Duff, A.; Fumero, B.; Fillenz, M.; Mas, M. *J Neurochem* **1991**, *57*, 22-29.

(32) Haas, H. L.; Konnerth, A. *Nature* **1983**, *302*, 432-434.

(33) Samaranayake, S.; Abdalla, A.; Robke, R.; Wood, K. M.; Zeqja, A.; Hashemi, P. *Analyst (Cambridge, U. K.)* **2015**, *140*, 3759-3765.

(34) Cahill, P. S.; Walker, Q. D.; Finnegan, J. M.; Mickelson, G. E.; Travis, E. R.; Wightman, R. M. *Analytical Chemistry* **1996**, *68*, 3180-3186.

(35) Duff, A.; O'Neill, R. D. *J Neurochem* **1994**, *62*, 1496-1502.

(36) Samaranayake, S.; Abdalla, A.; Robke, R.; Nijhout, H. F.; Reed, M. C.; Best, J.; Hashemi, P. *J Neurochem* **2016**.

(37) Roberts, J. G.; Toups, J. V.; Eyualem, E.; McCarty, G. S.; Sombers, L. A. *Anal Chem* **2013**, *85*, 11568-11575.

(38) Herr, N. R.; Park, J.; McElligott, Z. A.; Belle, A. M.; Carelli, R. M.; Wightman, R. M. *J Neurophysiol* **2012**, *107*, 1731-1737.

(39) Reinhoud, N. J.; Brouwer, H. J.; van Heerwaarden, L. M.; Korte-Bouws, G. A. *ACS Chem Neurosci* **2013**, *4*, 888-894.

(40) Pathirathna, P.; Samaranayake, S.; Atcherley, C. W.; Parent, K. L.; Heien, M. L.; McElmurry, S. P.; Hashemi, P. *Analyst (Cambridge, U. K.)* **2014**, *139*, 4673-4680.

(41) Smith, A. D.; Olson, R. J.; Justice, J. B., Jr. *J Neurosci Methods* **1992**, *44*, 33-41.

(42) Damsma, G.; Boisvert, D. P.; Mudrick, L. A.; Wenkstern, D.; Fibiger, H. C. *J Neurochem* **1990**, *54*, 801-808.

(43) Cumming, P.; Brown, E.; Damsma, G.; Fibiger, H. *J Neurochem* **1992**, *59*, 1905-1914.

(44) Glover, V.; Sandler, M.; Owen, F.; Riley, G. J. *Nature* **1977**, *265*, 80-81.

(45) Buu, N. T. *Biochem Pharmacol* **1989**, *38*, 1685-1692.

(46) Park, J.; Kile, B. M.; Wightman, R. M. *Eur J Neurosci* **2009**, *30*, 2121-2133.

(47) Zhao, Z.; Baros, A. M.; Zhang, H. T.; Lapiz, M. D.; Bondi, C. O.; Morilak, D. A.; O'Donnell, J. M. *Neuropsychopharmacol* **2008**, *33*, 3190-3200.

(48) Sayer, T. J.; Hannon, S. D.; Redfern, P. H.; Martin, K. F. *Br J Pharmacol* **1999**, *126*, 1777-1784.

(49) Gartside, S. E.; Umbers, V.; Sharp, T. *Psychopharmacology (Berl)* **1997**, *130*, 261-268.

CHAPTER 3: A COMPARISON OF *IN VIVO* SEROTONIN DYNAMICS IN THE MOUSE HIPPOCAMPUS AND PREFRONTAL CORTEX

(in preparation)

A Abdalla,[1] R Saylor,[1] A West,[1] Yunju Jin[2], Beidi Qiang[3,] Edsel Peña[3], David Linden[2], FH Nijhout,[4] MC Reed,[5] J Best,[6] P Hashemi[1*]

[1]Dept. of Chemistry and Biochemistry, University of South Carolina, SC, USA, [2]Solomon H. Snyder Department of Neuroscience, The Johns Hopkins University School of Medicine, 725. N. Wolfe Street, Baltimore MD 21205, [3]Department of Statistics, University of South Carolina, 1523 Greene Street, Columbia, SC 29208, [4]Department of Biology, Duke University, NC, USA, [5]Department of Mathematics, Duke University, NC, USA, [6]Department of Mathematics, The Ohio State University, OH, USA

3.1 ABSTRACT

Serotonin plays important roles in brain physiology and is implicated in several affective disorders. The principle mechanisms that regulate extracellular serotonin *in vivo* are not well-understood, making the diagnosis and treatment of psychiatric illnesses challenging. It is therefore critical to characterize serotonin chemistry, specifically in localities that are thought to be involved in specific disorders. In this paper, we utilize fast scan cyclic voltammetry to characterize two new stimulation-release circuitries for serotonin, specifically, the CA2 region of the mouse hippocampus and the medial prefrontal cortex. To gain further insight into the extracellular mechanisms that regulate serotonin in these areas, we utilize triple staining immunohistochemistry along with single-photon microscopy to determine the density of serotonin transporters in these discrete localities. Finally, we use fast-scan controlled adsorption voltammetry to measure ambient serotonin levels in these two regions to verify the effects of serotonin transporter density on extracellular levels. We determine that the dynamics of serotonin release and reuptake and ambient serotonin levels are distinctive to their respective regions and highly dependent on the density of serotonin transporters present. Our study is the first to use this powerful combination of tools to obtain information on the unique regional differences exhibited by the serotonergic system, that will be relevant to disease studies in local areas.

3.2 INTRODUCTION

Imbalances in serotonin neurochemistry are postulated to underlie psychiatric disorders, such as depression and anxiety.[1-3] The treatment of such disorders presents a challenge due to the poor characterization of serotonin chemistry in healthy and disease models. Thus, it becomes critical to characterize serotonin chemistry, specifically in localities that are thought to be involved in specific disorders.

The dorsal raphe nucleus (DRN) projects, in both ascending and descending pathways, to innervate most of the brain regions and the majority of these projections are serotonergic.[4] Two regions innervated by the ascending projections from the DRN are the hippocampus and the medial prefrontal cortex (mPFC)[4] - regions chosen for their importance in a variety of disorders. The mPFC and hippocampus have been studied for their roles in depression, cognition and impulsivity.[5-10] While both these regions have been previously studied using different methods[5,6,11-16], we are interested in characterizing the dynamics of serotonin utilizing the high temporal resolution offered by fast scan cyclic voltammetry (FSCV) for release and reuptake and ambient measurements afforded by fast scan adsorption controlled voltammetry (FSCAV). These techniques offer us an advantage of making measurements at specific localities, with minimal tissue damage at in real time.

In this letter, we characterize two novel stimulation-release circuitries for serotonin. We measure evoked release and reuptake after electrical stimulation of the medial forebrain bundle (MFB), in the mPFC and the CA2 region of the

hippocampus. We postulate that the dynamics of serotonin release and reuptake are characteristic of the region being studied. To better elucidate these differences, we utilize triple staining immunohistochemistry and single-photon microscopy to discern the differences in serotonin axons and transporter density in these regions and find that the voltammetry mirrors the local physiology. Subsequently, we use FSCAV to verify that high levels of serotonin transporter lower ambient levels of serotonin. Using this synergy of analytical and biological tools, we show that voltammetry can provide important information on local tissue physiology.

3.3 RESULTS AND DISCUSSION

FSCV is a background-subtracted method which necessitates the application of electrical stimulation, to induce a change that can be measured. This stimulation is performed by placing a stimulating electrode in the MFB; a bundle of neurons that originates in the DRN and innervates various brain regions as seen in **Figure 3.1A**. To measure serotonin release and reuptake, a nafion-coated carbon fiber microelectrode (CFM)[17] is inserted, either the mPFC or the CA2 region of the hippocampus (**Figure 3.1A),** and the Jackson waveform, for FSCV serotonin measurements,[18] is utilized.

Figure 3.1B (i), (**ii)**, and (**iii)**, display representative color plots for both regions. The analysis of color plots has been explained elsewhere in detail; [19] briefly, time is displayed on the x-axis, voltage on the y-axis and the current displayed in false color. The stimulation period (2 s) is denoted by a red bar below the color plots. Cyclic voltammograms (CVs), displayed in **Figure 3.1C (I)**, (**ii)**, and

(**iii)** are extracted at the vertical dashed lines in **Figure 3.1B (I)**, (**ii)**, and (**iii),** respectively.

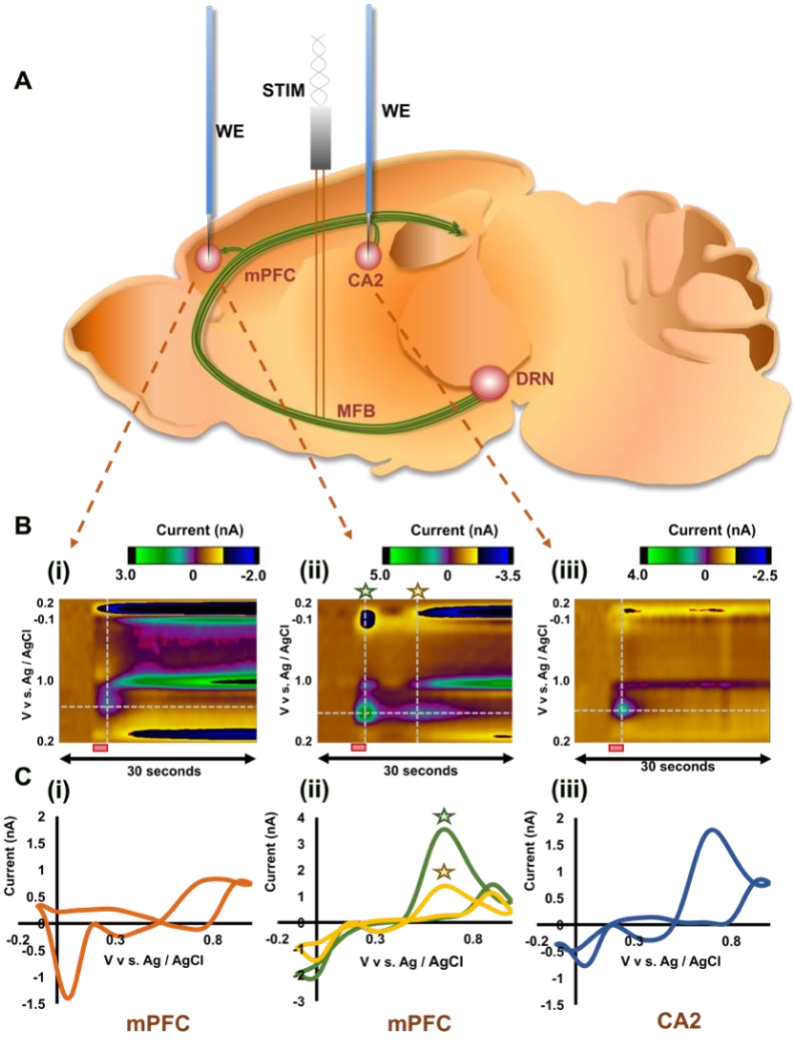

Figure 3.1. (A) Representation of a sagittal section of a mouse brain. Red circles denote different brain regions. WE are the working electrode and STIM is the stimulating electrode. Green track represents the serotonergic innervation that begins in the DRN, and make up the MFB to innervate different brain regions. **B)** Representative FSCV color plots of **(i)** and **(ii)** the mPFC and **(iii)** the CA2. The red bar below the color plots denote the stimulation period (2 s) **C)** Cyclic voltammograms extracted from the vertical dashed lines in **B**(**i), (ii),** and **(iii)** with current on the y-axis and voltage vs. Ag / AgCl on the x-axis. Green and yellow stars on **B(ii)** denote the two successive oxidation events seen in the mPFC. CVs extracted at both these positions are seen in **C (ii),** marked with their respective stars.

These CVs contain the characteristic serotonin oxidation and reduction peaks found at 0.65 – 0.75 V and 0 V, respectively, verifying that the signal measured in these 2 regions is serotonin. Interestingly, in the mPFC, two different kinds of signals were observed. In **Figure 3.1B (i) and 3.1C (i)**, a typical color plot and CV can be seen, with a single serotonin oxidation and reduction event. On the other hand, **Figure 3.1B (ii)** and **3.1C (ii)** show a different signal, not previously observed with serotonin FSCV. This response constitutes 2 distinct and successive redox events, one being more delayed than the other. Upon extraction and examination of CVs from both these events, the first at 7s and the second at 15 s, it is strongly implied by the position of the redox peaks that they are both serotonin redox events. There are various explanations for this observed phenomenon, including release by two populations of axons or a secondary messenger, and more work is currently being carried out to allow us to determine the exact cause of this response. The CA2 region shows a single serotonin redox event (**Figure 3.1B (iii)**), with the CV extracted displaying the characteristic serotonin redox peaks, as can be seen in **Figure 3.1C (iii)**.

The placement of the CFM in the mPFC and the CA2 was confirmed using histology displayed in **Figure 3.2A (iii)** and **3.2B (ii)**, respectively. Coronal slices of brains collected post *in vivo* experiments are presented, with 5 circles representing the 5 mice used in a region (green=mPFC and blue=CA2). For the mPFC, 5 mice were used for each response, thus coronal slices show 10 separate circles. The small lesions seen on the thionin stained coronal slices on the left of

both figures are an actual indication of the placement of the CFM in both regions in a representative brain.

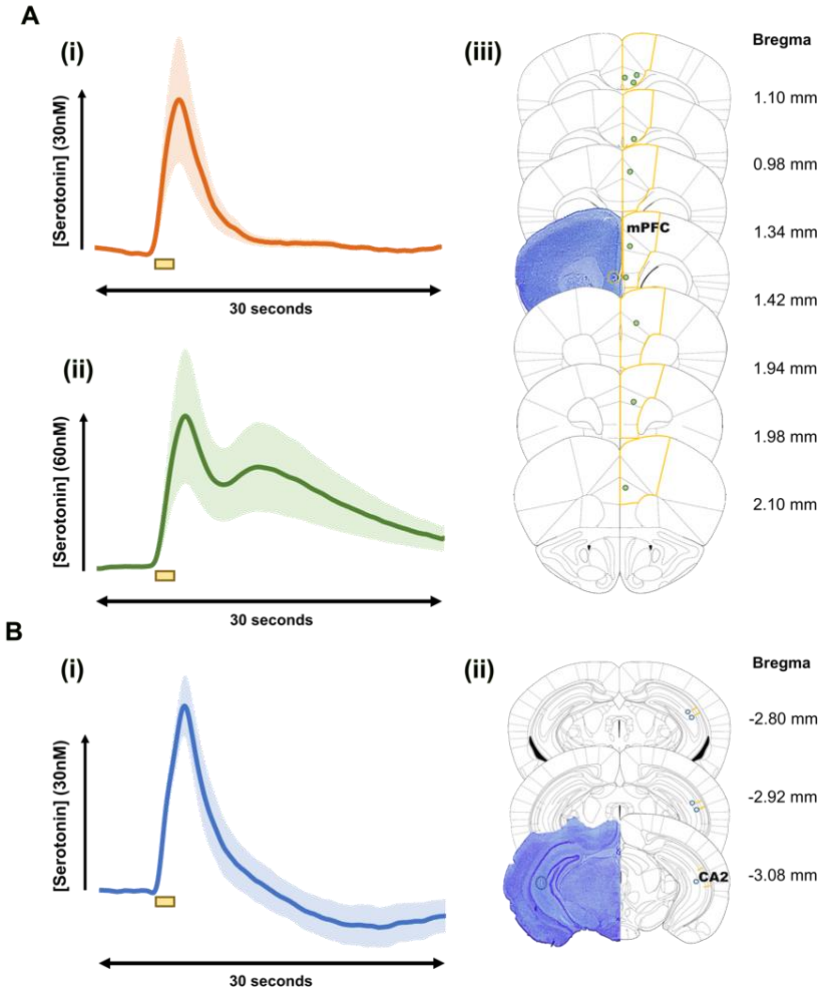

Figure 3.2. Averaged [Serotonin] – time profiles (n=5 ± SEM) and histological placements of CFMs in **A)** mPFC and **B)** CA2. **A(i)** is the averaged plot for the single response and A **(ii)** is the averaged plot for the "double peak" response in the mPFC. Yellow bars beneath the plot denote the stimulation period (2 s). **A(iii)** Thionin stained representative brains displayed on the left with a yellow circle denoting the actual placement of the CFM. On the right, yellow lines represent the outlines of the mPFC region, and the green circles denote the placement of the CFM in each individual mouse, for both type of responses (n=10). **B(ii)** Thionin stained representative brain displayed on the left with blue circle denoting the actual placement of the CFM. On the right, yellow lines represent the outlines of the CA2 region, and the blue circles denote the placement of the CFM in each individual mouse (n=5). Bregma coordinates are shown to the right of each coronal slice. Region specific coordinates are further explained in the methods section.

The FSCV [serotonin] vs. time signal (obtained from the horizontal dashed lines in **Figure 3.2B)** comprises a rapid increase, occurring upon electrical stimulation, that peaks, then decays in a manner determined by inactivation mechanisms. Wood *et. al*., modeled the uptake of serotonin in the SNr via two mechanisms.[19] The first, designated Uptake 1 is the serotonin transporters (SERTs) reuptaking serotonin with high affinity and low efficiency. Thus the [serotonin] vs. time curve is seen to decay slowly with a single slope. The second, Uptake 2, transpires due to the activity of non-serotonin (non-SERT) transporters, that uptake serotonin with high efficiency, but with low capacity. This generates a decay curve with a single slope that reaches baseline quickly. When there is a combination of SERTs and non-SERTs, the result is a hybrid signal, with a curve that decays quickly for a few seconds, followed by a slow decay until it reaches baseline, resulting thus in a decay curve with 2 different slopes.

Figures 3.2A (i), (ii) and Figure 3.2B (i) display the average [serotonin] vs. time profiles (n=5 animals ± SEM) for the mPFC and the CA2, respectively. F**igure 3.2A (i)**, shows the [serotonin] vs. time profile for the "single peak" mPFC response that has a mixed uptake profile. The decay in the [serotonin] vs. time profile for the second "double peak" mPFC response (**Figure 3.2A (ii)**), is comprised of a short "fast" decay for a few seconds, which is then, interestingly, overcome by another rise in concentration, albeit smaller than the initial one. This rise decays at a much slower rate than the initial decay. Both decays have single slopes, which makes it likely that the "fast" decay is Uptake 2 controlled, whereas the "slow" decay is Uptake 1 controlled. The CA2 profile (**Figure 3.1B (i)**), on the other hand, exhibits

a pattern of predominantly Uptake 2 controlled response, along with a small Uptake 1 component. Both regions are suggestive of a mixed SERTs and non-SERTs presence. Previous research into the localization and functions of transporters across the brain has uncovered the presence of both SERTs and non-SERTs in the hippocampus as well as the prefrontal cortex.[20,21] Among the non-SERTs found in both regions are dopamine transporters (DATs)[22,23], norepinephrine transporters (NETs)[23], and organic cation transporters (OCTs)[24]. Our chemical data allows us to postulate that a higher density of SERTs must be present in the mPFC.

To confirm our hypothesis, we performed triple staining immunohistochemistry on Slc6a4-EGFP mice. By using triple staining, EGFP/NeuN/SERT, followed by single-photon microscopy, we were able to visualize the serotonin axons in green (EGFP), the neuronal cell bodies in cyan (NeuN), and the SERTs in red, as can be seen in **Figure 3.3A and B**, for the CA2 and the mPFC, respectively. The yellow seen in both images is a result of having both green and red i.e. both serotonin axons and SERTs in the same spot, thus the amount of yellow, along with pure red, should signify the density of SERTs present. As can be seen from **Figure 3.3,** the CA2 region contains a lower density of green axons, signifying a lower density of serotonin axons, which along with the lower density of red and yellow, signifies a lower density of SERTs in this region. The mPFC on the other hand, contains a denser innervation of serotonin axons, signified by a larger network of green axons seen in **Figure 3.3B.** In addition, the larger spread of red dots and yellow in this image signifies a higher amount of

SERTs. L1 and L2/3 are different layers of the mPFC. It is interesting to note vast changes in the distribution and density of SERTs and serotonin axons between the two layers. It is possible that the different responses obtained in the mPFC could be due to the placement of the CFM in the different layers of the mPFC, a notion we are working to verify.

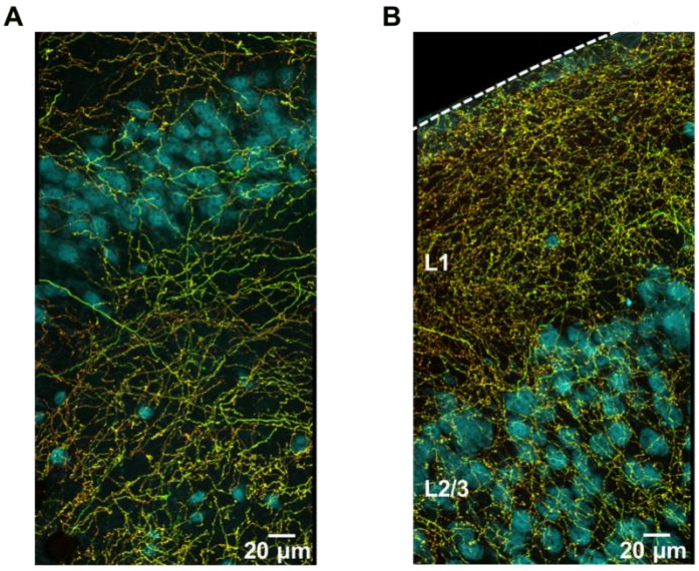

Figure 3.3. EGFP/NeuN/SERT triple staining immunohistochemistry followed by single-photon microscopy for the **A)** CA2 and **B)** mPFC of Slc6a4-EGFP mice. Green represents serotonin axons, cyan is neuronal cell bodies, and red are SERTs. Yellow is a result of green serotonin axons and red SERTs being at the same spot. **B)** L1 and L2/3 are different layers of the mPFC.

The observed differences in SERT density thus explain uptake differences observed between the mPFC and CA2. We further hypothesize that the magnitude of SERTs present should determine ambient serotonin levels because of the high capacity of SERTs for serotonin. We utilized fast-scan controlled adsorption voltammetry (FSCAV) to measure serotonin's extracellular concentration in these two brain regions.

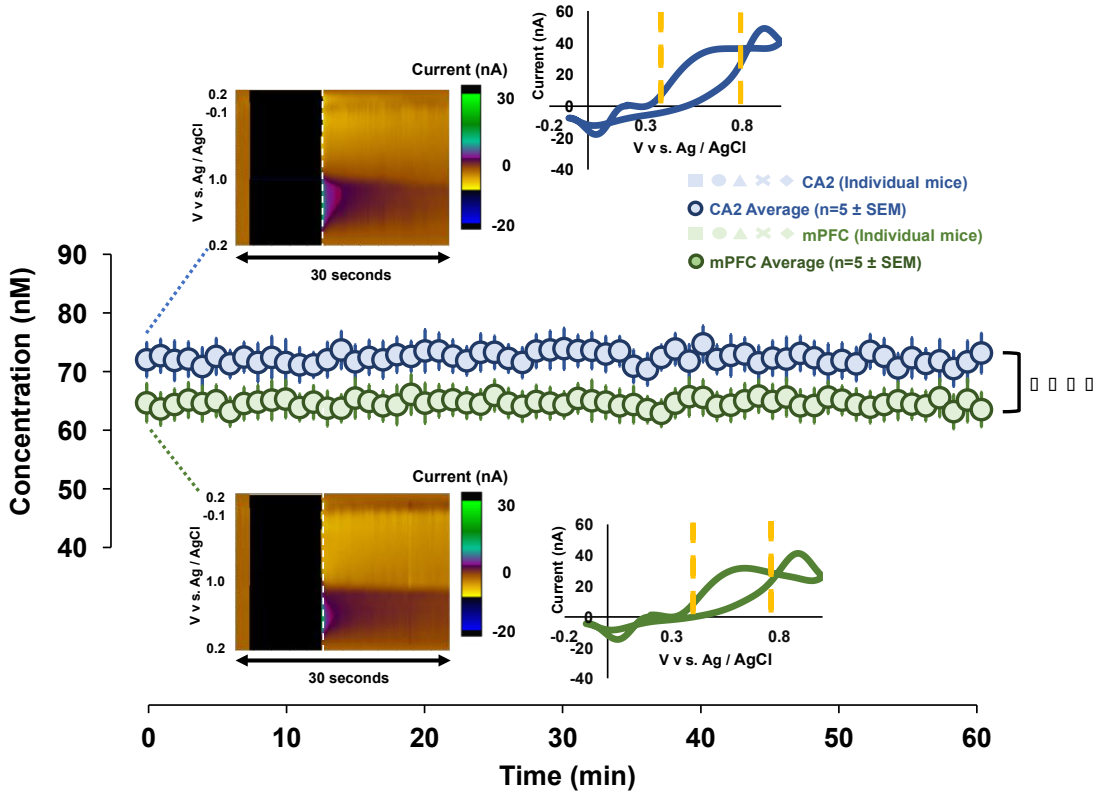

Figure 3.4. Dark blue and green circles represent the weighted averaged response (n=5 mice ± SEM), and faint blue and green markers represent individual mice responses Files were collected for 60 mins to obtain a baseline reading. Representative FSCAV color plots and CVs (extracted from vertical dashed lines) are inset, on top for the CA2 and at the bottom for mPFC. Yellow lines on the CV denote the limits of integration. ****p<0.0001

First MFB stimulation was employed in mice to verify the presence of serotonin with FSCV. FSCAV was then performed on the same CFM for 60 mins to obtain a baseline reading of ambient serotonin concentration. The dark blue and green circles on the central trace of **Figure 3.4** represent the weighted average response (n=5 ± SEM) in the CA2 and mPFC respectively. Individual mice traces are displayed by faint markers, of similar color, on the same plot. Representative *in vivo* color plots, along with CVs extracted from the 3rd scan (vertical dashed line), post controlled adsorption period, can be seen on **Figure 3.4**. The color plot and

CV collected in the CA2 are on the top, while those collected in the mPFC are at the bottom. Both CVs demonstrate the characteristic redox serotonin peaks, thus confirming the identity of the signal measured.

To report the ambient concentration of serotonin in these 2 regions, we used a chemometric approach, to take into account the variability between the CFMs used, along with the *in vivo* variability. This approach was explained by us in detail elsewhere; [25] in brief, a linear functional model was developed using *in vitro* calibrations performed on the electrodes post *in vivo* experiments. Using 5 mice for each region, the weighted average ambient serotonin level in the CA2 was 66.9 ± 0.57 nM (n = 5 mice, weighted average ± standard error), whilst the level in the mPFC was 59.8 ± 1.25 nM (n = 5 mice, weighted average ± standard error). A paired 2-sample t-test performed on these concentrations confirms a statistically significant difference between the basal levels in the 2 regions ($p < 0.0001$). Earlier reports on extracellular concentration of serotonin at different brain regions, collected with microdialysis, report significantly lower values.[26-30] As previously clarified in the paper published by Abdalla *et.al*. [25] the higher values can be explained by the different spatial resolution offered by the comparatively smaller CFM's, along with signal optimization achieved through electrode placement (verified by stimulated serotonin measurement), which allows for measurements from areas with higher serotonergic activity.

Ambient neurotransmitter concentration is partly controlled by type and density of transporters present.[31] We observed significantly more SERTs in the mPFC and this lead us to hypothesize that the ambient serotonin levels (if activity

of neurons is assumed the same) in the mPFC should be lower than in the CA2 because the SERTs have much higher affinity for serotonin. Indeed, we found this to be true. It must be noted that the electrical stimulation is aphysiological and although we see reuptake by Uptake 2 transporters with elicited serotonin release in the CA2, it is likely that serotonin is much more confined to the synapses where high affinity SERT dominate ambient levels.

Determining the different mechanisms that control serotonin neurochemistry in the different brain regions is challenging due to the inability of one single method to provide a complete picture of how serotonin is controlled and regulated in the brain. In this letter, we present a synergy of methods, electrochemical and biological to afford further insight into two discrete brain regions: the CA2 region of the hippocampus and the mPFC. We determine key differences in serotonin regulation in these 2 regions can be attributed, at least in part, to SERT density. This study highlights the power of electrochemistry in providing physiological information about local tissue.

3.4 METHODS

Carbon-Fiber Microelectrodes

CFM's were constructed through the aspiration of a single T-650 carbon fiber (7 μm, Goodfellow, Coraopolis, PA) through a cylindrical glass capillary (internal diameter: 0.4 mm, external diameter: 0.6 mm, A-M Systems, Carlsborg, WA). This capillary was then placed in a vertically pipette puller (Narishige Group, Setagaya-Ku, Tokyo, Japan) to make a carbon – glass seal by gravity. The protruding carbon fiber was then cut to about 150 μm in length. Subsequently, a

solution of nafion (Liquion-1105-MeOH, Ion Power, DE) was electrodeposited as previously described onto the exposed carbon fiber. [17] The CFM was then dried for 10 minutes at 70°C.

Animal Surgery

6 to 8 weeks old C57BL/6J male mice, between 20-25 g, were procured from Jackson Laboratories (Bar Harbor, ME). Mice were offered food and water ad libitum and housed in 12 hours light/dark cycles. The Guide for the Care and Use of Laboratory Animals, as accepted by the Institutional Animal Care and Use Committees (IACUC) of the University of South Carolina, was followed in all animal care and procedures. Anesthetic urethane, (25% dissolved in 0.9% NaCl solution, Hospira, Lake Forest, IL) was administered intraperitoneally (*i.p.*) at a volume of 7 µL per 1 g mouse weight, followed by stereotaxic surgeries (David Kopf Instruments, Tujunga, CA). To maintain the ideal mouse body temperature of 37° C, a heating pad from Braintree Scientific was utilized. For stereotaxic coordinates of MFB [AP: -1.58, ML: +1.0, DV: -4.8 to -5.0], CA2 [AP: -2.9, ML: +3.35, DV: -2.5 to -3.0], and mPFC [AP: +1.7, ML: +0.2, DV: -2.0 to -3.0], bregma was used as a reference from Franklin and Paxinos (2008). In order to access the MFB, CA2, and, mPFC holes were drilled in line with the above stereotaxic coordinates. For stimulation, a stainless-steel electrode (diameter 0.2 mm; Plastics One, Roanoke, VA) was inserted into the MFB. For measurements, the nafion-coated CFM was then inserted into either the CA2 or the mPFC. The reference electrode is made of a silver wire (diameter: 0.010 in; A-M Systems, Sequim, WA), which was electroplated with chloride through immersion of in hydrochloric acid (0.1 M, 4 V

vs. tungsten). This is then placed into the contralateral hemisphere of the CFM placement. A 60 Hz biphasic 360 μA, 120 pulse stimulation, that is 2 ms per phase was then used through employing a linear constant current stimulus isolator (NL800A Neurolog; Digitimer Ltd.).

Data Collection

FSCV and FSCAV were both performed through instrumentation and software (WCCV 3.05) developed by Knowmad Technologies LLC (Tucson, AZ). FSCAV was applied through a CMOS precision analog switch, ADG419 (Analog Devices), which is used in order to control the application of the computer-generated "Jackson" waveform to the CFM. The logic was software - controlled to either apply a series of ramps (0.2 V to 1.0 V to -0.1 V to 0.2 V, scan rate = 1000 V/s) every 10 ms (100 Hz), or apply a constant potential of 0.2 V to the CFM for a specified controlled adsorption period (10 s).

Data analysis

Signals collected from FSCV and FSCAV were processed using software written in-house using LabVIEW 2009. The processing used includes signal deconvolution, filtering, and smoothing. For FSCAV, the CV at the 3rd scan (following the controlled adsorption period) was extracted to integrate the serotonin oxidation peak approximately between 0.4V and 0.85V. The charge value found, in pC, was then plotted versus [serotonin] to generate calibration curves that were then used to calculate *in vivo* values.

Statistical Analysis

The *in vitro* calibration data was used to develop linear models, that relate charge with both the concentration and the different electrodes used *in vivo*, so as to accommodate for the varying responses between electrodes, as explained previously. [25] The data fitting was executed using the linear model via the lm command in the R program. Using the developed fitted linear models, along with the *in vitro* calibrations and the charge values collected *in vivo* for 60 mins, an estimation of the ambient serotonin levels at each of the time points were attained. In order to obtain an average concentration level estimate for each time point (60 mins), the concentration estimates from each of the 5 CFMs were used for a weighted pooling. These weights were calculated based on the inverse of the estimated variance of the concentration estimates. 95% point-wise confidence intervals were constructed by fitting the developed functional model to the pairs of time and concentration values through the use of the predict.lm command in the R package.

Exclusion Criteria

For all FSCV experiments, CV of the evoked signal was compared with well-established CVs and mice in which the CVs did not contain the characteristic serotonin redox peaks[17] was excluded. For FSCAV experiments, a stimulated serotonin response was collected prior to the start of FSCAV and the same aforementioned test was performed. In addition, mice that did not remain alive until the end of the collection time were excluded. All other animals were included in this study.

Histology

In order to confirm the spatial placement of the CFM *in vivo*, a small lesion was created at the end of the FSCV experiment, by applying a constant potential at the CFM (10 V for 1 min). Subsequently, the mice were euthanized and the brain was removed from the skull and stored in 4% paraformaldehyde in PBS solution. At least 2 days before sectioning, the brain is transferred into a 30% sucrose solution, until it sinks. The brain is then flash-frozen and sectioned into 30 µm slices mounted onto frosted glass slides, and stained with 0.2% thionin. The slices are then photographed with an optical microscope.

Immunohistochemistry

The Slc6a4-EGFP mice were anesthetized with urethane (25% dissolved in 0.9% NaCl solution, Hospira, Lake Forest, IL) administered intraperitoneally (*i.p.*) at a volume of 7 µL per 1 g mouse weight then perfused intracardially with phosphate-buffered saline (PBS) followed by 4% paraformaldehyde in PBS at 4 °C. The entire brain was removed and fixed in 4% paraformaldehyde for 3 hours at room temperature and then cryoprotected in 15% sucrose in PBS overnight at 4 °C, followed by a switch to 30% sucrose on the next day and continuing overnight. Sections of the mouse brain (40 µm thick) were prepared using a microtome and were washed with PBS and then blocked with 5% normal goat serum and 0.3 % Triton X-100 in PBS for 2 hours at room temperature. The sections were incubated in primary antibody diluted in blocking buffer, overnight at 4 °C. The primary antibodies used were chicken anti-GFP (1:5000, Aves Labs #GFP-1010), guinea pig anti-SERT (1: 1,000, Frontier Institute #HTT-GP-Af1400),

rabbit anti-TH (1: 1,000, Millipore #AB152), and mouse anti-NeuN (1:500, Millipore #MAB377). The sections were then washed with PBS and incubated in the secondary antibody in a blocking buffer for 2 hours at room temperature. The secondary antibodies used were Alexa Fluor 488-labeled goat anti-mouse (1:1000, Life Technologies #A11039), Cy3-labeled goat anti-guinea pig (1:800, Jackson ImmunoResearch Laboratories #106-165-003), Cy3-labeled goat anti-rabbit (1:800, Jackson ImmunoResearch Laboratories #111-165-003), and Cy5-labeled goat anti-mouse (1:200, Jackson ImmunoResearch Laboratories #115-175-146). Then, the sections were mounted on slides, and images were acquired using a single-photon confocal microscope (Zeiss).

3.5 REFERENCES

(1) Owens, M. J.; Nemeroff, C. B. *Clin Chem* **1994**, *40*, 288-295.

(2) Muller, C. L.; Anacker, A. M. J.; Veenstra-VanderWeele, J. *Neuroscience* **2016**, *321*, 24-41.

(3) Abi-Dargham, A.; Laruelle, M.; Aghajanian, G. K.; Charney, D.; Krystal, J. *J Neuropsychiatry Clin Neurosci* **1997**, *9*, 1-17.

(4) Michelsen, K. A.; Prickaerts, J.; Steinbusch, H. W. *Prog Brain Res* **2008**, *172*, 233-264.

(5) Thomas, A. J.; Hendriksen, M.; Piggott, M.; Ferrier, I. N.; Perry, E.; Ince, P.; O'Brien, J. T. *Neuropathol Appl Neurobiol* **2006**, *32*, 296-303.

(6) Hitti, F. L.; Siegelbaum, S. A. *Nature* **2014**, *508*, 88-92.

(7) Györfi, O.; Nagy, H.; Bokor, M.; Moustafa, A. A.; Rosenzweig, I.; Kelemen, O.; Kéri, S. *Frontiers in Neurology* **2017**, *8*, 84.

(8) Lemogne, C.; Delaveau, P.; Freton, M.; Guionnet, S.; Fossati, P. *J Affect Disord* **2012**, *136*, e1-e11.

(9) Chantiluke, K.; Barrett, N.; Giampietro, V.; Brammer, M.; Simmons, A.; Murphy, D. G.; Rubia, K. *Cereb Cortex* **2015**, *25*, 1757-1770.

(10) Konradi, C.; Zimmerman, E. I.; Yang, C. K.; Lohmann, K. M.; Gresch, P.; Pantazopoulos, H.; Berretta, S.; Heckers, S. *Arch Gen Psychiatry* **2011**, *68*, 340-350.

(11) Chai, X. J.; Whitfield-Gabrieli, S.; Shinn, A. K.; Gabrieli, J. D.; Nieto Castanon, A.; McCarthy, J. M.; Cohen, B. M.; Ongur, D. *Neuropsychopharmacol* **2011**, *36*, 2009-2017.

(12) Benes, F. M.; Kwok, E. W.; Vincent, S. L.; Todtenkopf, M. S. *Biol Psychiatry* **1998**, *44*, 88-97.

(13) Hashemi, P.; Dankoski, E. C.; Petrovic, J.; Keithley, R. B.; Wightman, R. M. *Anal. Chem. (Washington, DC, U. S.)* **2009**, *81*, 9462-9471.

(14) Jackson, B. P.; Dietz, S. M.; Wightman, R. M. *Anal Chem* **1995**, *67*, 1115-1120.

(15) Wood, K. M.; Zeqja, A.; Nijhout, H. F.; Reed, M. C.; Best, J.; Hashemi, P. *J. Neurochem.* **2014**, *130*, 351-359.

(16) Berumen, L. C.; Rodriguez, A.; Miledi, R.; Garcia-Alcocer, G. *ScientificWorldJournal* **2012**, *2012*, 823493.

(17) Hensler, J. G.; Artigas, F.; Bortolozzi, A.; Daws, L. C.; De Deurwaerdère, P.; Milan, L.; Navailles, S.; Koek, W. In *Advances in Pharmacology*, Eiden, L. E., Ed.; Academic Press, 2013, pp 167-197.

(18) Bai, J.; Blot, K.; Tzavara, E.; Nosten-Bertrand, M.; Giros, B.; Otani, S. *Cereb Cortex* **2014**, *24*, 945-955.

(19) Borgkvist, A.; Malmlof, T.; Feltmann, K.; Lindskog, M.; Schilstrom, B. *Int J Neuropsychoph* **2012**, *15*, 531-540.

(20) Matsui, T.; Nakata, T.; Kobayashi, Y. *Neurosci Lett* **2016**, *633*, 118-124.

(21) Abdalla, A.; Atcherley, C. W.; Pathirathna, P.; Samaranayake, S.; Qiang, B.; Pena, E.; Morgan, S. L.; Heien, M. L.; Hashemi, P. *Anal Chem* **2017**, *89*, 9703-9711.

(22) Mathews, T. A.; Fedele, D. E.; Coppelli, F. M.; Avila, A. M.; Murphy, D. L.; Andrews, A. M. *J Neurosci Methods* **2004**, *140*, 169-181.

(23) Zhang, J.; Jaquins-Gerstl, A.; Nesbitt, K. M.; Rutan, S. C.; Michael, A. C.; Weber, S. G. *Anal Chem* **2013**, *85*, 9889-9897.

(24) Gardier, A. M.; David, D. J.; Jego, G.; Przybylski, C.; Jacquot, C.; Durier, S.; Gruwez, B.; Douvier, E.; Beauverie, P.; Poisson, N.; Hen, R.; Bourin, M. *J Neurochem* **2003**, *86*, 13-24.

(25) Parsons, L. H.; Justice, J. B., Jr. *J Neurochem* **1993**, *61*, 1611-1619.

(26) Lee, W. H.; Ngernsutivorakul, T.; Mabrouk, O. S.; Wong, J. M.; Dugan, C. E.; Pappas, S. S.; Yoon, H. J.; Kennedy, R. T. *Anal Chem* **2016**, *88*, 1230-1237.

(27) Sun, W.; Shchepakin, D.; Kalachev, L. V.; Kavanaugh, M. P. *Neurochem Int* **2014**, *73*, 146-151.

CHAPTER 4*: IN VIVO* HISTAMINE VOLTAMMETRY IN THE MOUSE PREMAMMILLARY NUCLEUS

Reprinted with permission from Analyst

Samaranayake, S.; **Abdalla, A**.; Robke, R.; Wood, K. M.; Zeqja, A.; Hashemi, P.,

In vivo histamine voltammetry in the mouse premammillary nucleus. Analyst

2015, 140 (11), 3759 - 3765

I contributed both experimentally and intellectually and the results of this project directed me to my next project.

4.1 ABSTRACT

Histamine plays a major role in the mediation of allergic reactions such as peripheral inflammation. This classical monoamine is also a neurotransmitter involved in the central nervous system but its roles in this context are poorly understood. Studying histamine neurotransmission is important due to its implications in many neurological disorders. The sensitivity, selectivity and high temporal resolution of fast scan cyclic voltammetry (FSCV) offer many advantages for studying electroactive neurotransmitters. Histamine has previously been studied with FSCV; however, the lack of a robust Faradaic electrochemical signal makes it difficult to selectively identify histamine in complex media, as found *in vivo*. In this work, we optimize an electrochemical waveform that provides a stimulation-locked and unique electrochemical signal towards histamine. We describe *in vitro* waveform optimization and a novel *in vivo* physiological model for stimulating histamine release in the mouse premamillary nucleus via stimulation of the medial forebrain bundle. We demonstrate that a robust signal can be used to effectively identify histamine and characterize its' *in vivo* kinetics.

4.2 INTRODUCTION

The central nervous system holds four aminergic systems, dopamine, serotonin, norepinephrine and histamine. These messengers are in an intricate chemical interplay with one-another and other neurotransmitters to precisely modulate many aspects of brain function. It is critical to understand the fundamental neurochemistry of these four modulatory systems to better prevent, diagnose and treat brain disorders and diseases. Fast scan cyclic voltammetry (FSCV) at carbon fiber microelectrodes (CFMs) is a uniquely powerful method for *in vivo* analysis. CFMs are biocompatible, cause negligible damage to brain tissue and, because of their kinetically favorable surface kinetics, provide real-time output of electroactive neurotransmitters.

The dopaminergic system has been extensively studied with FSCV over the previous three decades leading to breakthroughs in understanding dopaminergic mechanisms in the brain.[1-3] More recently, FSCV has been recently developed for the detection of serotonin and norepinephrine [4, 5] and many important aspects of the two neurotransmitters are thus being unearthed.[6-10] Histamine is also an electroactive amine, and there have been previous reports of histamine induced FSCV signals in mast cells,[11-13] brain tissue slice preparations[14] and *in vivo,*[15] however mechanistic studies on histamine are limited. This is primarily because histamine electrochemistry is complex, and FSCV induced histamine signals are often interpreted via changes in the capacitative current on the electrode surface. This approach is fully quantitative; however, many analytes induce a capacitative

change at the electrode surface limiting selectivity and rendering *in vivo* studies very difficult.

Faradaic electrochemistry more selectively identifies analytes because of the unique potential position of redox peaks.[16] In this paper, we discuss the relevance of histamine adsorption to capacitative currents at CFMs. We describe a novel FSCV waveform that generates a robust oxidation peak in response to histamine. We show *in vitro*, that histamine can be detected selectively and with high sensitivity. Finally, we report and verify a robust histamine signature in the mouse premammillary nucleus (PM) in response to medial forebrain bundle (MFB) stimulation.

Our novel FSCV waveform for histamine provides a tool that will enable the same level of investigation for histamine as other, more established brain amines. Histamine's roles in the brain, in particular with respect to disorders in which it is implicated (e.g. Alzheimer's disease) can thus be systematically studied.

4.3 EXPERIMENTAL SECTION

Chemicals and Reagents

Standard solutions were prepared by dissolving histamine dihydrochloride, dopamine hydrochloride, serotonin hydrochloride and adenosine hydrochloride (Sigma-Aldrich, Co., MO, USA) respectively in Tris-buffer. Tris-buffer was constituted thus: 15 mM $H_2NC(CH_2)(OH)_3.HCl$, 140 mM NaCl, 3.25 mM KCl, 1.2 mM $CaCl_2$, 1.25 mM $NaH_2PO_4.H_2O$, 1.2 mM $MgCl_2$ and 2.0 mM Na_2SO_4 at pH=7.4 in deionized water (EMD Chemicals Inc. NJ, USA).

Carbon-Fiber Microelectrodes (CFMs)

CFMs were fabricated with 7µm diameter carbon-fibers (Goodfellow Corporation, PA, USA) aspirated in to glass capillaries (0.6 mm external diameter, 0.4 mm internal diameter, A-M systems, Inc., Sequim, WA). A carbon-glass seal was formed via a vertical micropipette puller (Narishige Group, Tokyo, Japan). The exposed length of the carbon fiber was trimmed to 150 µm under an optical microscope. Microelectrodes were electroplated with Nafion as described previously.[4]

Data Collection/Analysis

Waveform generation was via a PCIe-6341 DAC/ADC card (National Instruments, Austin, TX). Output current was measured by a CHEM-CLAMP potentiostat (Dagan corporation, MN). Custom built software was employed to drive the hardware, collect data and perform analysis including background subtraction, signal averaging and digital filtering (Knowmad Technologies LLC, Tucson, AZ). All potentials are quoted with respect to Ag/AgCl reference electrodes, which were fabricated via electrodeposition of Cl^- by holding a silver wire (A-M systems, WA) at 4.0 V for 5 s in 1 M HCl. All data represented with error bars represent the standard error of the mean (SEM). Statistical differences were determined using one-tailed student's-tests on paired data sets ($p<0.45$ was taken as statistically different).

Langmuir Adsorption Isotherms

A CFM was placed into histamine solution of standard concentration and an optimized histamine waveform was applied. An electronic relay (ADG-419, Analog

Devices) was used to switch between the applied waveform and a constant potential (-0.5 V) for 10 seconds to allow histamine adsorption at the electrode surface and reach equilibrium. After 10 seconds, the waveform was reapplied, and the first background-subtracted cyclic voltammogram was collected and analyzed for total adsorbed histamine. In house LabVIEW 2012 software integrated the oxidation peak from the background subtracted cyclic voltammogram and Faraday's law was used to convert this to a surface concentration ($\Gamma_{histamine}$). Measured data was fit to a linearized Langmuir adsorption isotherm as previously described,[17] and K is the equilibrium constant for adsorption. This experiment was performed in Tris buffer (15 mM).

Flow Injection Analysis

In vitro analyses were performed with flow injection analysis (FIA). CFMs were inserted into a flangeless short 1/8 nut (PEEK P-335, IDEX, Middleboro, MA) such that around 2 mm of the tip remained exposed outside of the nut. The microelectrode-containing nut was then fastened into a modified HPLC union (Elbow PEEK 3432, IDEX, Middleboro, MA). The other end of the elbow union was fastened into the out-flowing steam of the FIA buffer and two holes were drilled into the union for incorporation of the reference electrode and for a 'waste' flow stream. Flow was maintained with a syringe infusion pump (kd Scientific, model KDS-410, Holliston, MA) at 2 mL min^{-1}. A rectangular pulse of analyte was introduced into the flow steam for 10 s via a six-port HPLC loop injector (Rheodyne model 7010 valve, VICI, Houston, TX). For calibrations and waveform optimization, analytes were injected in random concentrations order to avoid carry-over effects.

Potentiometry

The open circuit potential between CFMs and Ag/AgCl was measured using a potentiostat with an integrated high impedance amplifier (eDAQ Pty Ltd, NSW, Australia). 200 µM of histamine was injected onto the CFM in Tris-buffer using FIA at pH = 7.4. Subsequent injections were after potential recovered to base line.

Animal Surgeries

Handling and surgery on male C57BL/6J mice weighing 20−25 g (Jackson Laboratory, Bar Harbor, ME) were in agreement with The Guide for the Care and Use of Laboratory Animals, approved by the Institutional Animal Care and Use.

Urethane (25% dissolved in 0.9% NaCl solution, Hospira, Lake Forest, IL) was administered via intraperitoneal (*i.p.*) injection, and stereotaxic surgery (David Kopf Instruments, Tujunga, CA) was performed. A heating pad sustained mouse body temperature around 37 °C (Braintree Scientific, Braintree, MA). Stereotaxic coordinates were taken in reference to bregma. A Nafion modified CFM was inserted into the PM (AP: −2.45, ML: +0.50, DV: −5.45 to −5.55.). A stainless-steel stimulating electrode (diameter: 0.2 mm, Plastics One, Roanoke, VA) was positioned into the MFB (AP: -1.07, ML: +1.10, DV: −5.00). 120 biphasic pulses were applied through a linear constant current stimulus isolator (NL800A, Neurolog, Medical Systems Corp., Great Neck, NY). The 60 Hz trains were 350 µA each phase, 2 ms in width, and 2 s in length. An Ag/AgCl reference electrode was implanted into the brain's opposite hemisphere.

Drugs

Tacrine hydrochloride (2 mg kg-1) and thioperamide maleate (20 mg kg-1) from TOCRIS bioscience (Bristol, UK) were dissolved in saline respectively and injected *i.p*. at a volume of 0.6 ml kg-1.

4.4 RESULTS AND DISCUSSION

Histamine Adsorption onto CFMs Underlies Capacitative FSCV Current

Histamine has previously been detected in mast cells and neural tissues with FSCV.[11-15] In the majority of these studies, the oxidation peak that appeared at or after the switching potential on the positive wave, as illustrated in **Figure 4.1**, was used for quantification. **Figure 4.1A (i)** is an FSCV color plot during flow injection of histamine (20 µM) onto a CFM with a serotonin sensitive waveform.[18] The interpretation of color plots is described in detail elsewhere,[19] briefly, potential is displayed on the y-axis, time on the x-axis and current in false color and injection time is denoted by the star.

A cyclic voltammogram (CV) taken from the vertical white dashed line of the color plot displays an oxidation peak at around 0.8 V that appears after the switching potential (on the returning positive scan). In previous work, a stimulation-locked signal in the rat substantia nigra (SNr) displayed a similar CV and was pharmacologically determined to be histamine.[15] In the absence of pharmacology however, it is not possible to selectively verify histamine with this waveform, this is because other electroactive species give identical CVs. **Figure 4.1A (ii)** is a color plot taken during FIA of adenosine (10 µM). The corresponding CV (**Figure 4.1B**) is almost identical to that of histamine's. In a region containing both adenosine and

histamine, therefore, it is not possible to distinguish between these analytes electrochemically. Furthermore, other work has shown similar CVs for H_2O_2 and gonatropin-releasing hormone,[20,21] further complicating selective histamine detection.

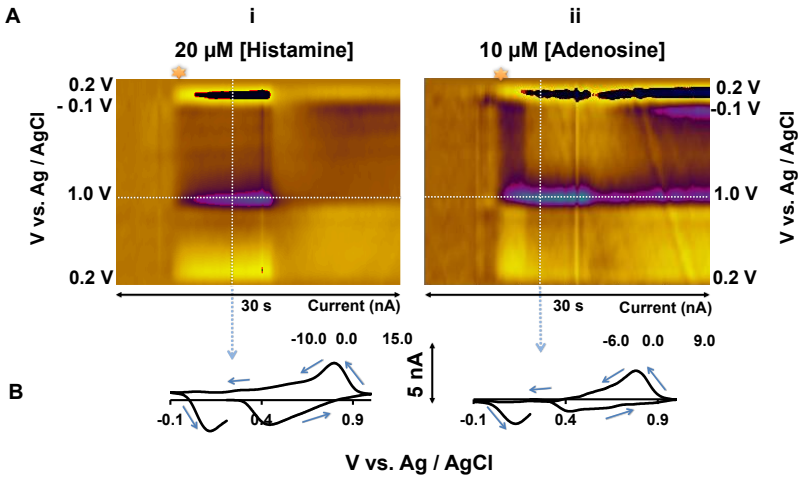

Figure 4.1. ***(A)*** shows color plots for FIA of **(i)** 20 µM histamine **(ii)** 10 µM adenosine. **B)** shows CVs extracted from the vertical dashed lines from **(i)** and **(ii)**.

Histamine electrochemistry is kinetically limited within the oxidation potential window of previously utilized waveforms. In fact, the electrochemical oxidation scheme for histamine is not known, presumably because it involves charge transfer. We therefore postulate that the peaks observed in **Figure 4.1** are due to non-Faradaic processes. These processes arise on the CFM surface when spontaneous adsorption of histamine causes changes in the electrical bilayer. The electrical bilayer on electrode surfaces acts as a capacitor, discharging current into the electrode, particularly at switching potentials. Capacitative or charging currents are a well-known phenomenon in FSCV because of the high scan rates employed.[16] FSCV is background-subtracted, specifically to remove such background charging currents which do not reflect Faradaic processes associated

with analytes of interest. However, adsorption of histamine changes the background capacitative current which cannot be subtracted out, this effect manifests as the features in the CVs in **Figure 4.1**.

In **Figure 4.2**, FIA was utilized to inject histamine (200 µM) onto CFMs while the open field potential was measured vs. Ag/AgCl (**Figure 4.2A**). **Figure 4.2B** shows that the potential of the CFMs rapidly peaks in response to histamine injections. Because there is no driving potential, this implies that histamine spontaneously adsorbs to and changes the potential of the CFM. The features on histamine's CV in **Figure 4.1** are likely a consequence of the current that arises from this adsorption. To further verify this histamine adsorption, Langmuir isotherms were constructed for histamine with a previously described method [22] confirming monolayer coverage of the CFM (**Figure 4.2C**).

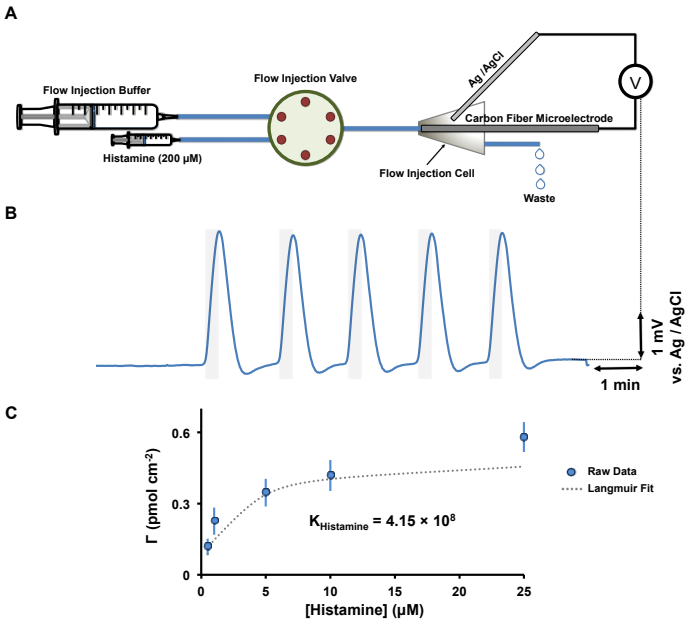

Figure 4.2. ***(A)*** shows the schematic diagram of the experimental setup used for potentiometric experiments. **B)** shows the experimental potentiometric data for five consecutive injections of histamine (200 µM) on CFM. **C)** Langmuir isotherm for histamine adsorption on CFMs in Tris buffer.

While charging current peaks can quantify histamine, little selectivity is offered since many analytes adsorb onto CFMs. We therefore designed a novel waveform to capture histamine electrochemistry before the switching potential.

Histamine Selective Waveform (HSW)

Histamine contains an imidazole ring and an aliphatic amine group. This molecule's ability to readily bind metals such as Cu,[23,24] because of its electronegative sites, means that it is readily amenable to oxidation. However, histamine electro-oxidation differs from serotonin and dopamine in that it likely involves charge transfer. This mechanism introduces kinetic limitations that have not yet enabled stimulation-locked peaks on the positive direction of the wave in FSCV studies. Therefore, preliminary we utilized a triangular waveform and expanded the potential window to cover a large range thereby allowing histamine oxidation to occur within a single scan. Through trial and error, we determined that, *in vitro*, a waveform scanning from -0.7 to 1.1 V (resting at -0.7 V at 600 Vs^{-1}) provided an oxidation peak during the positive scan. However, this waveform was not successful *in vivo*, showing rapid degradation (fouling). By changing the resting potential to -0.5 V, we found that electrode degradation was eliminated, and *in vivo* detection was possible. A possible explanation for this phenomenon is that at -0.7 V, fouling species (e.g. proteins) may preferentially adsorb onto the electrode surface.

Our optimized waveform, the histamine selective waveform (HSW), therefore is -0.7 V to 1.1 V, resting at -0.5 V, with a scan rate of 600 Vs^{-1}. **Figure**

4.3 compares histamine detection with the previously described serotonin waveform[15] to the HSW.

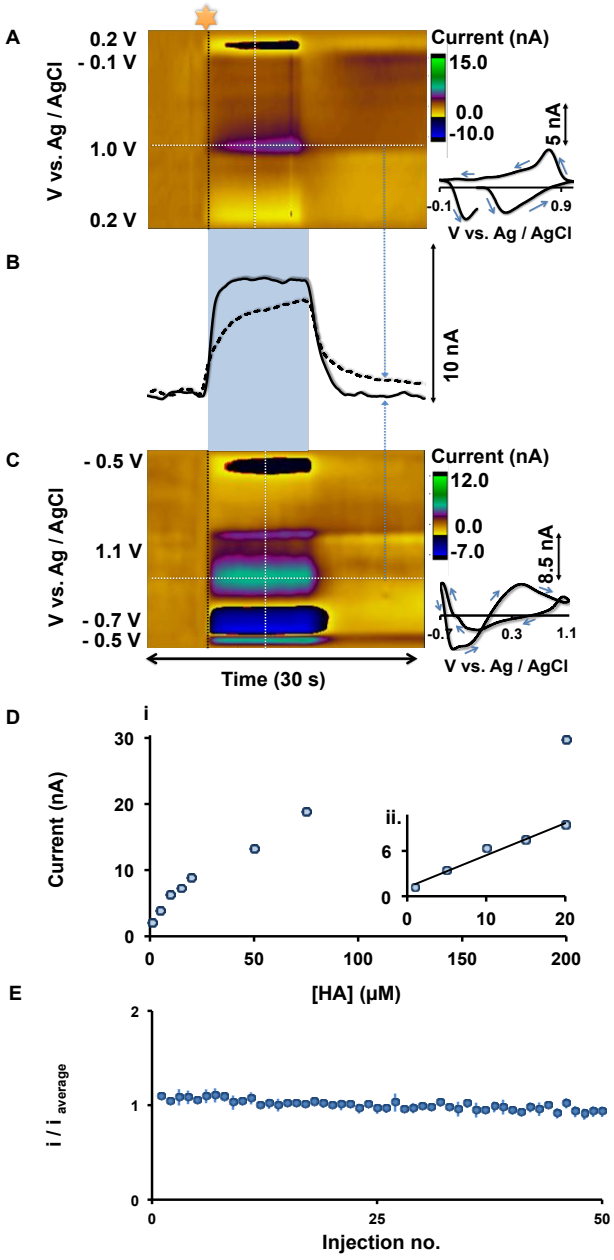

Figure 4.3. ***(A & C)*** show color plots for FIA of 20 μM histamine with the serotonin and HSW waveforms respectively. CVs extracted from vertical dashed lines are shown on the right. **B)** shows current vs. time traces from the horizontal dashed lines from color plots. **D)** shows **(i)** Calibration curve, **(ii)** Linear dynamic range (n=4 ± SEM). **E)** Stability of CFM over 50 consecutive injections of 10 μM histamine (n=4 ± SEM).

Figure 4.3A (serotonin waveform) and **C** (HSW) show color plots and CVs during FIA of histamine (20 µM). The HSW detects histamine oxidation at around + 0.3 V vs. Ag/AgCl, and in contrast to the serotonin waveform, this peak occurs before the switching potential on the positive wave. Furthermore, current vs. time traces, extracted from horizontal dashed lines from the color plots (**Figure 4.3B)**, show that the HSW response is a square injection while the serotonin waveform response does not reach steady state. This makes it possible to more accurately describe histamine *in vivo* kinetics (i.e. histamine clearance kinetics) with the HSW. The HSW has a linear dynamic range up to 20 µM of histamine **(Figure 4.3D (ii)),** a sensitivity of 0.354 ± 0.032 nA/µM and a limit of detection of 1 µM. Finally, histamine measurements with this waveform show good stability, as evidenced by the negligible loss in signal (normalized oxidation current) during 50 successive flow injections of histamine (10 µM) (**Figure 4.3E**).

HSW Selectivity

We sought to develop a waveform to produce a histamine oxidation peak before the switching potential on the positive scan to increase the selectivity of FSCV towards histamine. To assess the selectivity of the waveform *in vitro*, we tested dopamine, serotonin and adenosine, which are electroactive species that are chemically similar to histamine and commonly found in brain regions containing histamine.[25,26,27] **Figure 4** shows CVs obtained during FIA of histamine (20 µM), dopamine (100 nM), serotonin (10 nM) and adenosine (1 µM). These concentrations were chosen to mimic previously reported evoked *in vivo* concentrations.[11,26,28] Adenosine's peak still occurs at the switching potential with

this waveform and is therefore unlikely to interfere. The oxidation peak for histamine appears at around 0.3 V vs. Ag/AgCl (green dashed line) and is in a different position from dopamine and serotonin oxidation peaks (around 0.5 and 0.6 V vs. Ag/AgCl (red and blue dashed lines), respectively).

The HSW therefore shows good selectivity *in vitro*. However, the *in vivo* matrix is far more complicated than can be reproduced on the bench. We next assessed the ability of our novel waveform to measure histamine *in vivo*.

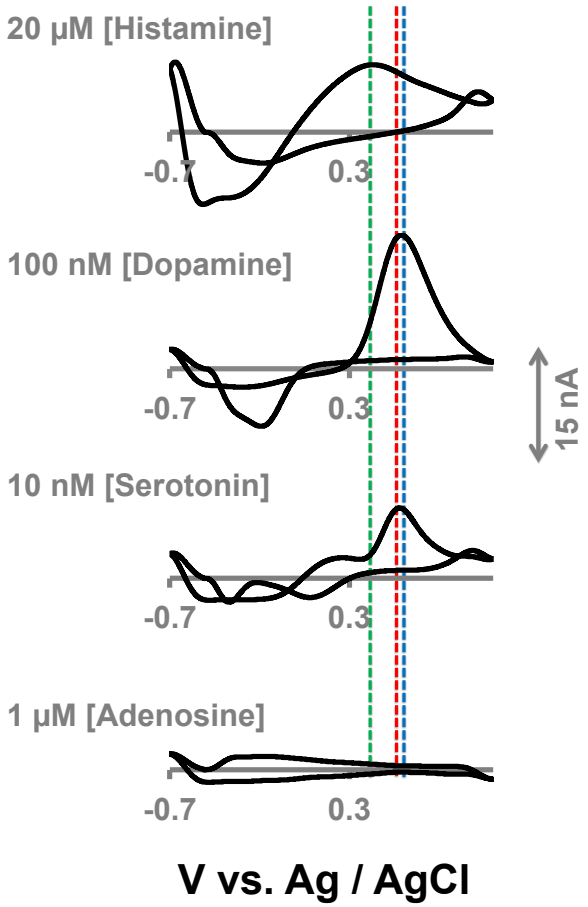

Figure 4.4. CVs for 20 µM histamine, 100 nM dopamine, 10 nM serotonin and 1 µM adenosine with *in vitro* FIA using HSW on CFMs. Vertical dashed lines indicate potential positions of peaks.

In Vivo Histamine

Histamine and serotonin were previously found to be co-released in the SNr upon electrical stimulation of the MFB.[15] We were interested in isolating a histamine signal in a novel physiological circuitry involving the histamine cell bodies. Histamine cell bodies are confined to the posterior hypothalamus, the tuberomamillary nucleus (PM), and send their afferents to the forebrain via the MFB.[29,30,31] By utilizing a retrograde-stimulation[15] of the MFB, we reasoned that we would be able to detect histamine in the PM since histamine has previously been measured in this region with microdialysis.[32]

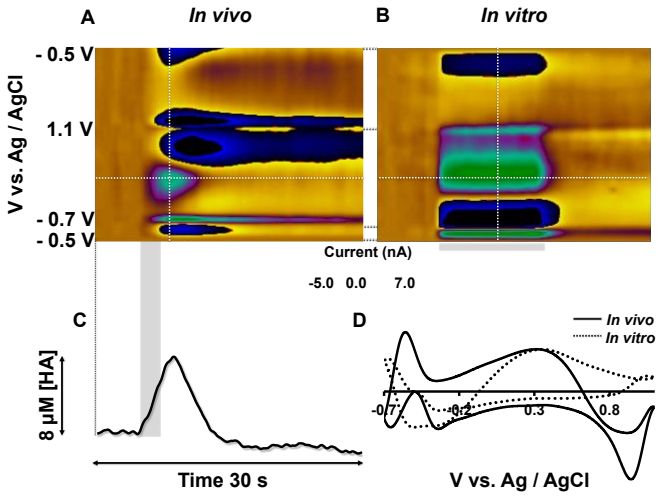

Figure 4.5. ***(A)*** shows a representative colors plot of in the PM upon MFB stimulation. **B)** shows a representative *in vitro* color plot of histamine (20 µM) using FIA. **C)** shows [histamine] vs. time extracted from the horizontal dashed line from color plot **A**. **D)** shows normalized CVs of *in vivo* and *in vitro* (5 µM histamine) signals taken from vertical dashed lines.

Figure 4.5A shows a color plot in the mouse PM upon MFB stimulation (at 5-7 seconds indicated with the blue bar). An event at around 0.3 V vs. Ag/AgCl is clearly visible: a vertical dashed line through the maximum amplitude of this event (at 7 s) provides the CV in **Figure 4.5D**. When a CV collected for histamine *in vitro*

(**Figure 4.5B**) was normalized and superimposed onto this *in vivo* CV, there was very good agreement between the oxidation peaks at 0.3 V. The additional features of the *in vivo* CV are due to the capacitative changes on the electrodes surface because of changes in the *in vivo* environment (ionic fluxes, pH changes). Where it not for the peak at 0.3V, it would be impossible to disentangle histamine's electrochemistry from this other electrochemistry occurring at the switching potential.

Figure 4.5C shows how histamine changes with time, determined by extracting current vs. time from the horizontal dashed line of the color plot and the calibration curve in **Figure 4.3D**. Histamine levels elevate in response to electrical stimulation to around 8 µM and then clear after the stimulation, similar in magnitude to histamine release from mast cells.[11] This profile is similar to dopamine and serotonin reuptake.[10,33] This is an important finding since it implies a similar reuptake system for histamine, however a histamine transporter is yet to be identified.[34]

Although the electrochemistry is supportive of histamine's identity. It is necessary to perform pharmacological experiments to validate the histamine response. Histamine neuropharmacology is not well explored in voltammetry models and there are very few histamine selective compounds that can cross the blood brain barrier. As a first step, we utilized tacrine, a pharmaceutical therapy for Alzheimer's disease. Tacrine is thought to primarily inhibit acetylcholinesterase, however it also is a potent inhibitor of histamine N-methyltransferase (HNMT) (histamine metabolizing enzyme).[35-37] **Figure 4.6** shows the effect on the evoked

PM signal (schematic of circuitry shown in **Figure 4.6A**) upon *i.p.* tacrine (2 mg kg^{-1})[38] administration (n=5 animals ± SEM). Consistent with tacrine's pharmacokinetic profile in rodents,[39] there was a clear effect 50 minutes after administration, whereby the $t_{1/2}$ of histamine clearance increased significantly from 10.9 ± 1.1 s to 15.44 ± 2.6 s (p=0.01) (**Figure 4.6B**). This is an expected result of inhibition of histamine metabolism: because HNMT is located intracellularly, [40, 41] inhibition of this enzyme raises cystolic histamine levels which slows down the reuptake equilibria back into the cell.

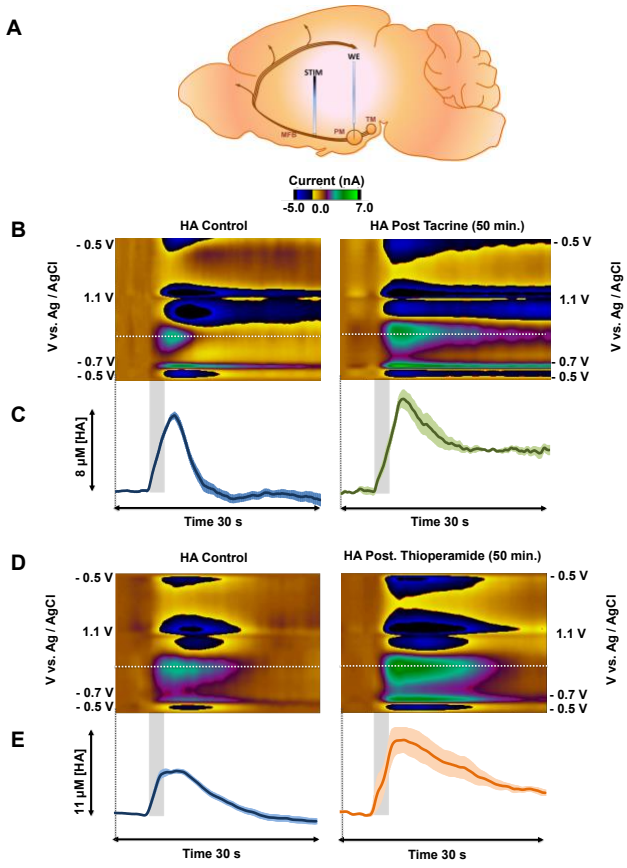

Figure 4.6. *(A)* shows the positions of electrodes (stimulation and CFM) in mouse brain. **B & D** show representative color plots of stimulated release of histamine using HSW - before and after tacrine (2 mg Kg^{-1}) and thioperamide (20 mg Kg^{-1}). **C & E** show concentration vs. time traces extracted from horizontal dashed line from **B & D** respectively, (n=5 ± SEM). The 2 s stimulation starting at 5 s is shown by the blue bar.

Because tacrine is non-selective, we performed a further pharmacological experiment to verify the PM signal. Thioperamide is a selective H3 receptor antagonist. We would expect thioperamide administration to affect the kinetics of histamine release and clearance via inhibition of these histamine autoreceptors in the PM.[42]

Figure 4.6C and **D** show that 50 minutes after thioperamide (20 mg kg^{-1}),[43] there was a pronounced increase in histamine release from 7.9 ± 2.1 to 11.8 ± 4.6 μM (p=0.02). Increases in evoked release have previously been seen with dopamine and autoreceptor antagonism.[44, 45] A significant increase in the $t_{1/2}$ of histamine clearance was also observed from 13.3 ± 3.4 s to 18.8 ± 3.2 s (p=0.03), which was seen in prior studies with serotonin autoreceptor antagonism.[10] The time course of this experiment is also consistent with thioperamide's pharmacokinetics in rodents.[46]

These pharmacological experiments, in addition to the electrochemical characterization allow us to confidently verify the histamine nature of this signal in the PM.

4.5 CONCLUSION

Histamine has important, but not well studied roles as a neurotransmitter. FSCV is an ideal tool for histamine detection because of its sensitivity, selectivity and high temporal resolution. Previous FSCV studies have not been able to selectively identify histamine because the CV features were due to capacitative processes on the electrode surface that are not selective. Here, we developed the HSW that provides a robust

oxidation peak before the switching peak. We described *in vitro* waveform optimization and a novel *in vivo* physiological model for retrograde stimulation of histamine release in the mouse PM. We verified this signal pharmacologically as histamine. This novel FSCV method will enable detailed *in vivo* characterizations of this important neuromodulator.

4.6 ACKNOWLEDGEMENTS

The authors would like to thank Ellen Strawsine for technical assistance. WSU funded this research. A Rumble fellowship supported Srimal Samaranayake.

4.7 REFERENCES

(1) Robinson, D. L.; Venton, B. J.; Heien, M. L.; Wightman, R. M. *Clinical chemistry* **2003**, *49*, 1763.

(2) Howe, M. W.; Tierney, P. L.; Sandberg, S. G.; Phillips, P. E.; Graybiel, A. M. *Nature* **2013**, *500*, 575.

(3) Ford, C. P.; Gantz, S. C.; Phillips, P. E.; Williams, J. T. *The Journal of neuroscience : the official journal of the Society for Neuroscience* **2010**, *30*, 6975.

(4) Hashemi, P.; Dankoski, E. C.; Petrovic, J.; Keithley, R. B.; Wightman, R. M. *Analytical Chemistry* **2009**, *81*, 9462.

(5) Park, J.; Kile, B. M.; Wightman, R. M. *Eur J Neurosci* **2009**, *30*, 2121.

(6) Wood, K. M.; Hashemi, P. *ACS Chem Neurosci* **2013**.

(7) Hashemi, P.; Dankoski, E. C.; Lama, R.; Wood, K. M.; Takmakov, P.; Wightman, R. M. *Proc Natl Acad Sci U S A* **2012**, *109*, 11510.

(8) Park, J.; Takmakov, P.; Wightman, R. M. *J Neurochem* **2011**, *119*, 932.

(9) Park, J.; Bucher, E. S.; Fontillas, K.; Owesson-White, C.; Ariansen, J. L.; Carelli, R. M.; Wightman, R. M. *Biol Psychiatry* **2013**.

(10) Wood, K. M.; Zeqja, A.; Nijhout, H. F.; Reed, M. C.; Best, J.; Hashemi, P. *J Neurochem* **2014**.

(11) Pihel, K.; Hsieh, S.; Jorgenson, J. W.; Wightman, R. M. *Anal Chem* **1995**, *67*, 4514.

(12) Pihel, K.; Hsieh, S.; Jorgenson, J. W.; Wightman, R. M. *Biochemistry* **1998**, *37*, 1046.

(13) Travis, E. R.; Wang, Y. M.; Michael, D. J.; Caron, M. G.; Wightman, R. M. *Proc Natl Acad Sci U S A* **2000**, *97*, 162.

(14) Chang, S. Y.; Jay, T.; Munoz, J.; Kim, I.; Lee, K. H. *Analyst* **2012**, *137*, 2158.

(15) Hashemi, P.; Dankoski, E. C.; Wood, K. M.; Ambrose, R. E.; Wightman, R. M. *J Neurochem* **2011**, *118*, 749.

(16) Bard, A.; Faulkner, L. *Electrochemical Methods: Fundamentals and Applications*; John Wiley & Sons, Inc, 2001.

(17) Pathirathna, P.; Samaranayake, S.; Atcherley, C. W.; Parent, K. L.; Heien, M. L.; McElmurry, S. P.; Hashemi, P. *Analyst* **2014**, *139*, 4673.

(18) Jackson, B. P.; Dietz, S. M.; Wightman, R. M. *Anal Chem* **1995**, *67*, 1115.

(19) Michael, D.; Travis, E. R.; Wightman, R. M. *Anal Chem* **1998**, *70*, 586A.

(20) Sanford, A. L.; Morton, S. W.; Whitehouse, K. L.; Oara, H. M.; Lugo-Morales, L. Z.; Roberts, J. G.; Sombers, L. A. *Analytical chemistry* **2010**, *82*, 5205.

(21) Glanowska, K. M.; Venton, B. J.; Moenter, S. M. *The Journal of neuroscience : the official journal of the Society for Neuroscience* **2012**, *32*, 14664.

(22) Pathirathna, P.; Yang, Y.; Forzley, K.; McElmurry, S. P.; Hashemi, P. *Anal Chem* **2012**, *84*, 6298.

(23) Torreggiani, A.; Tamba, M.; Bonora, S.; Fini, G. *Biopolymers* **2003**, *72*, 290.

(24) Xerri, B.; Flament, J.-P.; Petitjean, H.; Berthomieu, C.; Berthomieu, D. *The Journal of Physical Chemistry B* **2009**, *113*, 15119.

(25) RICHELSON, E. *Journal of clinical psychopharmacology* **1996**, *16*, 1S.

(26) Heien, M. L. A. V.; Khan, A. S.; Ariansen, J. L.; Cheer, J. F.; Phillips, P. E. M.; Wassum, K. M.; Wightman, R. M. *Proceedings of the National Academy of Sciences of the United States of America* **2005**, *102*, 10023.

(27) van Dijk, A.; Klompmakers, A. A.; Feenstra, M. G. P.; Denys, D. *Journal of Neurochemistry* **2012**, *123*, 897.

(28) Swamy, B. E.; Venton, B. J. *Anal Chem* **2007**, *79*, 744.

(29) *Histamine in the Nervous System*, 2008; Vol. 88.

(30) Vanhala, A.; Yamatodani, A.; Panula, P. *The Journal of comparative neurology* **1994**, *347*, 101.

(31) Auvinen, S.; Panula, P. *The Journal of comparative neurology* **1988**, *276*, 289.

(32) Russell, W. L.; Henry, D. P.; Phebus, L. A.; Clemens, J. A. *Brain Res* **1990**, *512*, 95.

(33) Wu, Q.; Reith, M. E. A.; Wightman, R. M.; Kawagoe, K. T.; Garris, P. A. *Journal of Neuroscience Methods* **2001**, *112*, 119.

(34) Hough, L. B. *Progress in neurobiology* **1988**, *30*, 469.

(35) Morisset, S.; Traiffort, E.; Schwartz, J. C. *Eur J Pharmacol* **1996**, *315*, R1.

(36) Musial, A.; Bajda, M.; Malawska, B. *Curr Med Chem* **2007**, *14*, 2654.

(37) Taraschenko, O. D.; Barnes, W. G.; Herrick-Davis, K.; Yokoyama, Y.; Boyd, D. L.; Hough, L. B. *Methods Find Exp Clin Pharmacol* **2005**, *27*, 161.

(38) Nishibori, M.; Oishi, R.; Itoh, Y.; Saeki, K. *Japanese journal of pharmacology* **1991**, *55*, 539.

(39) Telting-Diaz, M.; Lunte, C. E. *Pharmaceutical research* **1993**, *10*, 44.

(40) Maintz, L.; Novak, N. *Am J Clin Nutr* **2007**, *85*, 1185.

(41) Pollard, H.; Bischoff, S.; Schwartz, J. C. *J Pharmacol Exp Ther* **1974**, *190*, 88.

(42) Brown, R. E.; Stevens, D. R.; Haas, H. L. *Progress in neurobiology* **2001**, *63*, 637.

(43) Bernaerts, P.; Lamberty, Y.; Tirelli, E. *Behavioural Brain Research* **2004**, *154*, 211.

(44) Kita, J. M.; Parker, L. E.; Phillips, P. E.; Garris, P. A.; Wightman, R. M. *J Neurochem* **2007**, *102*, 1115.

(45) Clark, D.; Exner, M.; Furmidge, L. J.; Svensson, K.; Sonesson, C. *European journal of pharmacology* **1995**, *275*, 67.

(46) Bordi, F.; Mor, M.; Plazzi, P. V.; Silva, C.; Caretta, A.; Morini, G. *Farmaco (Societa chimica italiana : 1989)* **1992**, *47*, 1095.

CHAPTER 5: A VOLTAMMETRIC AND MATHEMATICAL ANALYSIS OF HISTAMINERGIC MODULATION OF SEROTONIN IN THE MOUSE HYPOTHALAMUS

Reprinted with permission from Journal of Neurochemistry

Samaranayake, S.; **Abdalla, A.;** Robke, R.; Nijhout, H. F.; Reed, M. C.; Best, J.; Hashemi, P., A Voltammetric and Mathematical Analysis of Histaminergic Modulation of Serotonin in the Mouse Hypothalamus. J Neurochem 2016, 138 (3), 374 - 383

I contributed both experimentally and intellectually towards this project

5.1 ABSTRACT

Histamine and serotonin are neuromodulators which facilitate numerous, diverse neurological functions. Being co-localized in many brain regions, these two neurotransmitters are thought to modulate one another's chemistry and are often implicated in the etiology of disease. Thus, it is desirable to interpret the *in vivo* chemistry underlying neurotransmission of these two molecules to better define their roles in health and disease. In this work, we describe a voltammetric approach to monitoring serotonin and histamine simultaneously in real time. Via electrical stimulation of the axonal bundles in the medial forebrain bundle, histamine was evoked in the mouse premammillary nucleus. We found that histamine release was accompanied by a rapid, potent inhibition of serotonin in a concentration dependent manner. We developed mathematical models to capture the experimental time courses of histamine and serotonin, which necessitated incorporation of an inhibitory receptor on serotonin neurons. We employed pharmacological experiments to verify that this serotonin inhibition was mediated by H_3 receptors. Our novel approach provides fundamental mechanistic insights that can be used to examine the full extent of interconnectivity between histamine and serotonin in brain.

5.2 INTRODUCTION

Serotonin and histamine are neuromodulators thought to carry a variety of roles in the brain [1-3]. These two modulators are co-localized in many brain regions [4,5] and are postulated to closely modulate one another [6,7]. However, while there is much focus on serotonin's roles in affective, sleep and cognition processes [8,9], histamine's contribution to the same processes remains relatively neglected. In recent years, we established fast scan cyclic voltammetry (FSCV) at carbon fiber microelectrodes (CFMs) to investigate *in vivo* serotonin dynamics [10]. We are systematically studying the array of *in vivo* processes that regulate serotonin extracellular levels [11,12] with the ultimate goal of identifying distinct mechanistic abnormalities that underlie different pathophysiological states. Because of histamine's close association with serotonin, in particular the electrophysiological, histological and slice voltammetry studies that imply histamine inhibits serotonin release [6,13-15] we now find it of great importance to direct our efforts to voltammetrically defining histamine and serotonin co-modulation *in vivo*.

In this paper, we extend on recent work where we described the first voltammetrically selective waveform for real time FSCV histamine measurements *in vivo* in the mouse [16], to detail simultaneous *in vivo* measurements of serotonin and histamine. To achieve this, CFMs were implanted in the mouse premammillary nucleus (PM), a hypothalamic region rich in serotonin and histamine [4,5,17]. To assess the effects of histamine release on endogenous serotonin chemistry, we identified a discrete location in the medial forebrain bundle (MFB) that, when electrically stimulated, evoked histamine but not serotonin in the PM. This robust

experimental model allowed us to observe histamine release rapidly followed by potent, long lasting serotonin inhibition. We found that both histamine release and serotonin inhibition were dependent on stimulation parameters in a manner that indicated an inversely correlative relationship. We mathematically modeled both responses and found that an inhibitory receptor term was necessary to fit both sets of data. We postulated that this inhibitory receptor was the H_3 receptor and provided pharmacological evidence, in the form of manipulations with thioperamide, an H_3 receptor antagonist, in favor of our hypothesis.

We thus provide not only an important technological advance, but our physiological findings also represent an opportunity to more closely scrutinize histamine's roles in controlling serotonin chemistry in the context of disease.

5.3 MATERIALS AND METHODS

Chemicals and Reagents

Standard solutions were prepared by dissolving histamine dihydrochloride and serotonin hydrochloride (Sigma-Aldrich, Co., MO, USA) respectively in Tris-buffer. Tris-buffer was constituted thus: 15 mM $H_2NC(CH_2OH)_2$.HCl, 140 mM NaCl, 3.25 mM KCl, 1.2 mM $CaCl_2$, 1.25 mM $NaH_2PO_4.H_2O$, 1.2 mM $MgCl_2$ and 2.0 mM Na_2SO_4 (EMD Chemicals Inc. NJ, USA) in deionized water at pH=7.4 Thioperamide maleate (2, 20, or 200 mg kg^{-1}) from TOCRIS bioscience (Bristol, UK) was dissolved in sterile saline and administered via intra-peritoneal injection at a volume of 0.6 ml kg^{-1}.

Carbon-Fiber Microelectrodes (CFMs)

CFMs were fabricated employing 7µm diameter carbon-fibers (Goodfellow Corporation, PA, USA) aspirated into glass capillaries (0.6 mm external diameter, 0.4 mm internal diameter, A-M systems, Inc., Sequim, WA). A carbon-glass seal was formed using vertical micropipette puller (Narishige Group, Tokyo, Japan). The exposed length of the carbon fiber was trimmed to 150 µm under an optical microscope. Microelectrodes were electroplated with Nafion as described previously [10].

Data Collection

Waveform generation, data acquisition and signal processing were achieved by a commercial potentiostat (Dagan corp.), custom-built hardware, software written in house using LabVIEW 2009 and interfacing a PCIe-6341 DAC/ADC card (National Instruments, Austin, TX). Custom built software was employed to drive the hardware and perform data analysis including background subtraction, signal averaging and digital filtering (Knowmad Technologies LLC, Tucson, AZ). All potentials are quoted with respect to Ag/AgCl reference electrodes, which were fabricated via electrodeposition of Cl^- by holding a silver wire (A-M systems, WA) at 4.0 V for 5 s in 1 M HCl. All data represented with error bars represent the standard error of the mean (SEM).

Data Analysis

All the Current vs time data were extracted from custom made software. Histamine current was transferred to its concentration using 2.825 µM/nA factor. Conversion factor for serotonin was 11 nM/nA. Statistical differences were

obtained using one-tailed Student's *t*-tests on paired data sets. ($p < 0.05$ was taken as significantly different)

Data Modeling

Simulations were carried out in MatLab R2014a (MathWorks, Natick, MA, USA) using ODE solver ode23s, implemented on an iMac with operating system OS X Version 10.6.8. We modeled our experimental data with two differential equations:

$$\frac{d[eha]}{dt} = A_{H3}(t)\,fire_{ha}(t)[vha] - V_u([eha]) + a_1[cha] - V_{ug}([eha]) - a_2[gha] \quad (1)$$

The left-hand side is the rate of change of the extracellular histamine [eha]. The first term on the right side multiplies the fractional release, $A_{H3}(t)$, caused by autoreceptor inhibition by the firing rate, $fire_{ha}(t)$, and the vesicular histamine concentration, [uha]. The remaining terms are reuptake into the terminal, $V_u([eha])$, leakage from the terminal, $a_1[cha]$, uptake into glial cells, $V_{ug}([eha])$, and leakage from the glial cells, $a_2[gha]$. There is a similar differential equation for serotonin in the extracellular space:

$$\frac{d[e5ht]}{dt} = A_{H3}^{5ht}(t)\,fire_{5ht}(t)[v5ht] - V_{sert}([e5ht]) + a_3[c5ht] - V_{ug}([e5ht]) - a_4[g5ht] \quad (2)$$

The term A_{H3}^{5ht} is the time course of fractional serotonin release caused by the H_3 receptors on serotonin neurons. All other terms in equation 2 are analogous to the terms in equation 1.

Flow Injection Analysis

Flow injection analysis *(FIA)* was used for *in vitro* analyses. CFMs were inserted into a flangeless short 1/8 nut (PEEK P-335, IDEX, Middleboro, MA) in order for 2 mm of the tip to be exposed outside of the nut. The microelectrode-containing nut was then fastened into a modified HPLC union elbow (PEEK 3432, IDEX, Middleboro, MA). The other end of the elbow union was fastened into the out-flowing stream of the FIA buffer and incorporation of the reference electrode and for a 'waste' flow stream by drilling into the union. *In vitro* experiments were carried out at 2 mL min^{-1} flow rate using syringe infusion pump (kd Scientific, model KDS-410, Holliston, MA). Starting at 5s, a rectangular pulse of analyte was introduced into the buffer stream for 10 s via a six-port HPLC loop injector (Rheodyne model 7010 valve, VICI, Houston, TX). In order to avoid carry-over effects, analytes were injected randomly.

Animal Surgeries

Handling and surgery on male C57BL/6J mice weighing 20−25 g (Jackson Laboratory, Bar Harbor, ME) were in agreement with University of South Carolina Guide for the Care and Use of Laboratory Animals, approved by the Institutional Animal Care and Use. Urethane (25% dissolved in 0.9% NaCl solution, Hospira, Lake Forest, IL) was injected intraperitoneally (*i.p*) and once deep anesthesia was confirmed, animals were secured into a stereotaxic instrument (David Kopf Instruments, Tujunga, CA) and stereotaxic surgery was performed. A heating pad sustained mouse body temperature around 37 °C (Braintree Scientific, Braintree, MA). Stereotaxic coordinates were taken in reference to bregma. A Nafion

modified CFM was in the PM (AP: −2.45, ML: +0.50, DV: −5.45 to −5.55.). A stainless steel stimulating electrode (diameter: 0.2 mm, Plastics One, Roanoke, VA) was positioned into the MFB (AP: -1.07, ML: +1.10, DV: −5.00). Biphasic pulse trains applied through a linear constant current stimulus isolator (NL800A, Neurolog, Medical Systems Corp., Great Neck, NY) provoked histamine efflux. The 60 Hz trains were 350 μA each phase, 2 ms in width, and 2 s in length. To determine the effects of different stimulation parameters on histamine and serotonin, stimulation frequency, width and amplitude were systematically altered. The time in between stimulations (2 minutes) was determined sufficient to produce negligible effects on serotonin and histamine in subsequent stimulations. A Ag/AgCl reference electrode (constructed by plating Cl^- ions onto a Ag wire) was implanted into the brain's opposite hemisphere.

5.4 RESULTS

Simultaneous Measurements of Serotonin and Histamine

In this experiment, we implanted a CFM in the PM of an anesthetized mouse and electrically stimulated the MFB. A representation of this experimental model, illustrating the relative positions of the working and stimulations electrodes can be found in **Figure 5.1A (i)**. Directly underneath this, in **Figure 5.1B (i),** is a raw data color plot showing the resultant electrochemical signal at the CFM. The interpretation of color plots is described elsewhere in detail [18]. Concisely, background subtracted cyclic voltammograms collected at 10 Hz for 30 seconds are displayed as voltage (y-axis) vs. time (x-axis) and current (false color). The green bar directly under the color plot denotes the occurrence and duration of the

electrical stimulation. Upon stimulation there are several events, typical of *in vivo* FSCV measurements whereby other electroactive species, pH changes and ionic fluxes affect the measurement [19,20]. Of interest is the discrete event occurring at 0.3 V which is denoted by the horizontal dashed line and the blue star. A cyclic voltammogram (CV) extracted from the vertical dashed line through this event is displayed in **Figure 5.1C (i)** (solid line).

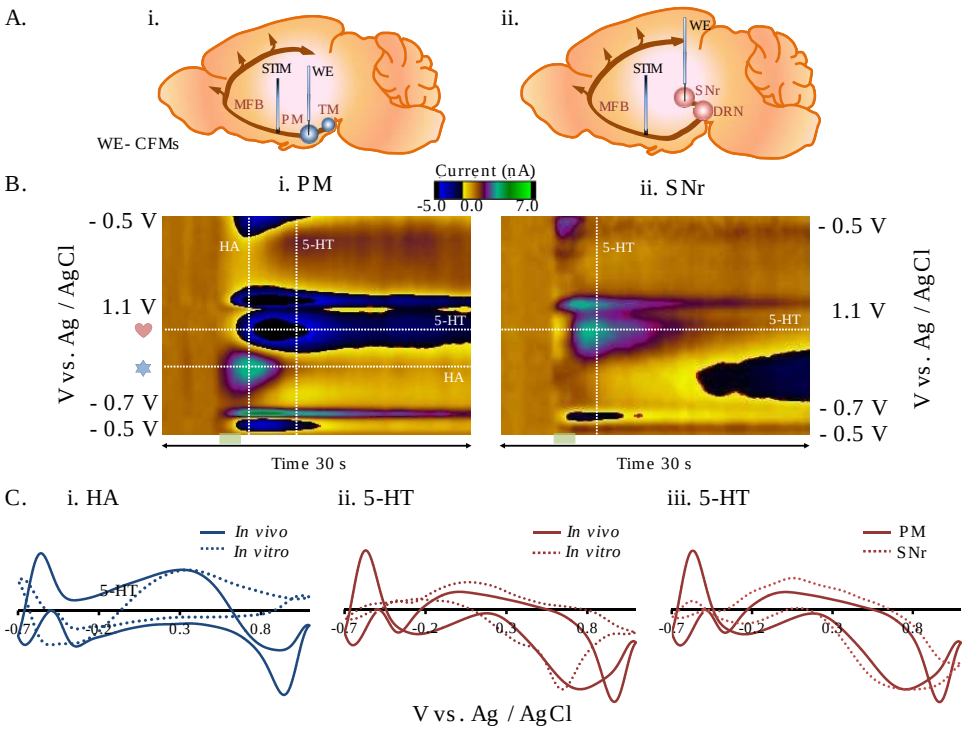

Figure 5.1. (Ai & Aii) The position of electrodes (stimulation and CFM) in mouse brain. **B(i) & B(ii)** Representative color plots of the stimulated release of histamine and serotonin in the premammillary nucleus (PM) and stimulated release of serotonin in the substantia nigra (SNr) respectively. (Ci & ii) Superimposed cyclic voltammograms of *in vivo* and *in vitro* histamine and serotonin signals taken from vertical dashed lines in the PM. **Ciii)** Comparison of normalized CVs of *in vivo* serotonin signals taken from vertical dashed lines in both PM and SNr. HA= histamine, 5-HT = serotonin.

The oxidation peak at 0.3 V shows excellent agreement with the oxidation peak extracted from an *in vitro* injection of histamine (dashed) normalized to maximum current and superimposed onto this *in vivo* CV. In our prior work, we showed electrochemically and pharmacologically that this event is histamine release [16]. Histamine's electro-oxidation scheme has not yet been described. It is likely that the peak at 0.3V occurs because of a proton transfer type oxidation between the aliphatic amine group and imidazole amine group in the histamine molecule. Because this is an internal proton transfer oxidation, it follows that it should occur at a potential lower than observed for classic serotonin and dopamine electrooxidation (i.e. 0.6 - 0.8 V) [21].

An additional event of interest occurs at around 0.7 V and is denoted by the horizontal dashed line and red heart. Because FSCV is background subtracted, ambient levels cannot be determined, thus according to the false color scale, this event signals a decrease in concentration. A CV collected at the vertical dashed line through this event is presented in **Figure 5.1C (ii)**. A CV taken from an *in vitro* injection of serotonin was inverted on the current axis (to mimic a decrease in concentration), normalized to maximum current and superimposed (dashed) onto the *in vivo* CV. The good agreement between the peaks at 0.7 V strongly implies that this event is caused by serotonin. To further confirm this notion, we made a measurement of serotonin with this waveform via an experimental model of MFB stimulation and measurement in the substantia nigra pars reticulata (SNr) that we have well established for serotonin FSCV [22]. This experimental model is depicted in **Figure 5.1A (ii)** and the color plot arising from the *in vivo* experiment is shown

in **Figure 5.1B (ii).** The stimulated serotonin event occurs at the same horizontal (potential) position on the color plot. The CV extracted from this color plot, inverted, normalized to maximum current and superimposed to the *in vivo* CV collected in the PM shows in excellent agreement in **Figure 5.1C (iii)**.

Serotonin Inhibition Following Histamine Release

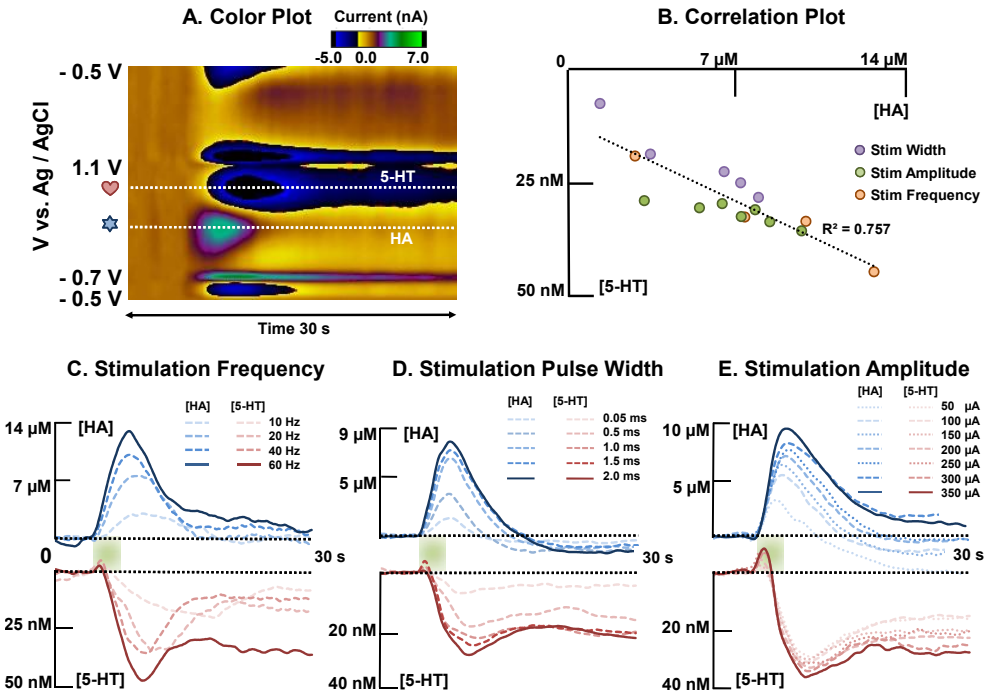

Figure 5.2. (A) Representative color plot of the stimulated release of histamine and serotonin inhibition in the PM. **(B)** Correlation plot between [histamine] and [serotonin] for all stimulation parameters. **(C)** Averaged current vs. time traces along the two horizontal dashed lines of histamine and serotonin with respect to different stimulation frequencies (n=5). **(D)** Averaged current responses to various stimulation pulse widths of histamine and serotonin (n=5). **(E)** Averaged current responses to various stimulation amplitudes of histamine and serotonin (n=5). [HA] = [histamine], [5-HT] = [serotonin].

The event immediately following histamine release proceeds in the negative false color current direction. FSCV cannot determine basal concentrations (*vide supra*) thus one can only determine changes from ambient levels. This result,

therefore, is indicative of a reduction in the ambient concentration of serotonin after stimulation. **Figure 5.2A** is a representative color plot showing simultaneous histamine release and serotonin inhibition in the PM upon MFB stimulation. **Figure 5.2C-E** shows serotonin and histamine concentrations with time for different stimulation parameters (dark solid lines = maximum responses and lighter dashed lines = lower responses) extracted from the horizontal dashed lines from the color plot (n=5 animals). The decrease in serotonin concentration is delayed around 2 seconds with respect to histamine release, implying that serotonin inhibition may be dependent on histamine release. To probe this notion, we systematically altered stimulation parameters to assess whether the profile of histamine release affects serotonin inhibition. The dark solid line shows the maximum responses for the 60 Hz stimulation frequency in **Figure 5.2C**. The lighter colored dashed lines in **Figure 5.2C** shows the result of altering the stimulation frequency from 10 - 40 Hz (n=5 animals). There is a clear correlation between histamine release and the serotonin inhibition profiles. This is apparent in terms of both time course (i.e. 10 Hz stimulation leading to lower, more prolonged histamine release and subsequent serotonin inhibition) and amplitude (higher level of histamine release corresponds to higher level of serotonin inhibition). This pattern holds true for stimulation pulse width and amplitude (**Figure 5.2D and E**) (n=5 animals). In **Figure 5.2B**, the relationship between histamine release and serotonin inhibition was more formally explored by directly plotting amplitude of histamine release vs. amplitude of serotonin inhibition for the three stimulation parameters explored. We found a

linear relationship (R^2 = 0.757) connecting histamine release to serotonin inhibition for all three parameters explored.

Mathematical Modeling of Serotonin and Histamine Co-regulation

We needed to vary only three functions, $fire_{ha}(t)$, $A_{H3}(t)$, and A_{H3}^{5ht}(t), from equations 1 and 2 to obtain excellent model fits to our experimental data. **Figures 5.3A** and **B** show the model fits (dotted lines) to the experimental curves (solid lines) for control and 20 mg kg^{-1} thioperamide, respectively. Thioperamide selectively acts as an H_3 receptor (auto and hetero) antagonist on both histamine and serotonin pre-synaptic neurons [23]. In our model, the electrical stimulation is mimicked by raising $fire_{ha}(t)$ above its tonic level of 5 spikes/sec. **Figure 5.3C** shows $fire_{ha}(t)$ vs. time that best fits the control and thioperamide experiments. $fire_{ha}(t)$ returns to baseline at 9 seconds and the rates are higher after thioperamide.

To fit the slow decline in histamine after stimulation, it was necessary to incorporate an autoreceptor function as per our previous serotonin model [12] **Figure 5.3D** shows fractional histamine release, $A_{H3}(t)$, as a function of H_3 autoreceptors activation following stimulation before and after thioperamide. In the control experiment, tonic inhibition was $A_{H3}(t)$= 0.7 up to 9 seconds, then dropped to $A_{H3}(t)$= 0 up to 15 seconds (complete inhibition), and then returned to $A_{H3}(t)$= 0.4 from 15 seconds to 30 seconds. For thioperamide, $A_{H3}(t)$= 0.9, and the smallest fractional release is $A_{H3}(t)$ = 0.5. Our model shows that the H_3 autoreceptor effect is delayed (starting at 9 seconds) and lasts throughout our file collection window (30 seconds).

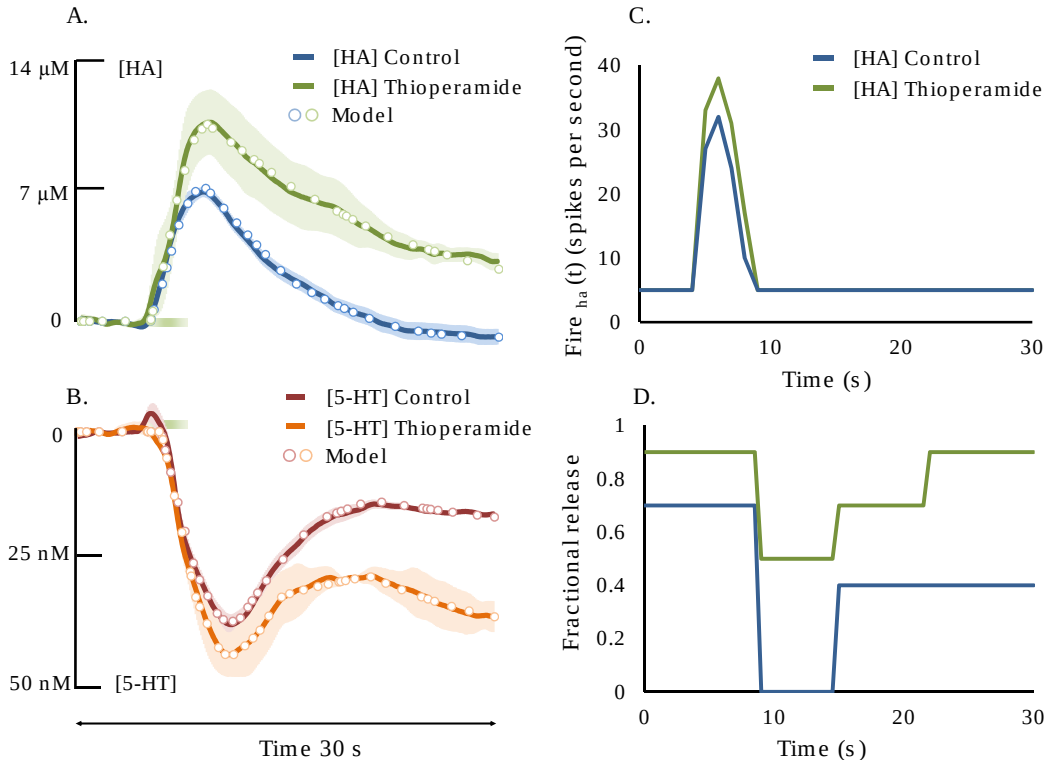

Figure 5.3. (A) [Histamine] vs. time plots comparing *in vivo* (solid traces) and the results of the mathematical model (large dots) in the control case. (B) [Serotonin] vs. time plots comparing *in vivo* (solid traces) and the results of the mathematical model (large dots) in the presence of thioperamide (20 mg kg^{-1}) (C) Firing rate of the histamine neurons as a function of time in the two cases control (blue) and drug (green), respectively. (D) Assumed fractional release of histamine from the histamine neurons as a function of time in the two cases. [HA] = [histamine], [5-HT] = [serotonin].

We next modeled our serotonin curves. Since the serotonin neurons are not stimulated, $fire_{5ht}(t)$ remains at a tonic level of 5 spikes/sec. We varied A_{H3}^{5ht}(t) (fraction of serotonin release permitted by the H_3 receptors on serotonin neurons). For the control experiment, A_{H3}^{5ht}(t) starts at 0.9, goes down to 0.45, and then returns to 0.9. For thioperamide, A_{H3}^{5ht}(t) starts at 0.9, goes down to 0.36, and then returns to 0.8 at 30 seconds (graphs not shown). As above, the H_3 receptor effect is prolonged throughout file collection (> 60 seconds).

H_3 Receptor Mediated Inhibition of Serotonin

Three different doses of thioperamide, an H_3 receptor antagonist [23], were administered to different groups of mice. This agent's effects on histamine release and serotonin inhibition was observed 50 minutes after administration, which is a sufficient time period for thioperamide to exert its effects [24,25]. The results are shown in **Figure 5.4**. Here, histamine before drug is displayed in blue and after drug in green, serotonin before drug is red, and after drug is orange. Error bars showing SEM (n=5 ± SEM) are lighter versions of these respective colors.

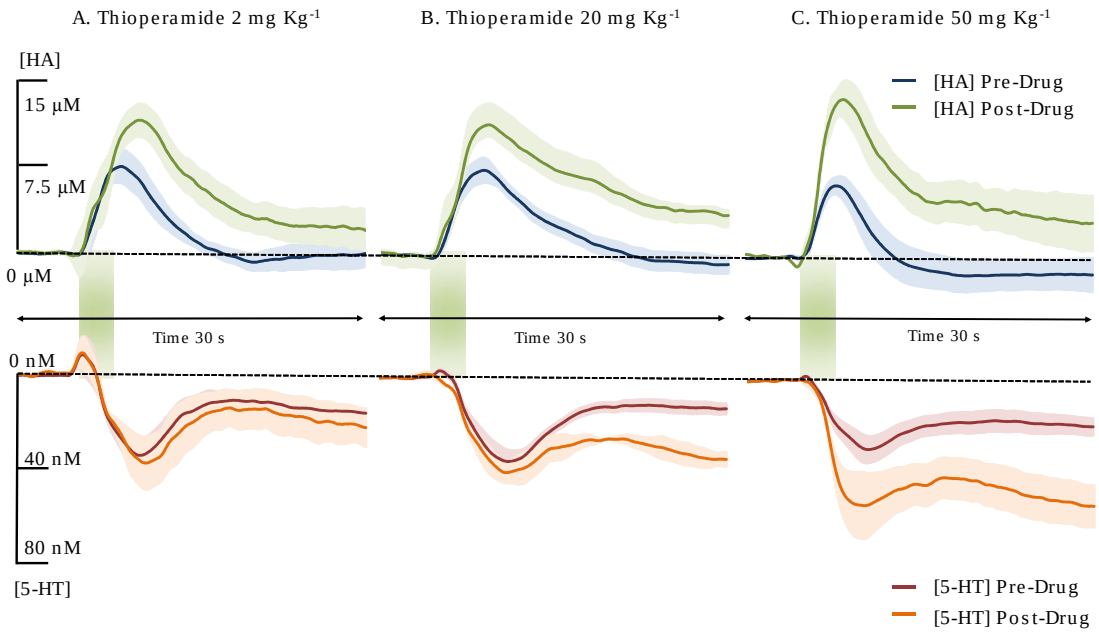

Figure 5.4. [Histamine] vs time traces are shown in blue and green for pre and post drug administration respectively. [Serotonin] vs time traces are shown in red and orange for before and after the drug. Error bars showing SEM (n=5 ± SEM) are lighter versions of these respective colors. **(A)** thioperamide 2 $mgKg^{-1}$ **(B)** thioperamide 20 $mgKg^{-1}$ **(C)** thioperamide 50 $mgKg^{-1}$. [HA] = [histamine], [5-HT] = [serotonin].

Thioperamide, administered at 2 mg kg^{-1} caused a significant increase in the amplitude of histamine release from 7.5 ± 1.4 µM to 11.5 ± 1.4 µM (p = 0.004),

but not in rate of histamine clearance ($t_{1/2}$ from 11.5 ± 1.5 s to 14.3 ± 2.4 s, p = 0.07). The effects of 2 mg kg^{-1} on the amplitude and time course of serotonin inhibition were negligible. Maximum serotonin inhibition changed from 34.2 ± 7.5 nM to 37.5 ± 11.9 nM (p = 0.55), whereas, inhibition at 30 s enhanced from 15.8 ± 1.5 nM to 22.1 ± 8.9 nM (p = 0.31). Thioperamide administered at 20 mg kg^{-1} dose affected both the amplitude and clearance time of histamine response. Histamine elevated from 7.9 ± 2.1 µM to 11.9 ± 4.2 µM (p = 0.03) and $t_{1/2}$ from 14.7 ± 2.8 s to 19.6 ± 2.3 s (p = 0.02), but only the time course of the serotonin response (maximum inhibition from 38.8 ± 5.01 nM to 44.8 ± 4.5 nM (p = 0.31). Furthermore, serotonin inhibition at 30 s increases from 16.5 ± 5.3 nM to 37.7 ± 9.6 nM, (p = 0.002). At the highest dose, thioperamide greatly affected histamine release from 6.8 ± 1.9 µM to 14.3 ± 4.1 µM (p = 0.006) and reuptake such that histamine does not return to baseline during the 30 second file acquisition window. The effects on serotonin are also highly significant. Maximum inhibition elevated from 37.3 ± 9.6 nM to 68.2 ± 20.0 nM (p = 0.04), whereas, inhibition at 30 s enhanced from 24.4 ± 7.9 nM to 65.9 ± 14.8 nM (p = 0.03).

5.5 DISCUSSION

FSCV: A Powerful Tool for Simultaneous, Real-time Serotonin and Histamine Measurements

FSCV at CFMs is a powerful tool for neurotransmitter analysis because of FSCV's rapid, sensitive and selective analysis capabilities in addition to the minimally invasive dimensions of CFMs. A traditional drawback of FSCV is its limited *in vivo* analytical scope (measuring primarily dopamine) [26-28], which has

been systematically challenged in recent years via advances to measure serotonin [10], adenosine [29], H_2O_2 [30] and gonadotropin-releasing hormone [31]. We are primarily interested in deciphering the *in vivo* dynamics that regulate extracellular serotonin levels, and we were thus oriented towards histamine. There is a significant body of literature that suggests histamine inversely modulates serotonin in the brain [6,15]. Many of these studies propose that dysregulations in histamine underlie disorders that are primarily considered to be serotonin mediated (e.g. depression) [32-34]. In 2011 we described simultaneous histamine and serotonin measurements in the rat SNr [22]. However, the FSCV peaks utilized to quantify histamine occurred at the anodic switching potential. These so called 'switching peaks' occur when spontaneous adsorption of analytes changes the electrical bilayer, hence capacitative current on the CFM. While switching peaks can be used to quantify histamine in a well-controlled environment (i.e. *in vitro* or tissue slice preparations), they cannot be used *in vivo* because other analytes that adsorb to the CFM provide identical, indistinguishable CVs [16].

In 2015, we addressed the issue of selective *in vivo* histamine analysis by developing a detection waveform that displayed a distinct Faradaic-like peak corresponding to histamine oxidation. We successfully applied this waveform *in vivo* to selectively quantify histamine [16]. In this study, we show that this novel waveform can simultaneously and selectively measure not only histamine, but also serotonin (*vide infra*), which greatly aids our interests in establishing how histamine modulates serotonin chemistry.

MFB Stimulation Rapidly, Potently Inhibits Ambient Serotonin in the PM

Figure 5.1 shows histamine release upon MFB stimulation in a hypothalamic region, the PM. We and others previously established this stimulation and measurement model to be robust and successful in evoking histamine [35,36] since the PM is home to a dense population of histamine cell bodies [36] and the region of the MFB that we stimulate contains histamine axons [37,38]. The PM region also contains serotonin terminals [5,17], therefore we postulated that the PM seemed a promising area to study histamine/serotonin modulation, particularly because our data imply that the electrical stimulation does not evoke serotonin. This finding is supported by the presence of fewer serotonin axons in the anterior area of the MFB (our stimulation location) [39,40]. Importantly, this model allows us to investigate histamine's effects on serotonin chemistry in the absence of stimulated serotonin release. This type of measurement can be greatly facilitated in the future with the development of optogenetic tools that selectively target histamine.

In accord with our postulation, in **Figure 5.1**, an event following the evoked histamine event by around 2 seconds is apparent. Via comparison of CVs collected *in vitro* and *in vivo* in the SNr (an area we have well established for serotonin FSCV) [21,41], we can electrochemically verify this second event to be caused by serotonin. The small deviation in the peak positions in **Figure 5.1C (ii)** is typical when comparing *in vivo* and *in vitro* responses and is likely due to differences in ohmic drop between *in vitro* and *in vivo* preparations. Of great interest, our data indicate that the serotonin levels are *decreasing* in response to the stimulation.

Because FSCV is a background subtracted method, ambient levels cannot be established therefore the conclusion of this data is that MFB stimulation inhibits ambient serotonin activity by around 40 nM. FSCV most commonly observes increased neurotransmitter activity; thus, our experiment represents an exciting opportunity to study inhibition of ambient activity.

We next hypothesize that this inhibition is, at least partially, mediated by histamine based on prior histamine/serotonin modulation studies [6,15]. In the next sections we take experimental, mathematical and pharmacological approaches towards this hypothesis.

Histamine Mediates Serotonin Inhibition in the PM

i) Serotonin Inhibition is Concentration and Time Correlated to Histamine Release

To show that histamine, rather than another result of MFB stimulation inhibits serotonin in the PM, we systematically altered our stimulation parameters to change the profile of histamine release. **Figure 5.2** shows excellent agreement between the time course and amplitude of histamine release and serotonin inhibition. The raw data in **Figures 5.2 C, D and E** show that the profile of serotonin inhibition closely tracks histamine release, and the **Figure 5.2B** highlights this correlation more formally by plotting maximum histamine release amplitude vs. maximum serotonin inhibition amplitude. The linear relationship between histamine and serotonin with all stimulation parameters is strong evidence for chemical rapport between these two molecules in the PM.

ii) Mathematical Modeling of Serotonin Inhibition Necessitates an Autoreceptor Function.

The power of interpreting experimental data through mathematical models is the ability to test a number of physiological hypotheses. Above, we hypothesized that serotonin inhibition is histamine mediated, we now test this notion mathematically. Our model necessitates ambient (basal) histamine and serotonin levels which we are not yet able to determine with FSCV. For histamine, a value of 1.5 μM was chosen, because our data show that after stimulation histamine levels fall 1 μM or more below baseline (**Figures 5.2, 5.3, 5.4**). Similarly, for the same reason we chose 65 nM as the basal concentration of serotonin in the extracellular space. We found that we could fit the data closely via simple manipulations of H_3 heteroreceptor and autoreceptor strengths in our model. H_3 heteroreceptors on serotonin terminals [15,42] have previously been postulated to inhibit serotonin [6]. Our model supports this hypothesis, particularly given that is unlikely that the serotonin inhibition we observe is attributable to other slower mechanisms such as synthesis inhibition. Thus, to probe this idea further, we took a pharmacological approach.

iii) H_3 receptor Mediation of Serotonin Inhibition

Given the results of our mathematical modeling and the large body of prior work implicating H_3 heteroreceptors as an inhibitory mechanism for serotonin [15,42] we decided to probe H_3 receptor mediation of serotonin. **Figure 5.4** shows the results of systemically administering varying doses of a potent H_3 receptor antagonist, thioperamide, to different mice. The low dose (2 mg kg^{-1}) increased the

amplitude of histamine release (consistent with prior studies with dopamine and D2 autoreceptor antagonism) [43,44], but has no significant effect on serotonin. This phenomenon is not difficult to explain because the serotonin response is controlled by dual mechanisms of a) now increased histamine available to antagonize H_3 receptors and b) a larger percentage of H_3 receptors antagonized on serotonin neurons. The overall result is a manifestation of two opposing effects that cancel each other out.

The 20 mg kg^{-1} dose had effects on both histamine release and clearance (reuptake effects have been previously seen with serotonin autoreceptor antagonism) (Wood *et al.* 2014). The effect on the magnitude of serotonin inhibition was not significant, however it seems that the prolonged histamine in the synapse is outcompeting thioperamide for H_3 receptors on serotonin neurons to create prolonged serotonin inhibition (> 60 seconds).

H_3 heteroreceptors are likely more localized in the synapse, because of their position on serotonin terminals [45] than are H_3 autoreceptors on presynaptic histamine neurons. Autoreceptors are generally found outside of the direct synaptic space, asserting inhibition when a concentration threshold is reached [46]. The inhibition constant (K_i) of thioperamide is smaller than the Michaelis Menton constant (K_m) of histamine towards H_3 receptors [47,48]. However, after stimulation histamine concentrations are very high in the direct synaptic space (likely reaching mMs based on prior dopamine models) [49] and fall off exponentially with distance. Because the thioperamide concentration is assumed to be homogenous throughout this brain region, the histamine most certainly outcompetes

thioperamide for H_3 heteroreceptors on serotonin neurons. This notion is made apparent by the largest dose (50 mg kg^{-1}) of thioperamide which created significant and long-lasting serotonin inhibition.

In sum, we showcased the power of FSCV for simultaneous measurements of histamine and serotonin the PM. We showed that MFB stimulation released histamine but created a potent inhibition of serotonin. Voltammetrically, mathematically and pharmacologically we showed serotonin inhibition was dependent on histamine release, via an H_3 receptor mediated mechanism. Our approach signals a powerful advancement in FSCV technology that will facilitate the systematic study of histamine and serotonin dynamics in the variety of different brain processes involving these two molecules.

5.6 ACKNOWLEDGEMENTS

The authors would like to thank Glenn Dryhurst and Eberhard Schlicker for helpful insights into histamine electro-oxidation and H_3 receptor K_i respectively. The University of South Carolina start-up funds and the Eli Lily Young Investigator Award in Analytical Chemistry to PH and an NSF award, DMS-0931642, and a NSF CAREER Award, DMS-0956057, to JB funded this research funded this research.

5.7 REFERENCES

(1) Haas, H. L.; Sergeeva, O. A.; Selbach, O. *Physiological reviews* **2008**, *88*, 1183.

(2) Brown, R. E.; Stevens, D. R.; Haas, H. L. *Progress in neurobiology* **2001**, *63*, 637.

(3) Chase, T. N.; Murphy, D. L. *Annual review of pharmacology* **1973**, *13*, 181.

(4) Russell, W. L.; Henry, D. P.; Phebus, L. A.; Clemens, J. A. *Brain Res* **1990**, *512*, 95.

(5) Moore, R. Y.; Halaris, A. E.; Jones, B. E. *J Comp Neurol* **1978**, *180*, 417.

(6) Threlfell, S.; Cragg, S. J.; Kallo, I.; Turi, G. F.; Coen, C. W.; Greenfield, S. A. *J Neurosci* **2004**, *24*, 8704.

(7) Laitinen, K. S. M.; Tuomisto, L.; Laitinen, J. T. *European Journal of Pharmacology* **1995**, *285*, 159.

(8) Portas, C. M.; Bjorvatn, B.; Ursin, R. *Progress in neurobiology* **2000**, *60*, 13.

(9) Cowen, P.; Sherwood, A. C. *Journal of psychopharmacology (Oxford, England)* **2013**, *27*, 575.

(10) Hashemi, P.; Dankoski, E. C.; Petrovic, J.; Keithley, R. B.; Wightman, R. M. *Analytical Chemistry* **2009**, *81*, 9462.

(11) Wood, K. M.; Cepeda, D.; Hashemi, P. *Compendium of in Vivo Monitoring in Real-Time Molecular Neuroscience, Vol 1: Fundamentals and Applications* **2015**, 269.

(12) Wood, K. M.; Zeqja, A.; Nijhout, H. F.; Reed, M. C.; Best, J.; Hashemi, P. *J Neurochem* **2014**, *130*, 351.

(13) Fink, K.; Schlicker, E.; Neise, A.; Gothert, M. *Naunyn Schmiedebergs Arch Pharmacol* **1990**, *342*, 513.

(14) Hough, L. B. *Prog Neurobiol* **1988**, *30*, 469.

(15) Schlicker, E.; Betz, R.; Gothert, M. *Naunyn Schmiedebergs Arch Pharmacol* **1988**, *337*, 588.

(16) Samaranayake, S.; Abdalla, A.; Robke, R.; Wood, K. M.; Zeqja, A.; Hashemi, P. *Analyst* **2015**, *140*, 3759.

(17) Marvin, E.; Scrogin, K.; Dudas, B. *J Chem Neuroanat* **2010**, *39*, 235.

(18) Michael, D. J.; Joseph, J. D.; Kilpatrick, M. R.; Travis, E. R.; Wightman, R. M. *Analytical Chemistry* **1999**, *71*, 3941.

(19) Jones, S. R.; Mickelson, G. E.; Collins, L. B.; Kawagoe, K. T.; Wightman, R. M. *Journal of neuroscience methods* **1994**, *52*, 1.

(20) Takmakov, P.; Zachek, M. K.; Keithley, R. B.; Bucher, E. S.; McCarty, G. S.; Wightman, R. M. *Anal Chem* **2010**, *82*, 9892.

(21) Hashemi, P.; Dankoski, E. C.; Lama, R.; Wood, K. M.; Takmakov, P.; Wightman, R. M. *Proceedings of the National Academy of Sciences of the United States of America* **2012**, *109*, 11510.

(22) Hashemi, P.; Dankoski, E. C.; Wood, K. M.; Ambrose, R. E.; Wightman, R. M. *Journal of Neurochemistry* **2011**, *118*, 749.

(23) Bernaerts, P.; Lamberty, Y.; Tirelli, E. *Behavioural brain research* **2004**, *154*, 211.

(24) Akhtar, M.; Pillai, K. K.; Vohora, D. *Basic & Clinical Pharmacology & Toxicology* **2005**, *97*, 218.

(25) Bordi, F.; Mor, M.; Plazzi, P. V.; Silva, C.; Caretta, A.; Morini, G. *Farmaco (Societa chimica italiana : 1989)* **1992**, *47*, 1095.

(26) Millar, J.; Stamford, J. A.; Kruk, Z. L.; Wightman, R. M. *European Journal of Pharmacology* **1985**, *109*, 341.

(27) Zhou, F. M.; Liang, Y.; Dani, J. A. *Nature neuroscience* **2001**, *4*, 1224.

(28) Montague, P. R.; McClure, S. M.; Baldwin, P. R.; Phillips, P. E.; Budygin, E. A.; Stuber, G. D.; Kilpatrick, M. R.; Wightman, R. M. *The Journal of neuroscience : the official journal of the Society for Neuroscience* **2004**, *24*, 1754.

(29) Swamy, B. E.; Venton, B. J. *Anal Chem* **2007**, *79*, 744.

(30) Sanford, A. L.; Morton, S. W.; Whitehouse, K. L.; Oara, H. M.; Lugo-Morales, L. Z.; Roberts, J. G.; Sombers, L. A. *Analytical chemistry* **2010**, *82*, 5205.

(31) Glanowska, K. M.; Venton, B. J.; Moenter, S. M. *The Journal of neuroscience : the official journal of the Society for Neuroscience* **2012**, *32*, 14664.

(32) Schneider, C.; Risser, D.; Kirchner, L.; Kitzmuller, E.; Cairns, N.; Prast, H.; Singewald, N.; Lubec, G. *Neuroscience letters* **1997**, *222*, 183.

(33) Muller, C. P.; Carey, R. J.; Huston, J. P.; De Souza Silva, M. A. *Progress in neurobiology* **2007**, *81*, 133.

(34) Barbeau, A. *Canadian Medical Association Journal* **1962**, *87*, 802.

(35) Rozov, S. V.; Zant, J. C.; Karlstedt, K.; Porkka-Heiskanen, T.; Panula, P. *The European journal of neuroscience* **2014**, *39*, 218.

(36) Panula, P.; Yang, H. Y.; Costa, E. *Proceedings of the National Academy of Sciences of the United States of America* **1984**, *81*, 2572.

(37) Garbarg, M.; Barbin, G.; Feger, J.; Schwartz, J. C. *Science (New York, N.Y.)* **1974**, *186*, 833.

(38) Auvinen, S.; Panula, P. *The Journal of comparative neurology* **1988**, *276*, 289.

(39) Veening, J. G.; Swanson, L. W.; Cowan, W. M.; Nieuwenhuys, R.; Geeraedts, L. M. *The Journal of comparative neurology* **1982**, *206*, 82.

(40) Nieuwenhuys, R.; Geeraedts, L. M.; Veening, J. G. *The Journal of*

comparative neurology **1982**, *206*, 49.

(41) Dankoski, E. C.; Wightman, R. M. *Frontiers in Integrative Neuroscience* **2013**, *7*, 44.

(42) Esbenshade, T. A.; Browman, K. E.; Bitner, R. S.; Strakhova, M.; Cowart, M. D.; Brioni, J. D. *Br J Pharmacol* **2008**, *154*, 1166.

(43) Clark, D.; Exner, M.; Furmidge, L. J.; Svensson, K.; Sonesson, C. *Eur J Pharmacol* **1995**, *275*, 67.

(44) Kita, J. M.; Parker, L. E.; Phillips, P. E.; Garris, P. A.; Wightman, R. M. *J Neurochem* **2007**, *102*, 1115.

(45) Carlsson, A.; Carlsson, M. L. *Dialogues in clinical neuroscience* **2006**, *8*, 137.

(46) Langer, S. Z.; Galzin, A. M.; Costentin, J. *Presynaptic Receptors and Neuronal Transporters: Official Satellite Symposium to the IUPHAR 1990 Congress Held in Rouen, France, on 26–29 June 1990*; Elsevier Science, 2013.

(47) Liedtke, S.; Flau, K.; Kathmann, M.; Schlicker, E.; Stark, H.; Meier, G.; Schunack, W. *Naunyn Schmiedebergs Arch Pharmacol* **2003**, *367*, 43.

(48) Chen, J.; Liu, C.; Lovenberg, T. W. *Eur J Pharmacol* **2003**, *467*, 57.

(49) Garris, P. A.; Ciolkowski, E. L.; Pastore, P.; Wightman, R. M. *The Journal of neuroscience : the official journal of the Society for Neuroscience* **1994**, *14*, 6084.

CHAPTER 6: CONCLUSIONS AND FUTURE DIRECTIONS

A detailed characterization of the different facets of serotonin neurotransmission *in vivo* has remained a challenge since the discovery of serotonin over 50 years ago. In this dissertation, I introduce novel methods, developed in the Hashemi lab, to better understand the phasic and tonic properties of serotonin, along with a better understanding of the neuromodullatory relation between histamine and serotonin.

In **Chapter 2**, FSCAV was first introduced for the measurement of ambient serotonin *in vivo*. This method was shown to be selective, stable, and sensitive to serotonin over other interferences, both *in vitro* and *in vivo*. This combination of tools was then utilized in **chapter 3** to study different brain regions; the hippocampus and the medial prefrontal cortex. FSCV measurements in these specific localities has shown characteristic differences in their reuptake curves events, that was attributed mainly to the differences in SERTs and non-SERTs in these regions. This was further verified with triple staining immunohistochemistry, and the effects of these different SERT densities was reflected in the ambient serotonin levels measured with FSCAV.

In **chapter 4**, a novel FSCV waveform for the study of HA is optimized for *in vivo* studies. *In vivo*, HA was evoked in the PH following stimulation in the

MFB. In **chapter 5,** it was determined that within this same region, serotonin could also be measured simultaneously with HA. Our work has shown that histamine inhibits serotonin in the PH region of the brain. The modulation of serotonin by other neurotransmitters is believed to be one of the methods of serotonin regulation in the brain.

My work in this dissertation has laid the foundation for exploring new serotonin circuitries to further understand the neurochemistry of serotonin. Through this, further work can be done on different disease model to study the changes that arise from different pathophysiologies. The combination of FSCV and FSCAV, along with different statistical and mathematical models, is now able to provide a new approach to study the different complex aspects of serotonin neurochemistry.

APPENDIX A: SUPPLEMENTARY INFORMATION FROM CHAPTER 2

The fitting of the different electrodes used in the *in vitro* calibrations was performed using regression via the *lm* command in the R programming package.[1,2] The results of the regression demonstrate significant difference in the intercept and slope of the different electrodes. The fitted lines for the 15 electrodes are given in the **Figure S.1** below. The linear model that was fitted for the kth (k = 1, 2, …, 15) electrode is of form:

$$\text{Charge} = B_0 + E_k + B_1 * C + I_k * C + \text{Error}, \qquad (1)$$

where $E_0 = 0$ and $I_0 = 0$. In these linear models, E_k and I_k are kth-electrode specific effects, with I_k an interaction effect between Charge and the kth electrode, and C denotes the concentration. “Error” represents measurement error.

Using the model developed as explained in the Experiments section and based on the concentration estimates over time a linear-parabolic model was fitted. This model was motivated by the expectation that the concentration level is constant before the drug takes effect, and when the drug takes effect, then the concentration level is expected to increase for a certain period of time. Thus, the functional continuous model that was fitted using the pairs of time and the concentration estimates was linear over the time portion where there is no drug effect and was parabolic afterwards. Mathematically, this linear-parabolic model is given by

$$C(t) = w_0 + w_1 t + k_1[\max(0, T+d-t)] - k_2[\max(0, T+d-t)]^2 + \text{Error}, \quad (2)$$

where T is the time when the drug intervention was performed (T = 60 minutes), while d is the lag-time until the drug starts taking effect.

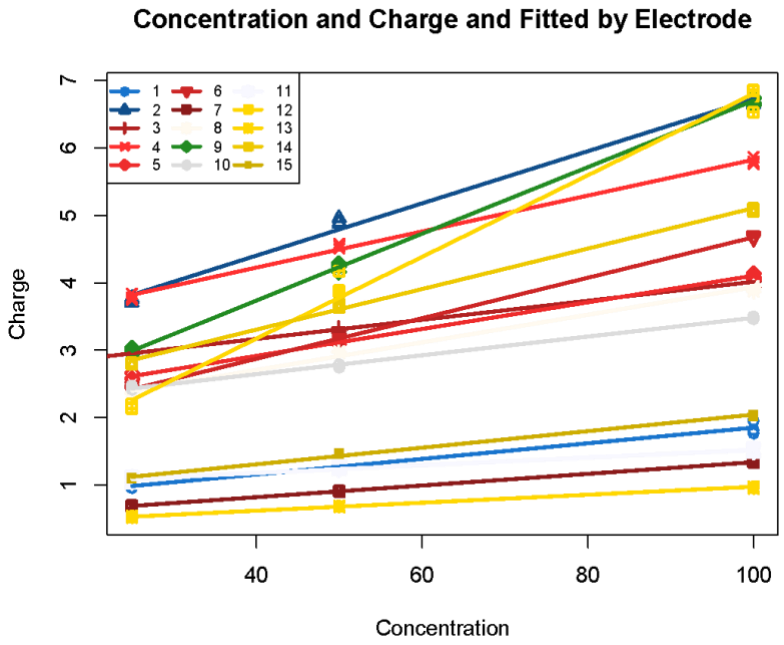

Figure A.1. Concentration (in nM) and charge (in pC) measurements obtained for 15 electrodes together with their fitted values based on linear models with interaction terms.

The weighted regression fitting of the model was done using the *lm* command in the R programming package, with weights equal to the inverse of the estimated variance of the concentrations. Point-wise confidence intervals (CI) were constructed based on the fitted linear-parabolic model using the *predict.lm* command in the R package.

Standard errors and tests of significance of the coefficients are:

Pargyline

Table A.1. Standard errors and tests of significance of the coefficients for Pargyline (75 mg/kg).

	Estimate	Standard Error	t value	Pr(>|t|)
(Intercept)	65.216532	0.304313	214.307	< 2e-16 ***
Time	0.004124	0.007753	0.532	0.596
Timelag	0.526824	0.031933	16.498	< 2e-16 ***
timelag2	-0.004234	0.000505	-8.385	1.25e-13 ***

GBR 12909

Table A.2. Standard errors and tests of significance of the coefficients for GBR 12909 (15 mg/kg)

	Estimate	Standard Error	t value	Pr(>|t|)
(Intercept)	5.882e+01	2.357e-01	249.533	<2e-16 ***
Time	5.460e-03	9.008e-03	0.606	0.546
time2	-8.779e-05	7.208e-05	-1.218	0.226

Desipramine

Table A.3. Standard errors and tests of significance of the coefficients for Desipramine (15 mg/kg)

	Estimate	Standard Error	t value	Pr(>|t|)
(Intercept)	7.154e+01	7.349e-02	973.500	<2e-16 ***
Time	1.274e-03	2.807e-03	0.454	0.651
time2	-4.159e-06	2.245e-05	-0.185	0.85

References

1. Fox, J., *applied linear regression analysis and generalized linear models*. 3rd ed.; Sage Publications: Thousand Oaks, CA, 2016.

2. John Fox, S. W., *An R Companion to Applied Regression*. 2nd ed.; Sage Publications: Thousand Oaks, CA, 2011.

APPENDIX B: PERMISSION OBTAINED FROM THE AMERICAN CHEMICAL SOCIETY TO REPRINT THE ARTICLE IN CHAPTER 2

Title:	In Vivo Ambient Serotonin Measurements at Carbon-Fiber Microelectrodes
Author:	Aya Abdalla, Christopher W. Atcherley, Pavithra Pathirathna, et al
Publication:	Analytical Chemistry
Publisher:	American Chemical Society
Date:	Sep 1, 2017

PERMISSION/LICENSE IS GRANTED FOR YOUR ORDER AT NO CHARGE

This type of permission/license, instead of the standard Terms & Conditions, is sent to you because no fee is being charged for your order. Please note the following:

- Permission is granted for your request in both print and electronic formats, and translations.
- If figures and/or tables were requested, they may be adapted or used in part.
- Please print this page for your records and send a copy of it to your publisher/graduate school.
- Appropriate credit for the requested material should be given as follows: "Reprinted (adapted) with permission from (COMPLETE REFERENCE CITATION). Copyright (YEAR) American Chemical Society." Insert appropriate information in place of the capitalized words.
- One-time permission is granted only for the use specified in your request. No additional uses are granted (such as derivative works or other editions). For any other uses, please submit a new request.

APPENDIX C: PERMISSION OBTAINED FROM THE ROYAL SOCIETY OF CHEMISTRY TO REPRINT THE ARTICLE IN CHAPTER 4

In vivo histamine voltammetry in the mouse premammillary nucleus

S. Samaranayake, A. Abdalla, R. Robke, K. M. Wood, A. Zeqja and P. Hashemi, Analyst, 2015, 140, 3759

DOI: 10.1039/C5AN00313J

- For reproduction of material from PCCP:

  Reproduced from Ref. XX with permission from the PCCP Owner Societies.

- For reproduction of material from PPS:

  Reproduced from Ref. XX with permission from the European Society for Photobiology, the European Photochemistry Association, and The Royal Society of Chemistry.

- For reproduction of material from all other RSC journals and books:

  Reproduced from Ref. XX with permission from The Royal Society of Chemistry.

If the material has been adapted instead of reproduced from the original RSC publication "Reproduced from" can be substituted with "Adapted from".

In all cases the Ref. XX is the XXth reference in the list of references.

If you are the author of this article you do not need to formally request permission to reproduce figures, diagrams etc. contained in this article in third party publications or in a thesis or dissertation provided that the correct acknowledgement is given with the reproduced material.

Reproduced material should be attributed as follows:

- For reproduction of material from NJC:

  [Original citation] - Reproduced by permission of The Royal Society of Chemistry (RSC) on behalf of the Centre National de la Recherché Scientifique (CNRS) and the RSC

- For reproduction of material from PCCP:

  [Original citation] - Reproduced by permission of the PCCP Owner Societies

- For reproduction of material from PPS:

  [Original citation] - Reproduced by permission of The Royal Society of Chemistry (RSC) on behalf of the European Society for Photobiology, the European Photochemistry Association, and RSC

- For reproduction of material from all other RSC journals:

  [Original citation] - Reproduced by permission of The Royal Society of Chemistry

If you are the author of this article you still need to obtain permission to reproduce the whole article in a third-party publication with the exception of reproduction of the whole article in a thesis or dissertation.

Information about reproducing material from RSC articles with different licenses is available on our Permission Requests page.

APPENDIX D: PERMISSION OBTAINED FROM THE JOURNAL OF NEUROCHEMISTRY TO REPRINT THE ARTICLE IN CHAPTER 5

Copyright Clearance Center RightsLink®

Title: A voltammetric and mathematical analysis of histaminergic modulation of serotonin in the mouse hypothalamus

Author: Srimal Samaranayake,Aya Abdalla,Rhiannon Robke,H. Frederik Nijhout,Michael C. Reed,Janet Best,Parastoo Hashemi

Publication: Journal of Neurochemistry

Publisher: John Wiley and Sons

Date: Jun 27, 2016

Order Completed

Thank you for your order.

This Agreement between Aya Abdalla ("You") and John Wiley and Sons ("John Wiley and Sons") consists of your license details and the terms and conditions provided by John Wiley and Sons and Copyright Clearance Center.

Your confirmation email will contain your order number for future reference.

printable details

License Number	4257700214829
License date	Dec 28, 2017
Licensed Content Publisher	John Wiley and Sons
Licensed Content Publication	Journal of Neurochemistry
Licensed Content Title	A voltammetric and mathematical analysis of histaminergic modulation of serotonin in the mouse hypothalamus
Licensed Content Author	Srimal Samaranayake,Aya Abdalla,Rhiannon Robke,H. Frederik Nijhout,Michael C. Reed,Janet Best,Parastoo Hashemi
Licensed Content Date	Jun 27, 2016
Licensed Content Pages	10
Type of use	Dissertation/Thesis
Requestor type	Author of this Wiley article
Format	Print and electronic
Portion	Full article
Will you be translating?	No
Title of your thesis / dissertation	ELECTROCHEMICAL METHODS TO STUDY REAL-TIME IN VIVO SEROTONERGIC AND HISTAMINERGIC NEUROCHEMISTRY
Expected completion date	Jan 2018
Expected size (number of pages)	145
Requestor Location	Aya Abdalla 1600 Park Circle Columbia, SC 29201 United States Attn:
Publisher Tax ID	EU826007151
Billing Type	Invoice
Billing address	Aya Abdalla 1600 Park Circle Columbia, SC 29201 United States Attn: Aya Abdalla
Total	0.00 USD